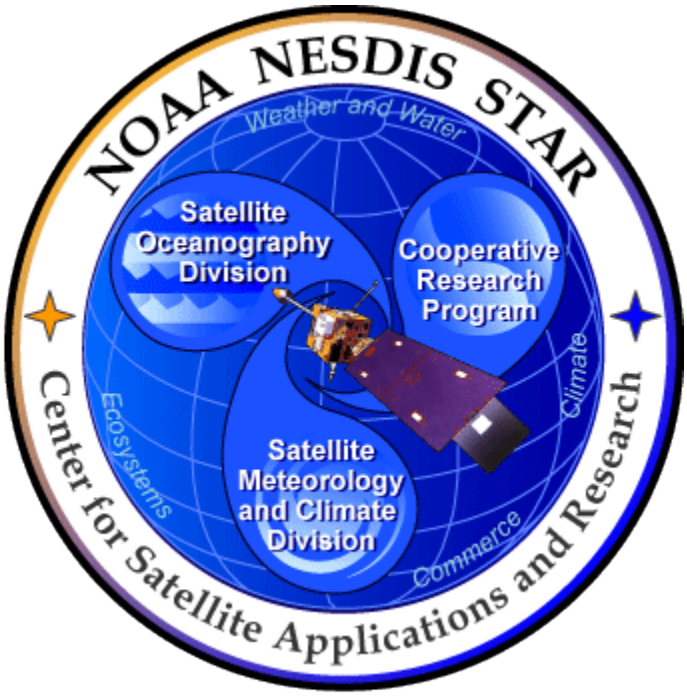

NOAA NESDIS
CENTER for SATELLITE APPLICATIONS and RESEARCH

EPS Aerosol Optical Depth (AOD) Algorithm Theoretical Basis Document

Prepared by
Istvan Laszlo (NOAA) and Hongqing Liu (IMSG)

Version 3.2
September 22, 2020

TABLE OF CONTENT

LIST OF FIGURES

LIST OF TABLES

LIST OF ACRONYMS

ABI	Advanced Baseline Imager
ACM	ABI cloud mask
AE	Ångström Exponent
AERONET	AErosol RObotic NETwork
AHI	Advanced Himawari Imager
AOD	Aerosol Optical Depth
APSP	Aerosol Particle Size Parameter
ASSISTT	Algorithms Scientific Software Integration and System Transition Team
ATBD	Algorithm Theoretical Basis Document
AVHRR	Advanced Very High Resolution Radiometer
BRDF	Bi-directional Reflectance Distribution Function
CMG	Climate Modeling Grid
EOS	Earth Observing System
EPS	Enterprise Processing System
FMW	Fine Mode Weight
GFS	Global Forecast System
IGBP	International Geosphere-Biosphere Programme
JPSS	Joint Polar Satellite System
LUT	Lookup Table
MISR	Multi-angle Imaging SpectroRadiometer
MODIS	Moderate Resolution Imaging Spectroradiometer
MSS	Multispectral Sensor
NASA	National Aeronautics and Space Administration
NDVI	Normalized Difference Vegetation Index
NESDIS	National Environmental Satellite, Data, and Information Service
NOAA	National Oceanic and Atmospheric Administration
POES	Polar Orbiting Environmental Satellites
POLDER	POLarization and Directionality of the Earth's Reflectances
RRPS	Risk Reduction Product Suite
RTM	Radiative Transfer Model
S-NPP	Suomi – National Polar-orbiting Partnership
SWIR	Shortwave Infrared
TM	Thematic Mapper
TOA	Top of Atmosphere
TPW	Total Precipitable Water
VCM	VIIRS Cloud Mask
VIIRS	Visible Infrared Imaging Radiometer Suite

ABSTRACT

This document describes the aerosol optical depth (AOD) and aerosol particle size parameter (APSP) retrieval algorithm developed for the NOAA Enterprise Processing System from inputs from the Visible Infrared Imaging Radiometer Suite (VIIRS), Advanced Baseline Imager (ABI), Advanced Himawari Imager (AHI) and METImage. AOD retrieval is performed globally in daylight except under cloudy or other unfavorable conditions. The AOD product consists of the vertically-integrated total-column extinction for a range of wavelengths from 0.4 to 2.25 μm including AOD at the mid-visible 0.55 μm wavelength. The AOD is retrieved by comparing satellite-observed top-of-atmosphere (TOA) reflectances with those calculated from radiative transfer for several atmospheric parameters, including discrete sets of aerosol models and AODs and sun-sensor geometries. The retrieved AOD is the one that leads to the best match between observed and calculated reflectances. In order to simplify the radiative transfer calculations the results of these calculations are saved in look-up tables (LUT). Because the reflective properties of ocean and land are very different, separate retrieval approaches are used. Over the ocean, the surface Bi-directional Reflectance Distribution Function (BRDF) is computed based on wind speed and direction, and the TOA reflectance is calculated by coupling the surface and atmosphere in the radiative transfer calculation. Over the land, the surface is assumed to be Lambertian; its reflectance is treated as unknown and retrieved simultaneously with AOD. In the retrieval surface reflectances are estimated from prescribed relationships between spectral surface reflectances in selected imager channels. Over dark land surface, two sets of these relationships corresponding to two different sets of channels are used. The preferred set is the set with the shorter wavelength channels; but when this set would lead to inferior results (predominantly for large AOD) the set with the longer wavelengths is used instead. Over bright land, the algorithm relies on ratios of spectral surface reflectances predetermined for 0.1^{o} x 0.1^{o} regions. The aerosol particle size parameter is provided only over ocean. It is reported as the Ångström Exponent calculated from the aerosol optical depth values at two different wavelengths. The aerosol algorithm is applied to every pixel at moderate resolution (e.g., 0.75 km at nadir for VIIRS, 2.0 km for ABI and AHI) to form a pixel-level product. A preliminary validation of the algorithm has been performed by comparing aerosol optical depth at 0.55 μm retrieved from VIIRS reflectances with ground measurements from the AErosol RObotic NETwork (AERONET); the quality of the AOD product is found to be comparable with that of the latest MODIS AOD product.

1 INTRODUCTION

Aerosols are liquid or solid particles suspended in the atmosphere. Aerosols modify the energy budget of the earth-atmosphere system in several ways. They directly scatter and absorb solar and thermal infrared radiation [e.g., Bohren and Huffman, 1983; Coakley et al., 1983; Charlson et al., 1992]; modify amount, life time, and microphysical and radiative properties of clouds and therefore indirectly change the Earth-leaving radiation [e.g., Twomey, 1977; Albretch, 1989; Rosenfeld and Lensky, 1998]. Absorption of radiant energy by aerosols leads to heating of the troposphere and cooling of the surface, which can change the relative humidity and atmospheric stability thereby influencing cloud formation and precipitation [Hansen et al., 1997; Koren et al., 2004; Ackerman et al., 2000]. Consequently, aerosols can influence land surface process [Yu, et al., 2002], the global surface temperature [Coakley et al., 1983; Charlson et al., 1992; Ramanathan et al., 2001], climate and the hydrological cycle [Ramanathan et al., 2001], and ecosystems [Chameides et al., 1999]. As complex mixtures of particles and particle aggregates of varying chemical composition, aerosols also affect regional air quality and human health [Pope et al., 2002]. Epidemiological studies have linked exposure to PM2.5 (particulate mass in units of $\mu g/m^3$ for particles smaller than 2.5 μm in median diameter) to a range of adverse health effects such as strokes, heart disease, respiratory ailments, and premature death (e.g. http://www.epa.gov/region4/sesd/pm25/p2.html).

Aerosols exhibit high spatial and temporal variability due to the heterogeneous distribution of sources, short lifetime, and episodic feature of emission events. Therefore continuous global and regional characterization can only be realized through satellite remote-sensing. Retrieval of aerosol optical depth and other aerosol products from reflected solar radiance in the visible and near-IR bands, measured by satellite, began in the 1970s. Retrievals were made initially with the Multispectral Sensor (MSS) and Thematic Mapper (TM) on board the Landsat series of satellites [Griggs, 1975; Fraser, 1976; Mekler et al., 1977], then from the Advanced Very High Resolution Radiometer (AVHRR) on board NOAA's Polar Orbiting Environmental Satellites (POES) [Rao et al., 1989; Stowe et al.,1990, 1997, Higurashi and Nakajima, 1999; Geogdzhayev et al., 2002] and using the Earth Observing System (EOS) era satellite sensors. The EOS-era satellite sensors in this category include the MODerate resolution Imaging Spectroradiometer (MODIS) [Remer et al., 2005; Levy et al. 2007], the Multi-angle Imaging SpectroRadiometer (MISR) [Diner et al., 1998; Kahn et al., 2010] and the POLarization and Directionality of the Earth's Reflectances (POLDER) [Tanré et al., 2011]. More recently, aerosol data are obtained using measurements made by the Visible Infrared Imaging Radiometer Suite (VIIRS) on board the Suomi National Polar orbiting Partnership (S-NPP) satellite [Jackson et al., 2013, Liu et al., 2014], and aboard the next generation of polar-orbiting environmental satellites, e.g., NOAA-20 of the Joint Polar Satellite System (JPSS) [Laszlo, 2018].

In addition to polar-orbiting satellites, aerosol retrievals have also been made from imager instruments on geostationary platforms. Real time monitoring of aerosol optical depth from the US Geostationary Operational Environmental Satellite (GOES) data dad been routinely conducted at the National Oceanic and Atmospheric Administration (NOAA) [Knapp et al., 2002; Prados, 2007] from the Imager instruments on the heritage GOES satellites and

now from the Advanced Baseline Imager (ABI) aboard the GOES-R series of NOAA geostationary meteorological satellites [Laszlo et al., 2008, Kondragunta et al., 2020]. In contrast to the heritage GOES imager, ABI measures radiances at multiple wavelengths from the UV through the IR at high spatial resolution [Schmit et al., 2005], and thus enabling one to perform aerosol retrievals similar to those applied with MODIS and VIIRS. Very similar capabilities are offered by measurements of the Advanced Himawari Imager (AHI) on board the Japanese Himawari 8 geostationary weather satellite [Bessho et al., 2016; Laszlo, 2018].

The aerosol-retrieval algorithm described in this document is designed to provide quality aerosol information in a timely manner to satisfy the needs of the air quality, research, applied, private, governmental and military communities.

1.1 Purpose of This Document

The Algorithm Theoretical Basis Document (ATBD) describes the theory and necessary assumptions for deriving aerosol optical depth from VIIRS and ABI. Details of the algorithm, the products, and their expected uncertainties are also discussed.

1.2 Who Should Use This Documents

The intended users of this document are those interested in understanding the physical basis of the algorithm and use the aerosol retrieval outputs of this algorithm in applications requiring aerosol data. This document also provides information useful to anyone maintaining or modifying the original algorithm.

1.3 Inside Each Section

Specifically, this document is broken down into the following main sections:

- **Observing System Overview**: Provides the objectives of the algorithm, relevant characteristics of the instruments, and provides a brief description of the aerosol products generated by this algorithm.

- **Algorithm Description**: Provides detailed description of the physical and mathematical basis of the algorithm, the look-up tables, and inputs and outputs.

- **Preliminary Validation**: Describes the preliminary validation results of the retrieved AOD against the ground measurements in terms of accuracy and precision.

- **Practical Considerations**: Provides an overview of the issues involving numerical computation, programming and procedures, quality assessment and diagnostics, and exception handling.

- **Assumptions and Limitations**: Provides an overview of the current limitations of the approach and gives the plan for overcoming these limitations with further algorithm development.

1.4 Related Documents

Joint Polar Satellite System (JPSS), VIIRS Aerosol Optical Thickness (AOT) and Particle Size Parameter (APSP) Algorithm Theoretical Basis Document (ATBD), 474-00049, Effective Date: February 4, 2015, Revision C.

GOES-R Advanced Baseline Imager (ABI) Algorithm Theoretical Basis Document for Suspended Matter/Aerosol Optical Depth and Aerosol Size Parameter; Version 3.0, June 30, 2012.

GOES-R Mission Requirements Document (MRD)

GOES-R Functional and Performance Specification Document (F&PS)

GOES-R ABI Performance and Operation Requirements Document (PORD)

1.5 Revision History

Version 3.2 – September 2020 (current version). Describes the Sep 2020 algorithm updates that includes adding the METImage imager aboard the METOP-SG polar orbiting satellite, and minor updates applied to the ABI and AHI geostationary satellite.

Version 3.1 – June 2020. Describes the algorithm delivered to ASSISTT in April 2020. That delivery includes updates of land surface spectral reflectance relationship derived from extended dataset, and some minor changes in the heavy aerosol test and quality control process.

Version 3.0.8 – January 2020. Added description of strategy implemented to mitigate GOES-17 Loop-Heat-Pipe anomaly impact.

Version 3.0.7 – May 2019 (Incorrectly labeled as version 3.1). Added updates needed for processing NOAA-20/VIIRS data.

Version 3.0.1 – June 2016. Updated flow charts and small editorial changes.

Version 3.0 – April 2016. Describes the algorithm delivered to ASSISTT in March 2016. That delivery includes some bug fixes, updates to the internal snow/ice test and capability to make retrievals from measurements of the Advanced Himawari Imager (AHI) on board the Japanese Himawari 8 geostationary weather satellite.

Version 2.0 – January 2016. Describes the algorithm delivered to ASSISTT in January 2016. It includes an updated AOD retrieval over bright land surface, and an updated description of inputs and outputs. (Prepared by Istvan Laszlo and Hongqing Liu with input from Hai Zhang on the retrieval over bright land surface.)

Version 1.0 – November 2015. Describes the state of maturity of the algorithm delivered to ASSISTT in April 2015. (Prepared by Istvan Laszlo and Hongqing Liu.)

2 OBSERVING SYSTEM OVERVIEW

2.1 Products Generated

The algorithm is designed to retrieve aerosol optical depth (AOD) over land and ocean and aerosol particle size parameter (APSP) over ocean from daytime clear-sky reflectances.

AOD (or aerosol optical thickness, τ) is a measure of extinction of radiation by aerosols due to absorption and scattering. It depends on the chemical composition and size of aerosol particles, and thus varies with the wavelengths of radiation. It also depends on the amount of aerosol in the atmosphere, and as such it is also a measure of aerosol loading. Mathematically, it is defined as the integrated extinction coefficient over a vertical column of unit cross section, and as such it is unitless. The primary product is AOD at 550 nm (AOD550 or τ_{550}). AODs in other bands (VIIRS: M1-M11; ABI: M3, M5, M7, M9, M10 and M11) are also calculated based on the aerosol model selected by the algorithm during the retrieval.

APSP is a proxy for average aerosol particle size. It is reported as the Ångström Exponent (AE), which characterizes the dependence of AOD on wavelength. This dependence is determined, among others, by the size of aerosol particles (the larger the exponent, the smaller the particles). APSP over ocean is represented by two Ångström Exponents corresponding to two pairs of wavelengths (VIIRS: 0.555/0.865 μm and 0.865/1.61 μm; ABI: 0.64/0.865 and 0.865/1.61 μm).

In addition to AOD and APSP, a single aerosol type over land, and a fine-mode and a coarse-mode aerosol model along with the corresponding fine-mode weight over ocean are retrieved.

The output is at the satellite-pixel level (0.75 km for VIIRS and 2 km nominal for ABI).

The requirements for AOD and APSP to be derived from VIIRS reflectances are listed in Table 2-1 and Table 2-2. AOD and APSP are retrieved for clear (cloud-free) pixels from daytime observations with zenith angles less than or equal to 80 degrees.

The requirements for AOD and APSP to be derived from ABI reflectances are listed in Table 2-1 and Table 2-4. AOD and APSP are retrieved for clear (cloud-free) pixels from daytime observations with zenith angles less than or equal to 60 degrees.

Table 2-1. JPSS RRPS AOD Supplement Requirements Table

Attribute	**Threshold**
Geographic Coverage	Global coverage
Horizontal Cell Size	0.8 km at Nadir
Vertical Cell Size	Total Column
Mapping Uncertainty, 3 Sigma	4 km
Measurement Range	-0.05 to 5
Measurement Precision	Over Ocean: 0.15 (Tau < 0.3) 0.35 (Tau ≥ 0.3) Over land: 0.15 (Tau < 0.1); 0.25 (0.1 ≤ Tau ≤ 0.8); 0.45 (Tau > 0.8)
Measurement Accuracy	Over Ocean: 0.08 (Tau < 0.3) 0.15 (Tau ≥ 0.3) Over land: 0.06 (Tau < 0.1); 0.05 (0.1 ≤ Tau ≤ 0.8); 0.20 (Tau > 0.8)
Product Refresh Rate	At least 90% coverage of the globe every 24hours (monthly average)
Latency	30 minutes after granule data is available
Timeliness	≤ 3hours

Table 2-2. JPSS RRPS APSP Supplement Requirements Table

Attribute	Threshold
Geographic Coverage	Global coverage
Horizontal Cell Size	0.8 km at Nadir
Vertical Cell Size	Total Column
Mapping Uncertainty, 3 Sigma	4 km
Measurement Range	-1 to +3 alpha units
Measurement Precision	Operational Over Ocean: 0.6 alpha units
Measurement Accuracy	Operational Over Ocean: 0.3 alpha units
Product Refresh Rate	At least 90% coverage of the globe every 24hours (monthly average)
Latency	30 minutes after granule data is available
Timeliness	≤ 3hours

Table 2-3. GOES-R ABI mission requirements for Aerosol Optical Depth

Name	Geographic Coverage	Vertical Resolution	Horizontal Resolution	Mapping Accuracy	Measurement Range	Measurement Accuracy	Refresh Rate/Coverage Time Option (Mode 3)	Refresh Rate Option (Mode 4)	Vendor Allocated Ground Latency	Product Measurement Precision
Aerosol Optical Depth	C, FD	Total Column	2 km	1 km	-1* – 5 in optical depth	Based on Aerosol Optical Depth ranges: Over land: <0.04: 0.06 0.04 – 0.80: 0.04 > 0.80: 0.12 Over water: < 0.40: 0.02 > 0.40: 0.10	CONUS:5 min Full Disk: 15 min	CONUS:5 min Full Disk: 15 min	CONUS:50 sec Full Disk:159 sec	Based on Aerosol Optical Depth ranges: Over land: <0.04: 0.13 0.04 – 0.80: 0.25 > 0.80: 0.35 Over water: < 0.40: 0.15 > 0.40: 0.23

Table 2-4. GOES-R ABI mission requirements for Aerosol Particle Size

Name	Geographic Coverage	Vertical Resolution	Horizontal Resolution	Mapping Accuracy	Measurement Range	Measurement Accuracy	Refresh Rate/Coverage Time Option (Mode 3)	Refresh Rate Option (Mode 4)	Vendor Allocated Ground Latency	Product Measurement Precision
Aerosol Particle Size	FD	Total Column	2 km	1 km	Fine/Coarse Angstrom exponent range: -1 to +3	Fine/Coarse Angstrom exponent: 0.3 over ocean and land	Full Disk: 15 min	Full Disk: 5 min	Full Disk: 266 sec	0.15*

* Recommended to relax from 0.15 to 0.6

2.2 Instrument Characteristics

The narrow band measurements of the VIIRS/ABI sensor in the 0.412 to 2.25 μm range are used to derive the aerosol parameters. Other bands are used to create the VIIRS/ABI Cloud Mask (VCM/ACM) which the aerosol algorithm uses as input and in internal tests to characterize surface conditions. Table 2-5 summarizes the bands used by the algorithm. The band names are those of the VIIRS Moderate Resolution Bands (M-bands); the corresponding ABI bands will also be referred to by these names in this document. The aerosol algorithm for VIIRS uses the following bands: M1, M2, M3, M5 and M11 to derive AOD over land; M4, M5, M6, M7, M8, M10 and M11 to derive AOD over water; M1, M2, M3, M5, M7, M8, M9, M11, M15 and M16 for internal tests over land; M1, M2, M3, M4, M5, M7, M9, M10, M11 and M15 for internal tests over water. When the input satellite data are from ABI the algorithm to retrieve AOD uses M3, M5, and M11 over land; M5, M7, M10, and M11 over ocean. The channels used for internal tests in this case are: M3, M5, M7, M9, M10, M15 and M16 over land; M3, M5, M7, M9, M10, M11 and M15.

The spatial resolution of VIIRS M bands are 0.742 x 0.776 km at nadir (1.60 x 1.58 km at edge of scan); the spatial resolution of the input ABI channels is 2 km aggregated from the 0.5-km (M5), 1-km (M3, M7, M10) and 2-km (M9, M11, M15, M16) channels.

Table 2-5. Bands used by the AOD algorithm.

Band name	Central Wavelength (μm)		Use in aerosol algorithm
	VIIRS	ABI	
M1	0.412		Inversion over land ^{V*}, internal tests land^{V} and ocean^{V}
M2	0.445		Inversion over land^{V}, internal tests land^{V} and ocean^{V}
M3	0.488	0.470	Inversion over land; internal tests land and ocean
M4	0.555		Inversion over ocean^{V}; internal tests ocean^{V}
M5	0.672	0.640	Inversion over land and ocean;

			internal tests land and ocean
M6	0.746		Inversion over ocean^{V} (if unsaturated)
M7	0.865	0.865	Inversion over ocean; internal tests land and ocean
M8	1.240		Inversion over ocean^{V}; internal tests land^{V}
M9	1.378	1.378	Internal tests land and ocean
M10	1.610	1.610	Inversion over ocean; internal tests land^{A} and ocean
M11	2.250	2.250	Inversion over land and ocean; internal tests ocean
M15	10.763	11.2	Internal tests land and ocean
M16	12.013	12.3	Internal tests land

*: superscript ^{V} for being used by VIIRS only, ^{A} for being used by ABI only

It should be noted that all spectrally dependent constants provided in this document are derived for S-NPP VIIRS channels; those for the JPSS VIIRS and ABI channels are listed in the Appendix.

3 ALGORITHM DESCRIPTION

This section describes the algorithm at the current level of maturity.

3.1 Algorithm Overview

The algorithm described in this ATBD retrieves aerosol optical depth from measurements made in the solar reflective bands of VIIRS and ABI. The visible and near infrared bands chosen to derive optical depth are all within window regions and their bandwidths are narrow. As a result, the chance for contamination by gas (such as O_2, O_3, H_2O) absorption is minimized, and absorption by gases can be parameterized in a relatively simple manner (Section 3.4.6).

The algorithm builds on the MODIS [Tanré et al., 1997; Remer et al., 2005; Levy et al. 2007], VIIRS [Jackson et al., 2013; VIIRS ATBD, 2015], and ABI [Laszlo et al., 2008; ABI ATBD, 2012] aerosol retrieval algorithms. AOD is retrieved by comparing TOA reflectances observed in multiple bands with those computed for a range of discrete AOD values and aerosol models by coupling atmospheric and surface contributions. Separate algorithms are used for retrieval over land and ocean due to the distinct surface properties and aerosol types. For efficient retrieval, look-up tables are used to store the pre-calculated atmospheric contributions for a wide range of geometries and for a finite number of candidate (typical) aerosol models.

Daytime pixels suitable for aerosol retrieval are selected using upstream cloud, sun-glint, fire and snow masks. Amounts of atmospheric gases, surface pressure, wind speed and direction are obtained from ancillary data. Land/water mask is used to select the appropriate (land or ocean) algorithm (Section 3.3.2).

In addition to the upstream masks, internal tests are used to screen out pixels not appropriate for aerosol retrieval. Results of these and other tests performed during the retrieval are applied to set quality flags (Sections 3.4.2.5 and 3.4.3.5).

Due to the relatively weak aerosol signal and large uncertainties associated with the surface reflectance the algorithm does not make retrieval over sun-glint areas over water. Over land, AOD is retrieved for dark, vegetated surface following the dark-target approach [Kaufman et al. 1997, Remer et al., 2005; Levy et al. 2007]. A method that extends the retrieval to bright snow-free land surface has also been implemented. The method chooses the shorter wavelength channels (M1, M2, M3 and M5) to retrieve AOD applying a static 0.1°x0.1° spectral surface reflectance ratio dataset to characterize surface contribution over such a surface.

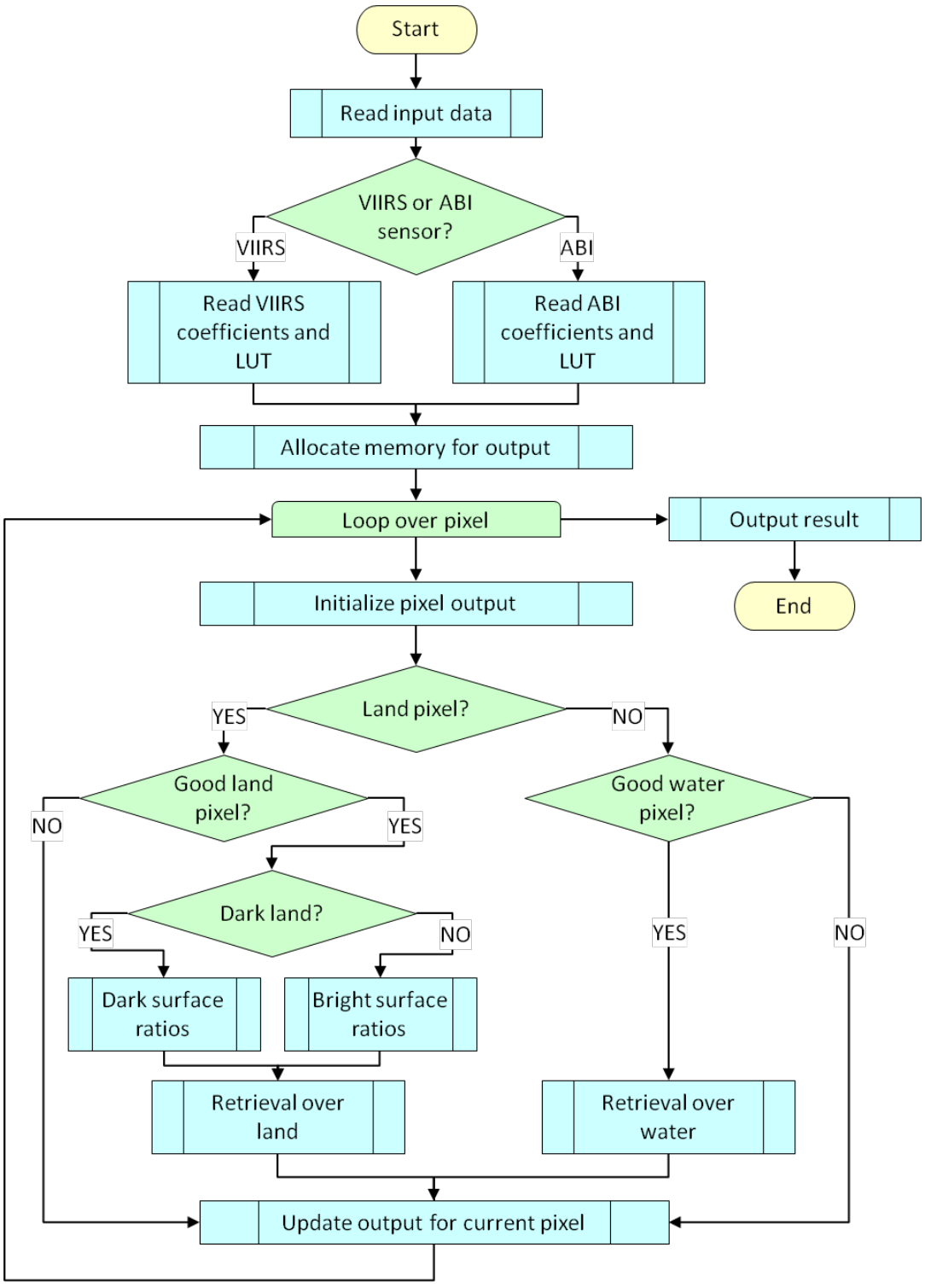

Figure 3-1. High level flowchart of the AOD retrieval illustrating the main processing sections.

3.2 Processing Outline

A high-level outline of the AOD retrieval algorithm is presented in
Figure 3-1. After reading in the input the algorithm determines whether they are from VIIRS or ABI, and then read in the appropriate, sensor-specific coefficients and look-up-tables. From this point on processing proceeds more or less independent of the type of sensor, limited only by the availability of channels from the particular sensor. The main steps are: 1) preparing input data for each pixel; 2) selecting land or water (ocean) algorithm based on whether the pixel is over land or water; 3) determining if AOD can be retrieved for the given pixel; 4) performing aerosol retrieval; 5) evaluating retrieval quality; and 6) output the result.

3.3 Algorithm Input

This section describes the input needed to process the aerosol retrieval.

3.3.1 Primary sensor data

Table 3-1 lists the primary sensor data used by the aerosol retrieval, including calibrated and geolocated reflectance from VIIRS/ABI observations, and its corresponding geolocation and geometry information.

Table 3-1. Primary sensor input data.

Name	Type	Description	Dimension
M1 reflectance	Input	Calibrated band M1 reflectance	pixel (xsize, ysize)
M2 reflectance	Input	Calibrated band M2 reflectance	pixel (xsize, ysize)
M3 reflectance	Input	Calibrated band M3 reflectance	pixel (xsize, ysize)
M4 reflectance	Input	Calibrated band M4 reflectance	pixel (xsize, ysize)
M5 reflectance	Input	Calibrated band M5 reflectance	pixel (xsize, ysize)
M6 reflectance	Input	Calibrated band M6 reflectance (assign missing values to saturated measurements)	pixel (xsize, ysize)
M7 reflectance	Input	Calibrated band M7 reflectance	pixel (xsize, ysize)
M8 reflectance	Input	Calibrated band M8 reflectance	pixel (xsize, ysize)
M9 reflectance	Input	Calibrated band M9 reflectance	pixel (xsize, ysize)
M10 reflectance	Input	Calibrated band M10 reflectance	pixel (xsize, ysize)
M11 reflectance	Input	Calibrated band M11 reflectance	pixel (xsize, ysize)
M15 brightness temperature	Input	Calibrated band M15 brightness temperature	pixel (xsize, ysize)
M16 brightness temperature	Input	Calibrated band M16 brightness temperature	pixel (xsize, ysize)
Longitude	Input	Pixel longitude	pixel (xsize, ysize)

Latitude	Input	Pixel latitude	pixel (xsize, ysize)
Solar geometry	Input	solar zenith and azimuth angles	pixel (xsize, ysize)
View geometry	Input	local zenith and azimuth angles	pixel (xsize, ysize)

The algorithm assumes the reflectance ρ is calculated from the calibrated radiance by dividing π times the radiance L by the product of the cosine of solar angle ϑ_0 and the extraterrestrial solar irradiance at the actual sun-earth distance E_d :

$$\rho = \frac{\pi L}{\cos \vartheta_0 \, E_d}$$

The dimensions "xsize" and "ysize" correspond to the number of pixels in the cross-track and along-track directions, respectively. All VIIRS sensor input data are at the same spatial resolution (0.75 km), and therefore have the same dimensions. For ABI, the sensor inputs vary in size due to the different spatial resolution (0.5, 1, and 2 km) of the channels; geolocation and geometry inputs are at 2-km to be consistent with the required resolution of the ABI aerosol product.

3.3.2 **Ancillary data**

The algorithm requires satellite-derived upstream products, Global Forecast System (GFS) model data, and global land cover type as ancillary data.

Satellite-derived upstream products (Table 3-2): Cloud, snow/ice, fire and glint masks are needed to identify pixels suitable for aerosol retrievals. There are four levels (confident clear; probably clear; probably cloud; and confident cloudy) in the input cloud mask, current algorithm consider the confident and probably clear as clear, and confident and probably cloudy as cloudy. Land/water mask is used to select the appropriate (land or ocean) algorithm. The cloud shadow mask is used to set the retrieval quality and the heavy aerosol mask is used to call-back (perform retrieval for) the pixel identified as cloud by the external cloud mask.

GFS model data (Table 3-3): GFS model surface wind speed and direction over ocean are required for calculation of ocean surface reflectance. Total precipitable water and ozone amount are used to account for gaseous absorption. Surface pressure data are used in calculating Rayleigh optical depth and transmission of gases other than water vapor and ozone. Because surface pressure can vary over small spatial scales in a complex terrain, the low-resolution (50 km) model surface pressure is pre-processed to VIIRS/ABI resolution. This pre-processing uses the hydrostatic equation and the equation of state to determine the surface pressure at pixel elevation:

$$P_{pixel} = P_{model} e^{-\frac{\Delta h * g}{R_d \overline{T_v}}} \qquad (3.3.1)$$

where P_{pixel} and P_{model} are actual pixel-level and model surface pressures ; Δh is the difference between the pixel and model surface elevations; g is the gravitational acceleration; R_d is the dry air constant; and $\overline{T_v}$ is the mean virtual temperature which is calculated as:

$$\overline{T_v} = \frac{T_{model}^{sfc}}{1-0.6*SH} - \gamma \frac{\Delta h}{2} \qquad (3.3.2)$$

where the first term on the right-hand side is the estimation of surface virtual temperature from the model surface air temperature T_{model}^{sfc} and the model surface specific humidity SH ; and γ is the moist air lapse rate (6.5 degree/km). The spatial and temporal interpolation of GFS model data is a common procedure to many algorithms, and is implemented at the framework level outside of the aerosol algorithm.

Global land-cover type (Table 3-4): Land cover type is used select the appropriate surface reflectance relationship in the over-land AOD retrieval. The table of land cover type contains the 13-class University of Maryland (UMD) classification at 1/120° spatial resolution. Currently this table is prepared by the NOAA Algorithms Scientific Software Integration and System Transition Team (ASSISTT). It can be updated using more recent data if needed and if such data are available.

Table 3-2. Dynamic ancillary input data

Name	Type	Description	Dimension
Land/water mask	input	land/water mask data	pixel (xsize, ysize)
Cloud mask	input	cloud mask data	pixel (xsize, ysize)
Snow/Ice mask	input	snow/ice mask data	pixel (xsize, ysize)
Fire mask	input	fire mask data	pixel (xsize, ysize)
Glint mask	input	glint mask data	pixel (xsize, ysize)
Cloud shadow mask	input	cloud shadow mask data	pixel (xsize, ysize)
Heavy aerosol mask	input	heavy aerosol mask data	pixel (xsize, ysize)

Table 3-3. Non-satellite dynamic ancillary input data

Name	Type	Description	Dimension	Unit
Model ocean surface wind speed	input	Global Forecast System (GFS) 10-meter wind speed data	pixel (xsize, ysize)	m/s
Model ocean surface wind direction	input	Global Forecast System (GFS) 10-meter wind direction data (clockwise from local north)	pixel (xsize, ysize)	Degree
Model total precipitable water	input	Global Forecast System (GFS) data	pixel (xsize, ysize)	Cm

Model total ozone	input	Global Forecast System (GFS) data	pixel (xsize, ysize)	atm-cm
Model surface pressure	input	Global Forecast System (GFS) surface pressure corrected to the pixel elevation	pixel (xsize, ysize)	Mb

Table 3-4. Non-satellite static ancillary input data

Name	Type	Description	Dimension
Table of land cover type	input	Land cover type model grid product (1/120°) from year 2007 with 13-class UMD classification	(21600, 43200) (Nlat, Nlon)

3.3.3 **Derived data**

Derived data (Table 3-5) include pre-calculated LUTs, table of retrieval coefficients and thresholds, and table and gridded dataset of parameters of spectral reflectance ratios.

There are two LUTs: atmospheric and sun-glint. The atmospheric LUT contains atmospheric (Rayleigh plus aerosol) and Rayleigh reflectance, transmittance and spherical albedo in the sensor channels used for retrievals, as well as aerosol normalized extinction coefficients (ratio of the aerosol optical depth in the sensor channels to that at 0.55 μm) which are used for calculating AODs in selected sensor channels (M1-M11 for VIIRS; M3, M5, M7, M9, M10 and M11 for ABI) once the 0.55-μm AOD and aerosol model are determined. The sunglint LUT contains direct-hemispheric reflectance and spherical albedo of water. Details of the LUTs are presented in Section 3.4.5.

The table of retrieval coefficients and thresholds contain the constants used for the atmospheric reflectance calculation, internal tests and quality control. It also includes parameters of spectral reflectance ratios to calculate surface reflectance over dark land surface.

The gridded 0.1°x 0.1° dataset of parameters is used to calculate the spectral reflectance ratios over bright snow-free surface. The parameters are functions of location and scattering angle in forward and backward reflection. Details of how these parameters were derived are presented in Section 3.4.3.4.1.

Table 3-5. Sensor derived input data

Name	Type	Description	Dimension
Atmospheric LUT	Input	atmospheric reflectance ρ_{R+A} as function of channel, aerosol model, aerosol optical depth and scattering angle	(7, 4, 20, 5527)* (7, 9, 20, 5527)** (Nchn,Nmodel,Ntau,Nscaang)
		atmospheric transmittance T_{R+A} as function of channel, aerosol model, aerosol optical depth and zenith angle	(7, 4, 20, 21)* (7, 9, 20, 21)** (Nchn, Nmodel, Ntau, Nzen)
		atmospheric spherical albedo S_{R+A} as function of channel, aerosol model and aerosol optical depth	(7, 4, 20)* (7, 9, 20)** (Nchn, Nmodel, Ntau)
		Rayleigh reflectance ρ_R as function of channel and scattering angle	(11, 5527) (Nchn, Nscaang)
		Rayleigh transmittance T_R as function of channel and zenith angle	(11, 21) (Nchn, Nzen)
		Rayleigh spherical albedo S_R as function of channel	(11) (Nchn)
		normalized aerosol extinction coefficient as function of channel, aerosol model and aerosol optical depth (land only)	(11, 4, 20)* (Nchn, Nmodel, Ntau) (11, 9)** (Nchn, Nmodel)
		mass extinction coefficients for each aerosol model	(4, 20) * (Nmodel, Ntau) (9, 2) ** (Nmodel, Nparameter)
Sunglint LUT	Input	water sunglint direct-hemispheric reflectance as function of channel, aerosol model, aerosol optical depth, solar zenith angle, local zenith angle, relative azimuth angle, and surface wind speed	(7, 9, 20, 21, 21, 21, 4) (Nchn,Nmodel, Ntau,Nsolzen, Nsatzen,Nrelazi,Nwndspd)
		water sunglint spherical albedo as function of channel and wind speed	(7, 4) (Nchn,Nwndspd)
Table of coefficients and threshold	Input	coefficients used for calculating gaseous absorption, molecular and water spectral reflection, spectral relationship of dark land reflectance, valid input value ranges, internal test thresholds, and quality control thresholds	N/A

Parameters of spectral reflectance ratios over bright land	Input	Offset and slope of the linear relationship for calculating the spectral reflectance ratios (M1/M5, M2/M5 and M3/M5) as a function of scattering angle. They are derived for each 0.1°x0.1° grids where bright land present, and for backward and forward scattering separately.	(2,2,3,348432) (Offset/Slope, Back/Forward-scattering, Nwav, Ngrids)

*: over land (dimensions only for VIIRS)
**: over ocean (dimensions only for VIIRS)

3.4 Theoretical Description

This section describes the physical basis of the aerosol retrieval over ocean and land. Description of the mathematics, including all simplifications, approximations, and numerical methods, as well as the algorithm outputs is also presented.

The feasibility of aerosol retrieval from satellite-observed radiances is based on the fact that these radiances are affected by aerosols [e.g., King et al., 1978; Kaufman et al., 1997]. However, extracting information on aerosols from these radiances is far from trivial because the aerosol "signal" is combined with radiation originating from the surface and scattered by molecules, and all of these are affected by gas absorption. Therefore, the wavelength bands of satellite sensors used for AOD retrieval are selected to minimize gas and other contaminants to the aerosol signal. Moreover, observations of TOA radiation at more than one wavelength can provide more information, and thus can reduce the number of unknowns and provide better constraints [King et al., 1978; Tanré et al., 1997].

The algorithm described in this document retrieves the aerosol optical depth and the most likely aerosol model simultaneously from reflectances observed in the visible and near infrared channels. It requires modeling the radiation received by the satellite sensor. The modeling must account for the contributions and modifications of the radiation in its path from sun-to-surface-to-satellite caused by atmospheric constituents and the surface and their interaction. The atmospheric path reflectance is pre-computed by a radiative transfer model (RTM), and saved in LUTs for multiple values of the AOD, extensive geometries and multiple aerosol models.

The surface contribution is estimated based on the assumptions that the reflectance of the ocean surface can be accurately computed, and that of land can be estimated based on the prescribed spectral relationships. Therefore there are two separate algorithms, one for ocean and one for land.

Aerosol retrievals are also affected by the presence of various "contaminants" in the pixel that can prevent the retrieval or degrade the quality of retrieved AOD. These include cirrus, snow/ice, glint and shallow water etc. [e.g., Remer et al., 2005, 2006]. As a result the algorithm needs to screen out pixels unfavorable for retrieval and assign various level of quality to the retrieval.

3.4.1 **Calculation of TOA reflectance**

Calculation of TOA reflectance is based on the formulation in the Second Simulation of the Satellite Signal, 6S radiative transfer model [Vermote et al., 1997, Kotchenova et al., 2006; 2007]. According to this formulation, the spectral reflectance at satellite level (ρ_{toa}) is the sum of two components ρ_{atm} and ρ_{surf} originating, respectively, in the atmosphere and at the surface. The atmospheric contribution is due to scattering by molecules and aerosols and absorption by aerosols and gases. The surface contribution comes from the multiple reflection of radiation between the surface and the atmosphere that is subsequently attenuated by the atmosphere as it travels upward to the satellite. The reflectance measured by the satellite sensor is calculated as:

$$\rho_{toa} = \rho_{atm} + \rho_{surf} \tag{3.4.1}$$

To facilitate the calculation of atmospheric reflection with varying gaseous amount and surface pressure, gas absorption, aerosol and Rayleigh scattering are decoupled in a layered model atmosphere. In this model, radiation produced in a layer with molecular scattering, aerosol extinction, and water vapor absorption is attenuated by absorption in the top layer by ozone, O_2, CO_2, N_2O, and CH_4. Ignoring the interaction between aerosol and Rayleigh scattering, the atmospheric contribution to TOA reflectance is computed as:

$$\rho_{atm} = T^{O_3} T^{og} \left[(\rho_{R+A} - \rho_R(P_0)) T^{\frac{1}{2}H_2O} + \rho_R(P) \right] \tag{3.4.2}$$

where, T^{O_3} is the transmittance from ozone absorption; T^{og} is the transmittance from gas absorption other than ozone and water vapor; $T^{\frac{1}{2}H_2O}$ is the transmittance from half-column water vapor absorption; ρ_{R+A} is the path reflectance by aerosols and molecules at standard surface pressure; $\rho_R(P_0)$ is the Rayleigh reflectance from molecular scattering at standard surface pressure P_0; $\rho_R(P)$ is the Rayleigh reflectance from molecular scattering at the actual surface pressure P. Here, ρ_{R+A} is pre-calculated and stored in the atmospheric LUT (see Section 3.4.5.1), while transmittances from gas absorption T and Rayleigh reflectance ρ_R are analytically modeled (see Sections 3.4.6 and 3.4.7). Rayleigh reflectance ρ_R is calculated at the given local surface pressure and at standard pressure, respectively (see Section 3.4.7). Note that the channel index has been dropped from the notation for convenience. Because the chemical composition and size distribution of aerosols over water and land are generally different, different aerosol models are used in calculating ρ_{atm} over water and land. Details of these models are shown in Sections 3.4.2.2 and 3.4.3.2.

Calculation of the surface contribution ρ_{surf} is formulated differently for water and land. Detailed description of surface contribution over water is presented in Section 3.4.2.3. The preparation of land surface spectral relationship is described in Section 3.4.3.3.1 for dark land surface and Section 3.4.3.4.1 for bright land surface, respectively.

3.4.2 Physical and mathematical description for aerosol optical depth retrieval over ocean

3.4.2.1 Strategy

The algorithm for aerosol retrieval over ocean (and inland water) is based on the MODIS heritage [Tanré et al., 1997; Remer et al., 2005]. It is assumed that the surface reflectance of water can be modeled with sufficient accuracy as shown by Cox and Munk [1954] and Koepke [1984]. Therefore, the essence of the multi-channel aerosol algorithm over water is the simultaneous retrieval of optical depth and aerosol model by matching calculated and observed TOA reflectances in selected sensor channels. The contribution of aerosol to the TOA reflectance is approximated by a linear combination of two aerosol modes corresponding to a fine and a coarse mode of the size distribution with a fine mode weight [e.g. Tanré et al., 1997]. Since an exact match of TOA reflectance in all selected channels is nearly impossible, the algorithm uses channel M7 (0.86μm) as the principal channel, where the aerosol optical depth at 550 nm (τ_{550}) and fine-mode weight (η) retrieval is performed to match the observed TOA reflectance. The 0.86-μm channel is chosen because of its negligible underwater reflectance, while the contributions from the fine and coarse mode aerosols are still significant. A residual constructed from the difference between calculated and observed reflectances in other channels is used to measure the degree of match. The minimum residual is considered the 'best' match. The process of checking for the minimum residual is repeated for the various combinations of AOD and η and the solution that gives the minimum residual is chosen as the final result. AOD at other wavelengths is determined by using the spectral dependence of aerosol optical properties unique to that aerosol model, which is included in the pre-calculated LUT.

The atmospheric reflectance ρ_{atm} is calculated from Eq. 3.4.2 using the aerosol models described in Section 3.4.2.2 below.

The surface contribution ρ_{surf} including contributions from water leaving radiation, diffuse reflection, whitecap and sun glint direct reflection, and the atmosphere-surface coupling are explicitly calculated in the algorithm. Dependence of ocean surface reflectance on surface wind is incorporated, which can be significant at mid-high latitudes where relatively large wind speed dominates. Details are provided in Section 3.4.2.3.

3.4.2.2 Aerosol models

Over ocean, the aerosol model is represented by a combination of fine-mode and coarse mode aerosols. Four fine-mode and five coarse-mode models have been adopted from MODIS [Remer et al., 2006]. The size distribution of these aerosols is assumed to be log-normal:

$$\frac{dN(r)}{d\ln r} = \sum_{i=1}^{2} \frac{N_0}{\sqrt{2\pi}\ln\sigma_{g,i}} exp\left[-\frac{(\ln r - \ln r_{g,i})^2}{2(\ln\sigma_{g,i})^2}\right] \qquad (3.4.3)$$

where $N(r)$ is the number density corresponding to particles of radii within (r, r+dr), $r_{g,i}$ is the median radius, and $\sigma_{g,i}$ is the associated standard deviation. The microphysical properties of the models are summarized in Table 3-6, which lists the complex refractive index, number median (r_g), standard deviation (σ_g), and the effective radius (r_{eff}). Using the relevant parameters in Table 3-6 as input to the Mie computer code in the 6S radiative transfer model (RTM) [Kotchenova et al., 2006; 2007] the optical properties of aerosols are calculated for the particle radius range of 0.05 to 15.0 μm. Figure 3-2 shows the resulting optical properties: phase functions at 0.55 μm, normalized extinction coefficients, single scattering albedos and asymmetry parameters of these models.

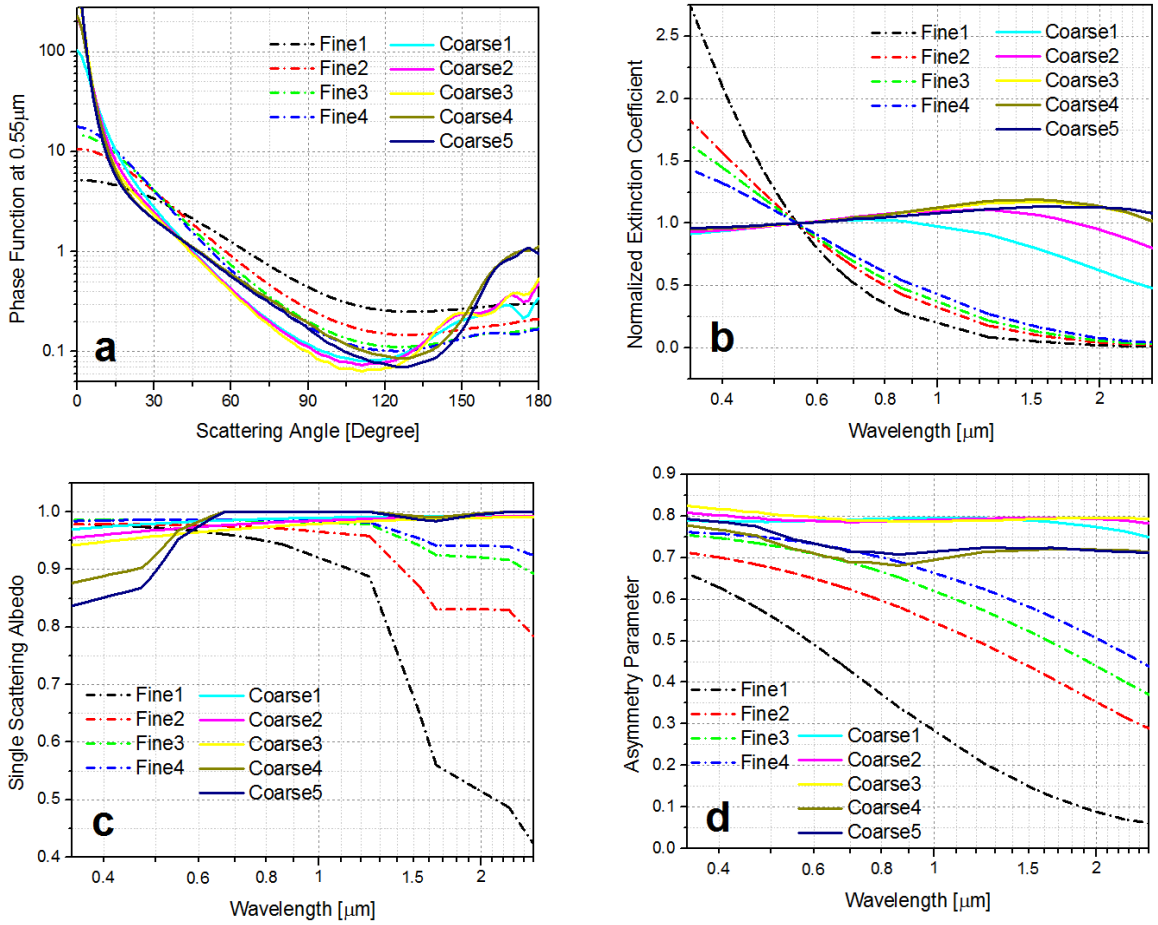

Figure 3-2. Optical properties of the candidate maritime aerosol models (four fine modes and five coarse modes): (a) phase function at 0.55μm, (b) normalized extinction coefficient (spectral extinction coefficient normalized to that at 0.55μm), (c) single scattering albedo, and (d) asymmetry parameter.

Table 3-6. Microphysical properties of oceanic aerosols used in the algorithm (fine modes: F1-F4; coarse modes: C1-C5; refractive indices, number median r_g, standard deviation σ_g, and effective radius r_{eff}).

Properties		F1	F2	F3	F4	C1	C2	C3	C4	C5
Refractive index	M1 (0.412μm)	1.45-0.0035i	1.45-0.0035i	1.40-0.0020i	1.40-0.0020i	1.35-0.0010i	1.35-0.0010i	1.35-0.0010i	1.53-0.0030i	1.53-0.0030i
	M2 (0.445μm)	1.45-0.0035i	1.45-0.0035i	1.40-0.0020i	1.40-0.0020i	1.35-0.0010i	1.35-0.0010i	1.35-0.0010i	1.53-0.0030i	1.53-0.0030i
	M3 (0.488μm)	1.45-0.0035i	1.45-0.0035i	1.40-0.0020i	1.40-0.0020i	1.35-0.0010i	1.35-0.0010i	1.35-0.0010i	1.53-0.0026i	1.53-0.0026i
	M4 (0.555μm)	1.45-0.0035i	1.45-0.0035i	1.40-0.0020i	1.40-0.0020i	1.35-0.0010i	1.35-0.0010i	1.35-0.0010i	1.53-0.0010i	1.53-0.0010i
	M5 (0.672μm)	1.45-0.0035i	1.45-0.0035i	1.40-0.0020i	1.40-0.0020i	1.35-0.0010i	1.35-0.0010i	1.35-0.0010i	1.53-0.0000i	1.53-0.0000i
	M6 (0.746μm)	1.45-0.0035i	1.45-0.0035i	1.40-0.0020i	1.40-0.0020i	1.35-0.0010i	1.35-0.0010i	1.35-0.0010i	1.53-0.0000i	1.53-0.0000i
	M7 (0.865μm)	1.45-0.0035i	1.45-0.0035i	1.40-0.0020i	1.40-0.0020i	1.35-0.0010i	1.35-0.0010i	1.35-0.0010i	1.53-0.0000i	1.53-0.0000i
	M8 (1.240μm)	1.45-0.0035i	1.45-0.0035i	1.40-0.0020i	1.40-0.0020i	1.35-0.0010i	1.35-0.0010i	1.35-0.0010i	1.53-0.0000i	1.53-0.0000i
	M9 (1.378μm)	1.44-0.0057i	1.44-0.0057i	1.40-0.0030i	1.40-0.0030i	1.35-0.0010i	1.35-0.0010i	1.35-0.0010i	1.46-0.0003i	1.46-0.0003i
	M10 (1.610μm)	1.43-0.0093i	1.43-0.0093i	1.39-0.0047i	1.39-0.0047i	1.35-0.0010i	1.35-0.0010i	1.35-0.0010i	1.46-0.0009i	1.46-0.0009i
	M11(2.250μm)	1.40-0.0050i	1.40-0.0050i	1.36-0.0030i	1.36-0.0030i	1.35-0.0010i	1.35-0.0010i	1.35-0.0010i	1.46-0.0000i	1.46-0.0000i
r_g		0.07	0.06	0.08	0.10	0.40	0.60	0.80	0.60	0.50
σ_g		1.49182	1.82212	1.82212	1.82212	1.82212	1.82212	1.82212	1.82212	2.2255
r_{eff}		0.10	0.15	0.20	0.25	0.98	1.48	1.98	1.48	2.50

3.4.2.3 **Calculation of ocean surface reflectance**

The reflectance of ocean/water surface is modeled as the sum of bi-directional sun-glint, Lambertian dark underwater and whitecap reflections. The calculation of each of these reflection terms contains wavelength-specific coefficients. These coefficients are derived for the visible-to-near-infrared channels using the 6S RTM, where the sunglint bi-directional reflectance distribution function (BRDF) is calculated from the Cox and Munk model [Cox and Munk, 1954].

The combined underwater and whitecap reflectance ρ_{w+wc} is calculated as

$$\rho_{w+wc} = (1 - \rho_{wc})\rho_w + \rho_{wc} \quad (3.4.4)$$

$$\rho_{wc} = \rho_{wc-eff} * 2.95 * 10^{-6}[ws]^{3.52} \quad (3.4.5)$$

where ρ_w and ρ_{wc} are reflectances from underwater and whitecap respectively, ws is the wind speed in m s^{-1} with a upper limit of 25 m/s. ρ_{wc} is the product of an effective whitecap reflectance ρ_{wc-eff} and whitecap coverage [Koepke, 1984]. For simplicity, chlorophyll concentration is fixed at 0.4 mg m^{-3}. The dependence of underwater reflectance on wind speed is week, and the wind-speed dependence of whitecap reflectance is accounted for by the wind-speed dependent whitecap coverage in Eq. (3.4.5). Table 3-7 contains the channel-dependent constants for ρ_w and ρ_{wc-eff}.

Table 3-7. Whitecap effective reflectance ρ_{wc-eff} and underwater reflectance ρ_w.*

Channel (wavelength: µm)	ρ_{wc-eff}	ρ_w
M4 (0.555)	0.2200	0.0071
M5 (0.672)	0.2200	0.0009
M6 (0.746)	0.2177	0.0
M7 (0.862)	0.2118	0.0
M8 (1.240)	0.1670	0.0
M10 (1.610)	0.1005	0.0
M11 (2.250)	0.0625	0.0

* Constants for NOAA-20 VIIRS are listed in Table B-1; Table C-1 for ABI

Calculation of sunglint directional reflectance ρ_{sgt} is adopted from the corresponding 6S subroutine [Vermote et al., 1997; Cox and Munk, 1954]. It requires inputs of wind speed ws (in m s^{-1}), index of refraction (n_r, n_i) and extinction coefficient of sea water, solar zenith angle θ_s, view zenith angle θ_v, and sun, view and wind azimuth angles ϕ_s, ϕ_v, ϕ_w (measured clockwise from local North). The index of refraction (Table 3-8) and extinction coefficient of sea water are calculated from the 6S RTM assuming a constant salinity of 34.3 ppt. Details of the sunglint directional reflectance calculation are given in Appendix A.

Table 3-8. Seawater index of refraction*

Channel (wavelength: μm)	Refractive Index	
	Real Part	Imaginary Part
M4 (0.555)	1.339	2.288E-09
M5 (0.672)	1.337	2.159E-08
M6 (0.746)	1.336	1.457E-07
M7 (0.862)	1.334	3.518E-07
M8 (1.240)	1.329	3.551E-05
M10 (1.610)	1.323	8.698E-05
M11 (2.250)	1.298	4.558E-04

* Constants for NOAA-20 VIIRS are listed in Table B-2; Table C-2 for ABI

Interaction between the atmosphere and the surface reflection is accounted for as the sum of two terms in Eq. (3.4.4) corresponding to the contributions from Lambertian reflection from underwater and whitecaps, and contributions from glint reflection. The latter includes five components: (1) directional sunglint reflection without atmospheric scattering; (2) diffuse downward radiation reflected by the surface and transmitted to the sensor without scattering; (3) direct downward radiation reflected by surface and scattered back to the sensor; (4) diffuse downward radiation reflected by surface and scattered back to the sensor; and (5) radiation reflected by the surface more than once.

For efficient calculations, a look-up table (Section 3.4.5.2) for the necessary terms (e.g., $\overline{\rho_{sgt}}$, $\overline{\rho'_{sgt}}$ and $\overline{\overline{\rho_{sgt}}}$) is generated using the 6S radiative transfer model [Vermote et al., 1997]. The diffuse atmospheric transmittance is calculated by subtracting the direct transmittance from the total transmittance. The glint contribution is weighted by the foam-free fraction $(1-W)$, where W the fraction is covered with whitecap and calculated as a function of wind speed (ws), $2.95 * 10^{-6}[ws]^{3.52}$[Koepke, 1984]. All terms are calculated for the central wavelength of the channels.

$$\rho_{surf} = T^{O_3}T^{og}T^{H_2O}\left[T^{\downarrow}_{R+A}T^{\uparrow}_{R+A}\frac{\rho_{w+wc}}{1-S_{R+A}\rho_{w+wc}} + (1-W)\left(t^{dir\downarrow}_{R+A}t^{dir\uparrow}_{R+A}\rho_{sgt} + t^{dif\downarrow}_{R+A}t^{dir\uparrow}_{R+A}\overline{\rho_{sgt}} + t^{dir\downarrow}_{R+A}t^{dif\uparrow}_{R+A}\overline{\rho'_{sgt}} + t^{dif\downarrow}_{R+A}t^{dif\uparrow}_{R+A}\overline{\overline{\rho_{sgt}}} + T^{\downarrow}_{R+A}T^{\uparrow}_{R+A}\frac{S_{R+A}\left(\overline{\overline{\rho_{sgt}}}\right)^2}{1-S_{R+A}\overline{\overline{\rho_{sgt}}}}\right)\right] \quad (3.4.6)$$

$$t^{dir\downarrow}_{R+A} = e^{-\tau_{R+A}/\cos\theta_s} \quad (3.4.7)$$

$$t^{dir\uparrow}_{R+A} = e^{-\tau_{R+A}/\cos\theta_v} \quad (3.4.8)$$

$$t^{dif\downarrow}_{R+A} = T^{\downarrow}_{R+A} - t^{dir\downarrow}_{R+A} \quad (3.4.9)$$

$$t^{dif\uparrow}_{R+A} = T^{\uparrow}_{R+A} - t^{dir\uparrow}_{R+A} \quad (3.4.10)$$

$$\tau_{R+A} = \tau_A + \tau_R(P) \quad (3.4.11)$$

where, $T^{\downarrow}_{R+A}$ is the total (direct and diffuse) downward atmospheric transmission; $T^{\uparrow}_{R+A}$ is the total (direct and diffuse) upward atmospheric transmission; $t^{dir\downarrow}_{R+A}$ is the direct downward atmospheric transmission; $t^{dir\uparrow}_{R+A}$ is the direct upward atmospheric transmission; $t^{dif\downarrow}_{R+A}$ is the diffuse downward atmospheric transmission; $t^{dif\uparrow}_{R+A}$ is the diffuse upward atmospheric

transmission; S_{R+A} is the atmospheric spherical albedo; ρ_{w+wc} is the surface Lambertian reflectance from underwater and whitecaps; ρ_{sgt} is the sunglint directional reflectance; $\overline{\rho_{sgt}}$ is the normalized integral of the downward irradiance reflectance by the sunglint directional reflectance; $\overline{\rho'_{sgt}}$ is the reciprocal quantity of $\overline{\rho_{sgt}}$ for the upward coupling; $\overline{\overline{\rho_{sgt}}}$ is approximated as the sunglint spherical albedo; θ_s is the solar zenith angle; θ_v is the local zenith angle; τ_{R+A} is the total column optical depth of molecules and aerosols; $\tau_R(P)$ is the Rayleigh optical depth at local actual pressure *P*, and τ_A is the total column aerosol optical depth. Note that $\tau_R(P)$ and τ_A should use the values for the specific wavelength. $T^{\downarrow}_{R+A}$, $T^{\uparrow}_{R+A}$, and S_{R+A} are obtained from the atmospheric look-up table, and require adjustment for actual surface pressure following Eq. (3.4.31) and Eq. (3.4.32). $\overline{\rho_{sgt}}$, $\overline{\rho'_{sgt}}$, and $\overline{\overline{\rho_{sgt}}}$ are obtained from the ocean surface reflectance look-up table.

3.4.2.4 **Aerosol retrieval algorithm over ocean**

The retrieval algorithm assumes that over ocean (and inland water) the aerosol reflectance ρ^t_λ for a given τ_{550} can be approximated by a linear combination of contributions from one fine (ρ^f_λ) and one coarse (ρ^c_λ) aerosol modes with a proper fine-mode weight η [Wang and Gordon, 1994; Kaufman and Tanré, 1996],

$$\rho^t_\lambda(\tau_{550}) = \eta\rho^f_\lambda(\tau_{550}) + (1-\eta)\rho^c_\lambda(\tau_{550}) \qquad (3.4.12)$$

In the retrieval, the algorithm searches for the pair of fine and coarse modes, along with the fine mode weight (η) and corresponding τ_{550} that gives the best match between calculated and observed TOA reflectances in multiple sensor channels.

Specifically, there are two levels of iteration and selection involved. The first iteration is on the combination of candidate fine and coarse modes, which are predetermined and built into the lookup table. In the current algorithm, there are four (fine mode) by five (coarse model) combination pairs. The second iteration (searching for η for any given pair of fine and coarse aerosol modes) uses bisection (interval halving), which repeatedly divides the fine-mode weight range in half and searches for the subinterval that includes the 'best' fit η with minimum residual. Ranges of the fine mode weight, starting with the full range of 0-1, are repeatedly bisected, AODs are retrieved and residuals are calculated. Altogether ten bisection steps are performed, regardless of measurement uncertainty. The process starts with dividing the range of η between 0 and 1 into four equal subintervals with ranges of 0.00-0.25, 0.25-0.50, 0.50-0.75, and 0.75-1.00. AODs are retrieved for the five boundary values of η (0, 0.25, 0.5, 0.75 and 1), and residuals are calculated. The smallest residual is identified among the five residuals and the half-interval containing the smallest residual is selected for further processing (bisection). So, for example, if the residuals corresponding to the five starting values of η are $R_{0.0}$, $R_{0.25}$, $R_{0.5}$, $R_{0.75}$ and $R_{1.0}$, and if $R_{0.0}$ (or $R_{0.25}$) is the smallest residual then the two intervals 0.0-0.25 and 0.25-0.50 are bisected leading to another five values of η (0.0, 0.125, 0.25, 0.375, 0.5). AODs and residuals are calculated for these η values. (Note that retrievals are already performed for the η values of 0, 0.25

and 0.5 in the previous step, so in reality they need to be done only for the η values of 0.125 and 0.375.) If $R_{0.5}$ is the smallest then the middle two subintervals (0.25-0.5 and 0.5-0.75) are used. If $R_{0.75}$ (or $R_{1.0}$) is the smallest the upper two subintervals (0.5-0.75 and 0.75-1.0) are used. The process is repeated ten times and usually reaches 0.1% accuracy, and the η (and AODs) corresponding to the smallest residual is selected as the solution. If two or more residuals are identical within machine precision, the first one in the sequence is selected.

The determination of τ_{550} for any specific aerosol model (combination of fine and coarse modes with known η) is performed by matching the calculated TOA reflectance at 0.86 μm with the measurement; extrapolation is allowed but flagged for $\tau_{550} > 5$ or $\tau_{550} < 0$ when τ_{550} is outside of the AOD550 range tabulated in the LUT. The best match is determined by comparing the residuals that are calculated as the root mean squared relative differences between calculated (ρ_λ^{cal}) and observed (ρ_λ^{obs}) TOA reflectances in channels M4, M5, M6 (if unsaturated), M8, M10 and M11 for VIIRS, or M5, M10 and M11 for ABI:

$$residual = \sqrt{\frac{\sum_{\lambda=1}^{n}\left(\frac{\rho_\lambda^{cal}-\rho_\lambda^{obs}}{\rho_\lambda^{cal}-\rho_\lambda^{ray}+0.01}\right)^2}{n}} \qquad (3.4.13)$$

where n = 6 (or 5 if M6 reflectance is saturated), the number of channels used for calculating the residual for VIIRS (n = 3 for ABI), and ρ_λ^{cal} corresponds to ρ_{toa} in Eq.(3.4.1) , and ρ_λ^{ray} is the Rayleigh reflectance corresponds to ρ_R in Eq.(3.4.26) (Section 3.4.7).

Once the solution of aerosol model and corresponding τ_{550} are determined, AODs in all sensor channels are calculated by the unique spectral dependence of the aerosol extinction coefficient for the retrieved combination of fine and coarse mode aerosol models and fine mode weight η. That is, the optical depth at wavelength λ is calculated as $\tau_{\lambda,fine/coarse} = n_{ext,\lambda,fine/coarse} * \tau_{550}$ for the retrieved fine and coarse mode aerosol models, respectively, where $n_{ext,\lambda}$ is the normalized extinction coefficient at wavelength λ included in the LUT for each fine and coarse mode aerosol model. The final AOD at wavelength λ is calculated as $\tau_\lambda = \tau_{\lambda,fine}\eta + \tau_{\lambda,coarse}(1-\eta)$.

The schematic illustration of the over-ocean retrieval algorithm is shown in Figure 3-3.

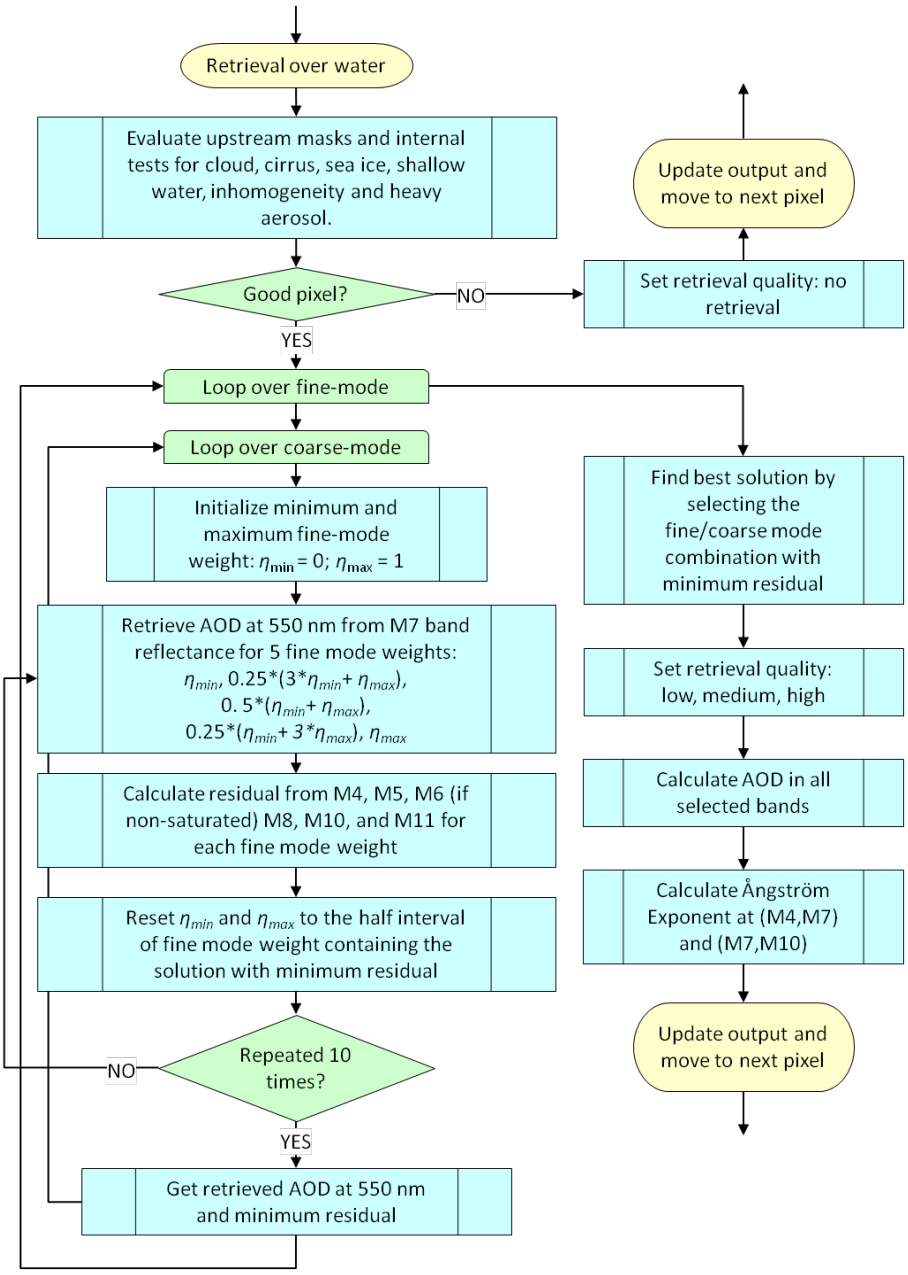

Figure 3-3. Flowchart of AOD and APSP retrieval over water.

3.4.2.5 **Internal Tests and Quality Control**

Producing a high quality global AOD product also requires an effective process to screen out contaminated pixels and identify low quality retrievals. In addition to the cloud, snow/ice, glint and land/water masks generated by upstream algorithms, several simple internal tests are also implemented to identify unfavorable retrieval conditions:

1) Internal cloud test: a brightness test $\rho_{M7}^{\text{obs-ray}} > 0.3$ is used to screen out thick cloud, where $\rho_{\lambda}^{\text{obs-ray}}$ is the satellite-measured reflectance corrected for Rayleigh scattering and gaseous absorption;

2) Internal heavy aerosol test: potential heavy aerosol is detected if $f''(\rho_{M2}^{obs-ray}) < -0.005$ (-0.05 for NOAA20 due to difference in the channel spectral response function) and $rdsi > 0.4$, here $f''(\rho_{M2}^{obs-ray})$ is a parameter proportional to the second spectral derivative of the Rayleigh-scattering-corrected TOA reflectance at channel M2 calculated as: $f''(\rho_{M2}^{obs-ray}) = 4.3\rho_{M1}^{obs-ray} - 7.6\rho_{M2}^{obs-ray} + 3.3\rho_{M3}^{obs-ray}$, and $rdsi$ is reflectance spectral difference index calculated as $rdsi = (\frac{\frac{\rho_{M3}^{obs} - \rho_{M11}^{obs}}{\rho_{M3}^{obs} + \rho_{M11}^{obs}}}{\rho_{M3}^{obs}})^2$. This test is based on the observation that usually the Rayleigh-scattering-corrected TOA reflectance is concave downward at channel M2 for heavy smoke and dust, which is caused by the enhanced absorption at M1 where the background Rayleigh scattering is much stronger than M2. The test on $rdsi$ is used to avoid the misidentification of the cloud, whose spectral contrast of reflectance is relatively small, as heavy aerosol. This heavy aerosol test is not available for ABI due to lack of deep-blue channels.

   An additional heavy aerosol test is included based on the VIIRS cloud mask (VCM) algorithm [JPSS, 2014]: if the input cloud mask is cloudy, but passes the internal cloud and cirrus test, then the pixel would be considered as potential heavy aerosol if the 3x3 TOA reflectance standard deviation at channel M11 (internal inhomogeneity test) is less than 0.002.

3) Internal cirrus test: cirrus is identified if $\rho_{M9}^{\text{TOA}} > 0.018$. To avoid the mis-identification of smoke plumes as cirrus, this test (and the thin cirrus test) is bypassed if heavy aerosol is detected by the internal test.

4) Internal thin cirrus test: Following the scheme of the VIIRS cloud mask (VCM) algorithm [JPSS, 2014], thin cirrus is identified if $\rho_{M9}^{obs} > TC$, where *TC* is the thin cirrus threshold calculated as $TC = a + b\frac{TPW}{\mu_v}$. Here μ_v is the cosine of viewing zenith angle (up to 71°) and the maximum value for $\frac{TPW}{\mu_v}$ is 16cm; (a, b) are constants specified as (0.0125, -3.597e-4).

5) Internal inhomogeneity test: spatially inhomogeneous pixel is identified if the 3 by 3 standard deviation of ρ_{M11}^{TOA} (σ_{M11}^{3x3}) is larger than 0.008.

6) Internal sea ice test: sea ice is detected if $\frac{\rho_{M4}^{obs-ray} - \rho_{M10}^{obs-ray}}{\rho_{M4}^{obs-ray} + \rho_{M10}^{obs-ray}} > 0.4$ and $\rho_{M4}^{obs-ray} > 0.1$ and $\rho_{M7}^{obs-ray} > 0.05$ and the brightness temperature at M15 is lower than 275K (for ABI, M5 replaces M4 in the test).

7) Internal shallow water test: retrieval over shallow water is avoided if $f''(\rho_{M5}^{\text{obs-ray}}) < -0.07$ and $\rho_{M1}^{\text{obs-ray}} > 0.02$. This test is based on the observation

that the Rayleigh-scattering-corrected TOA reflectance is usually concave downward at the channel M5 for shallow water. Here $f''(\rho_{M5}^{TOA\text{-}ray})$ is a parameter proportional to the second derivative of the spectral reflectance at channel M5, and calculate as $f''(\rho_{M5}^{obs-ray}) = 1.93\rho_{M4}^{obs-ray} - 3.1\rho_{M5}^{obs-ray} + 1.17\rho_{M7}^{obs-ray}$. For ABI, the test is $f''(\rho_{M5}^{obs\text{-}ray}) < -0.1$ and $\rho_{M5}^{obs-ray} > 0.02$, where $f''(\rho_{M5}^{obs-ray}) = 2.2\rho_{M3}^{obs-ray} - 3.9\rho_{M5}^{obs-ray} + 1.7\rho_{M7}^{obs-ray}$.

8) Internal glint test: retrieval over sunglint region is avoided if the glint angle is less than 36°. The glint angle is defined as the angle between the observing vector and the specular reflection direction, and calculated as $\vartheta_g = \cos^{-1}(\cos\theta_s \cos\theta_v - \sin\theta_s \sin\theta_v \cos\phi)$, where ϕ is the relative azimuth angle. This test is performed only when the input sunglint mask is not available.

Based on the input masks, internal tests as well as the retrieval residual, retrievals are categorized into four quality levels: no retrieval; low; medium; and high quality. The criteria used for assigning quality are listed in Table 3-9. In general, high quality retrievals are recommended for quantitative applications due to their better overall performance; however, the lower quality retrievals also have their merit for qualitative examination of local episodic events due to their greater spatial coverage.

Table 3-9 Criteria used for assigning retrieval quality over water.

Quality Level	Criteria
No Retrieval	1) Cloudy: external cloud mask is probably or confident cloudy and any internal cloud, cirrus or inhomogeneity test fails; 2) Sea ice (external mask or internal test); 3) Shallow water (internal test); 4) Sunglint (external mask or internal test) 5) Retrieval failed due to missing inputs or numeric error.
Low	1) Air mass (sum of inverse cosine solar and viewing zenith angles) > 5 (6 for ABI); 2) Fail internal cloud test (but external cloud mask is clear); 3) Fail internal cirrus test (but external cloud mask is clear); 4) External cloud mask is cloudy (but pass internal tests, and not heavy aerosol); 5) $\sigma_{M11}^{3x3} > 0.008$ ($\sigma_{M11}^{3x3} > 0.01$ for ABI) 6) Retrieval residual > 0.3
Medium	1) Cloud shadow (external mask); 2) Thin cirrus (internal test); 3) Adjacent to cloudy pixel; 4) Adjacent to snow pixel (within 3-pixel distance) 5) $\sigma_{M11}^{3x3} > 0.002$; 6) Retrieval residual > 0.25 7) Retrieved τ_{550} is out of range (-0.05, 5.0)
High	Remaining retrievals

3.4.3 Physical and mathematical description for aerosol optical depth retrieval over land

3.4.3.1 Strategy

Unlike water, land surface properties exhibit great variability and complexity, which prevent reliable modeling of the spectral reflectance. As a consequence, surface reflectance becomes an inherent unknown along with aerosol properties in the aerosol retrieval over land, and thus it must also be retrieved. Kaufman et al. [1997] observed that over vegetated and dark soil surfaces, the surface reflectance in the blue, red and shortwave-infrared (SWIR) wavelengths (channels M3, M5 and M11) are well-correlated; and this relationship can be established a priori. One way to use these relationships in aerosol retrieval is to estimate the surface reflectance in one band (say SWIR) where most aerosols are transparent and then predict the surface reflectances in the other two bands; thus reducing the number of unknowns by two. This approach was employed in an early version of the MODIS aerosol algorithm [Kaufman et al., 1997]. Another way to use the relationships is to observe that in the presence of aerosols the ratios of top-of-atmosphere (TOA) reflectances in the above channels are usually different from their surface values. AOD is then retrieved by computing, in a radiative transfer model, the channel reflectances for increasing amounts of AOD and comparing the ratios of computed reflectances to satellite-observed ratios. The AOD that produces a match is then taken as the retrieved value.

The algorithm applied to retrieve AOD over dark land surface belongs to the so-called "dark-target" class of algorithms. It adopts the methods used in the NPP/VIIRS [Vermote et al., 2008; Jackson et al., 2013], MODIS [Remer et al., 2005, 2006; Levy et al., 2007b] and the ABI [Laszlo et al, 2008; GOES-R ABI ATBD for AOD, 2012, 2018; Kondragunta et al., 2020] aerosol optical depth algorithms. The algorithm uses M3 as the primary channel to retrieve AOD because of the strong aerosol signal, darkness of surface, and the spectral adjacency to the nominal wavelength (0.55μm) where AOD is reported. Though surface reflectance is even weaker at shorter wavelengths (M1 and M2), the stronger Rayleigh scattering (molecular optical depth is 0.32 and 0.23) demands an accurate simulation of the interaction between aerosol and molecules, which could be challenging since the actual vertical profile of aerosol is not known. Also, the longer distance to the nominal wavelength requires a precise description of spectral variation of AOD in the prescribed aerosol model. At longer wavelengths (M5 and M11), the decrease of atmospheric scattering and increase of surface reflectance is better suited for retrieving surface reflectance than AOD. Therefore, the basic process for this multi-spectral algorithm is: (1) get the surface reflectance from M5 or M11, (2) retrieve AOD from M3 channel, and (3) select aerosol model based on the spectral shape at the remaining channels.

Depending on which channel (M5, or M11) is used to predict the M3 surface reflectance different algorithms can be designed. The MODIS algorithm [Remer et al., 2005, 2006; Levy et al., 2007b] uses the SWIR (M11) channel as the predictor, while the NPP/VIIRS

algorithm [Jackson et al., 2013] employs the red (M5) channel for this task. The current algorithm adopts both approaches. Section 3.4.3.3.2 describes how this is accomplished.

Dark target pixels, needed for the application of the surface reflectance relationships, are identified based on a threshold test which requires that the TOA reflectance observed in channel M11 (2.25 μm) should not be greater than 0.25. The relationships between the M1, M2, M3, M5 and M11 surface reflectances are presented in Section 3.4.3.3.1.

Over bright land, contribution of the surface ρ_{surf} can be comparable or even larger than the atmospheric path reflectance ρ_{atm}, and so aerosol retrieval for such bright surface is challenging. Moreover, the physical basis that connects surface reflectances in the red, blue and SWIR channels for dark land does not apply for bright land due to the lack of vegetation and water content. If, however, ratios of surface reflectances in selected channels can be established from "observations" for each bright land areas, and if the ratios of TOA reflectances in these channels differ from the surface values in the presence of aerosols, retrieval of AOD can be attempted. The current algorithm implements such an approach following Zhang et al., 2016. It relies on a surface reflectance ratio database prepared at 0.1° spatial resolution. The retrievals use the shorter wavelength channels (M1, M2, M3 and M5) owing to the relatively low surface reflectance in these bands.

3.4.3.2 **Aerosol models**

Four typical aerosol models, as described by Levy et al. [2007a] for MODIS collection C005, are adopted in the current algorithm. These represent generic, dust, smoke and urban aerosols. A bimodal lognormal distribution is used to describe each aerosol size distribution:

$$\frac{dV(r)}{d\ln r} = \sum_{i=1}^{2} \frac{C_{V,i}}{\sqrt{2\pi}\sigma_i} exp\left[-\frac{(\ln r - \ln r_{V,i})^2}{2\sigma_i^2}\right] \qquad (3.4.14)$$

where $V(r)$ is the volume corresponding to particles of radii within (r, r+dr). $C_{V,i}$ denotes the particle volume concentration, $r_{V,i}$ is the median radius, and σ_i is the associated standard deviation. Microphysical properties of the candidate aerosol models are listed below in Table 3-10. Aerosol radiative properties of the generic, urban and smoke aerosol models are calculated using the MIE code built in the 6S RTM assuming spherical particles, and using the spheroid kernel software of Dubovik [2006] for dust model to account for the non-spherical shape. The pre-calculated aerosol radiative properties are incorporated in the radiative transfer calculation for atmospheric reflectance, transmittance and spherical albedo stored in a lookup table. Note that the generic, urban, and smoke models are dominated by fine mode, whereas the dust model is coarse-mode dominated. As the size distributions of the three fine-dominated models are similar, the main differences are in their absorption properties and refractive indices. Figure 3-4 shows the optical parameters (phase function, normalized extinction coefficient, single scattering albedo and asymmetry parameter) of the candidate aerosol models for AOD at 0.55 μm of 0.3.

Table 3-10. Microphysical properties of land aerosols

Aerosol Model	Mode	Volume median radius r_V	Standard Deviation σ	Volume Concentration C_V (μm³/μm²)	Complex Refractive Index
Generic	Fine	0.145+ 0.0203 $\tau^{\&}$	0.3738+ 0.1365 τ	0.1642 $\tau^{0.7747}$	1.43 - (0.008-0.002τ)i$^{\#}$
	Coarse	3.1007+ 0.3364 τ	0.7292+ 0.098 τ	0.1482 $\tau^{0.6846}$	
Urban	Fine	0.1604+ 0.0434 τ	0.3642+ 0.1529 τ	0.1718 $\tau^{0.8213}$	1.42 - (0.007-0.0015τ)i
	Coarse	3.3252+ 0.1411 τ	0.7595+ 0.1638 τ	0.0934 $\tau^{0.6394}$	
Smoke	Fine	0.1335+ 0.0096 τ	0.3834+ 0.0794 τ	0.1748 $\tau^{0.8914}$	1.51 - 0.02i
	Coarse	3.4479+ 0.9489 τ	0.7433+ 0.0409 τ	0.1043 $\tau^{0.6824}$	
Dust	Fine	0.1416 $\tau^{-0.0519}$	0.7561 $\tau^{0.148}$	0.087 $\tau^{1.026}$	$(1.48\tau^{-0.021})$ – (0.0025 $\tau^{0.132}$)i at 0.47μm* $(1.48\tau^{-0.021})$ –0.002i at 0.55μm $(1.48\tau^{-0.021})$ – (0.0018 $\tau^{-0.08}$)i at 0.66μm $(1.46\tau^{-0.040})$ – (0.0018 $\tau^{-0.30}$)i at 2.12μm
	Coarse	2.20	0.554 $\tau^{-0.0519}$	0.6786 $\tau^{1.0569}$	

$^{\&}$ Aerosol optical depth (τ) is the spectral value at 0.55μm. The properties (r_v, σ and refractive index) of smoke and generic aerosol model are defined for τ<2.0, and τ=2.0 is used in calculation when τ>2.0. Likewise, parameters of urban and dust aerosol are defined for τ<1.0, and τ=1.0 is applied for higher τ.

***** Refractive index at other shortwave wavelength is estimated by spectral interpolation. No extrapolation is performed if wavelength is shorter than 0.47 μm or longer than 2.12 μm.

$^{\#}$ For NOAA-20, the imaginary part of the refractive index of the generic model was changed to -(0.008+0.002τ) based on the personal communication with MODIS dark-target aerosol team.

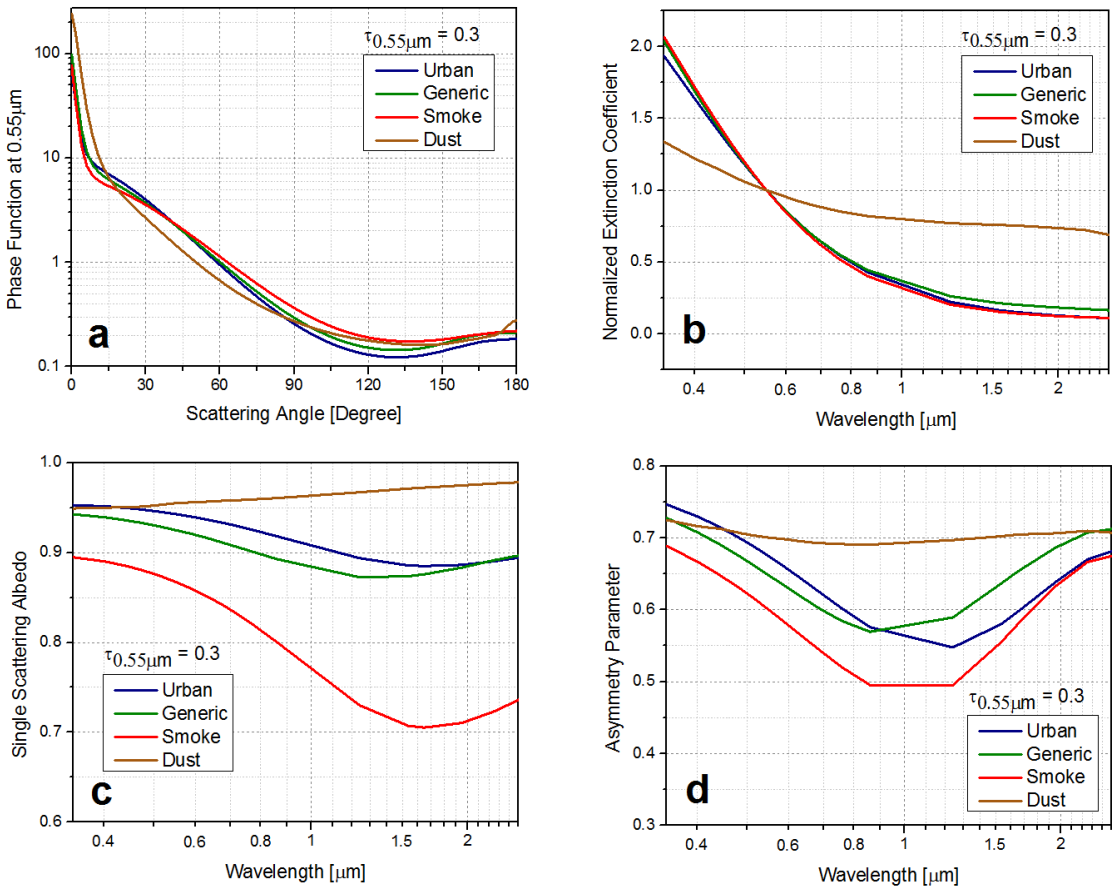

Figure 3-4. Optical parameters of the candidate land aerosol models for $\tau_{0.55\mu m}$=0.3: (a) phase function at 0.55μm, (b) normalized extinction coefficient (to 0.55μm), (c) single scattering albedo, and (d) asymmetry parameter.

3.4.3.3 **Retrieval over dark land surface**

3.4.3.3.1 Retrieval of dark land surface reflectance

For the dark target pixels ($\rho_{2.25\mu m} \leq 0.25$) a set of linear relationships is used to estimate the surface reflectance in channels M1, M2, M3, M5 and M11. The physical reason for the spectral relationship is the simultaneous carotenoid, chlorophyll and liquid water absorption at blue, red and SWIR wavelengths associated with healthy vegetation [Kaufman and Remer, 1994].

The surface reflectance relationship is established based on collocated satellite and AERONET measurements. Clear sky satellite measurements are collected over global AERONET stations for the period of 10/28/2012 – 07/05/2018. The criteria for selecting eligible pixels are: (1) separation between the pixel and station is less than 5 km horizontally and 100 meter vertically to ensure geographical adjacency, (2) average and

standard deviation of AERONET τ_{550} within one hour centered on the satellite observation time is less than 0.2 to ensure low aerosol amount, (3) at least 2 AERONET measurements within one hour and 200 VIIRS clear-sky pixels within a circle of 27.5 km radius to ensure clear-sky condition, (4) AERONET Ångström Exponent (AE) calculated for 0.48 vs. 0.67μm is smaller than 0.6 or larger than 1.6 to avoid ambiguous aerosol model identification, and (5) the TOA M11 reflectance is less than 0.25 to ensure the dark surface. Atmospheric correction is performed on the selected pixels with the AERONET τ_{550} and dust (AE < 0.6) or generic (AE > 1.6) aerosol model with 6S-V1.1 RTM, and the retrieved surface reflectance are used as a training dataset to establish the spectral relationship between four pair of channels, namely, M5 vs. M11, M3 vs. M5, M2 vs. M3, M1 vs. M3, and M11 vs. M5. The offset and slope of the linear relationships are parameterized as a linear function of $NDVI_{SWIR}$ (N), the M5/M4 (0.672/0.555 μm) TOA reflectance ratio (R), and the glint angle in degree (G), therefore, the spectral surface reflectance (ρ^{sfc}) can be related by the formula:

$$y = (c_0 + c_1 N + c_2 R + c_3 G) + (c_4 + c_5 N + c_6 R + c_7 G) * x \qquad (3.4.15)$$

The dependent variable y is ρ_{M5}^{sfc}, ρ_{M11}^{sfc}, ρ_{M3}^{sfc}, ρ_{M2}^{sfc}, and ρ_{M15}^{sfc}, and the independent variable x is ρ_{M11}^{sfc}, ρ_{M5}^{sfc}, ρ_{M5}^{sfc}, ρ_{M3}^{sfc}, and ρ_{M3}^{sfc}, respectively. The three parameters (N, R, G) are used to represent the scene "greenness" and "redness", and the angular distance from the specular reflection, where the $NDVI_{SWIR}$ is defined as:

$$NDVI_{SWIR} = \frac{\rho_{M8}^{obs} - \rho_{M11}^{obs}}{\rho_{M8}^{obs} + \rho_{M11}^{obs}} \qquad (3.4.16)$$

For ABI, the M8 channel is replaced with M7 for the NDVI calculation. Using the same formula, spectral relationship is further refined based on the land cover type. The training pixels are grouped into six categories: forest, wooded, shrubland, cropland/grass, urban, and barren surface using the land cover map that is in 1/120 degree resolution, and the linear fitting is performed for each category to derive the coefficients c_0 to c_7. Table 3-11 lists the fitting results as well as the corresponding RMSE, R^2 and percentage error. Compared with the general fitting with all training data, applying a dedicated relationship to each individual surface group may further reduce the uncertainty in the spectral relationship. Therefore, in this algorithm, the land cover type is identified for each pixel, and the corresponding spectral relationship, if available, is used instead of the general relationship.

Table 3-11. VIIRS coefficients in the spectral surface reflectance relationship for various categories of dark land cover types.

Channels	c_0	c_1	c_2	c_3	c_4	c_5	c_6	c_7	RMSE	R^2	%Error
Forest, land cover type 1-5, #: 324,838 (8.31%)											
M5 vs. M11	-0.041	-0.014	0.065	4.3E-05	-0.045	0.18	0.30	61.3E-03	0.0084	0.88	10.97
M3 vs. M5	0.014	1.6E-04	-0.034	2.4E-05	1.30	-0.17	-0.33	2.7 E-03	0.0044	0.91	10.85
M2 vs. M3	-0.0041	0.0042	-0.00006	-3.9E-05	1.21	-0.0058	-0.22	-7.7E-04	0.0022	0.97	6.67
M1 vs. M3	-0.009	0.011	0.0015	-4.7E-05	1.45	0.045	-0.48	-1.5E-03	0.0040	0.90	12.86
M11 vs. M5	0.12	-0.10	-0.039	-5.6E-05	0.96	0.13	0.053	1.6E-03	0.015	0.84	13.34
Woodland and woodedgrass, land cover type 6 and 7, #:783,044 (20.03%)											
M5 vs. M11	-0.012	-0.026	0.063	3.1E-05	-0.11	0.22	0.30	1.6E-03	0.012	0.86	11.45
M3 vs. M5	0.013	0.0026	-0.031	-2.7E-05	1.52	-0.37	-0.56	-1.7E-03	0.0055	0.91	9.98
M2 vs. M3	-0.0041	0.0055	-0.0017	-4.2E-05	1.33	-0.14	-0.30	-6.8E-04	0.0030	0.97	5.81
M1 vs. M3	-0.0008	0.008	-0.008	-4.5E-05	1.46	-0.13	-0.44	-1.3E-03	0.0051	0.89	11.78
M11 vs. M5	0.096	-0.089	-0.0084	4.6E-05	0.72	0.073	0.18	5.8E-04	0.021	0.81	13.42
Closed/open shrublands, land cover type 8 and 9, #:664,434 (16.99%)											
M5 vs. M11	-0.019	0.030	0.21	1.8E-04	1.13	-0.18	-0.62	1.03E-03	0.021	0.73	11.85
M3 vs. M5	0.051	-0.025	-0.060	-1.1E-04	1.33	-0.062	-0.43	-1.3E-03	0.0074	0.91	7.11
M2 vs. M3	0.0021	-0.0003	-0.0034	-5.4E-05	1.14	-0.053	-0.18	-4.5E-04	0.0035	0.97	3.87
M1 vs. M3	0.0082	0.0001	-0.0084	-4.6E-05	1.12	-0.062	-0.24	-9.8E-04	0.0066	0.89	8.20
M11 vs. M5	-0.093	0.064	0.14	6.2E-04	1.0	-1.1	-0.11	-1.6E-03	0.024	0.77	10.63
Grasses and cropland, land cover type 10 and 11, #:1,401,970 (35.86%)											
M5 vs. M11	0.023	-0.068	0.054	-2.2E-05	-0.39	0.43	0.47	2.4E-03	0.018	0.80	12.22
M3 vs. M5	0.016	0.0029	-0.033	-5.8E-05	1.51	-0.40	-0.55	-1.3E-03	0.0063	0.93	8.28
M2 vs. M3	-0.0045	0.0039	-0.001	-4.4E-05	1.39	-0.19	-0.35	-7.1E-04	0.0031	0.98	4.59
M1 vs. M3	0.0033	0.0004	-0.0092	-4.0E-05	1.48	-0.19	-0.47	-1.4E-03	0.0056	0.91	9.75
M11 vs. M5	0.010	-0.021	0.085	2.0E-04	0.76	-0.43	-0.035	3.9E-04	0.024	0.75	12.87
Urban, land cover type 13, #:655,612 (16.77%)											
M5 vs. M11	-0.061	-0.0057	0.094	8.7E-05	-0.02	0.95	0.48	1.8E-03	0.017	0.86	11.45
M3 vs. M5	0.019	-0.0032	-0.032	-1.2E-04	1.56	-0. 24	-0. 61	-9.6E-04	0.0058	0.96	6.24
M2 vs. M3	0.0083	-0.0052	-0.0071	-6.1E-05	1.08	-0.027	-0.14	-2.6E-04	0.0030	0.99	3.49
M1 vs. M3	0.019	-0.009	-0.013	-8.1E-05	1.11	-0.065	-0.27	-5.3E-04	0.0053	0.95	7.40
M11 vs. M5	-0.076	0.075	-0.11	3.5E-04	0.94	-0.61	-0.041	-1.7E-03	0.018	0.83	10.76
Barren, land cover type 12, #:33,730 (0.86%)											
M5 vs. M11	-0.15	0.062	0.18	-1.7E-04	0.57	0.28	-0.14	2.0E-03	0.022	0.75	9.42
M3 vs. M5	0.072	0.013	-0.082	-2.5E-04	1.51	-0.28	-0.56	-5.0E-04	0.0087	0.87	6.77
M2 vs. M3	0.014	0.0098	-0.018	-6.1E-05	1.21	-0.21	-0.18	-1.2E-04	0.0044	0.97	3.74
M1 vs. M3	0.037	0.034	-0.043	-1.1E-04	1.17	-0.43	-0.17	1.9E-04	0.0088	0.88	8.26
M11 vs. M5	-0.38	0.084	0.35	1.6E-03	2.6	-1.1	-1.4	-5.5E-03	0.022	0.75	8.28
All, land cover type 1-13, #:3,909,626 (100%)											
M5 vs. M11	-0.11	0.044	0.15	4.1E-05	0.54	-0.44	-0.15	2.0E-03	0.019	0.83	13.88
M3 vs. M5	0.027	-0.0074	-0.042	-7.2E-05	1.53	-0.27	-0.57	-1.5E-03	0.0066	0.95	8.96
M2 vs. M3	0.0023	0.001	-0.0055	-4.8E-05	1.22	-0.11	-0.22	-5.3E-04	0.0032	0.98	4.86
M1 vs. M3	0.0077	0.0012	-0.011	-5.0E-05	1.28	-0.14	-0.34	-1.0E-03	0.0057	0.93	10.05
M11 vs. M5	-0.00052	-0.027	0.091	2.4E-04	0.53	-0.15	0.53	9.5E-05	0.024	0.81	14.03

* Coefficients for NOAA-20 VIIRS are the same as NPP now; ABI coefficients are listed in Table C-5

For ABI, lack of M4 channel will remove the redness ratio (R) from the independent variables, and thus the linear relationship will be a function of $NDVI_{SWIR}$ (N) and the glint angle (G) only. The spectral relationship coefficients are listed in Table C-5.

The current over-land algorithm assumes that surface reflection is isotropic (Lambertian). Under this assumption, the interaction between atmosphere and surface can be modeled using the adding equation of radiative transfer [Chandrasekhar, 1960]. Therefore, the surface contribution to the TOA reflectance is calculated as:

$$\rho_{surf} = T^{O_3}T^{og}T^{H_2O}\left[T^{\downarrow}_{R+A}T^{\uparrow}_{R+A}\frac{\rho_{lam}}{1-S_{R+A}\rho_{lam}}\right] \quad (3.4.17)$$

Where ρ_{lam} is the Lambertian land surface reflectance retrieved using the process described below, and the other terms are the same as in Section 3.4.1.

3.4.3.3.2 Aerosol retrieval algorithm over dark land

The TOA reflectances ρ_{atm} required are calculated from Eq. 3.4.2 using the aerosol models described in Section 3.4.3.2. The surface contribution ρ_{surf} is calculated from Eq. 3.4.17 after retrieving ρ_{lam} simultaneously with AOD as described below.

With the prescribed spectral relationship of surface reflectance (Section 3.4.3.3.1), the five unknown surface reflectances (M1, M2, M3, M5, M11) are reduced to a single one (M5 or M11). As mentioned above the current algorithm implements two choices. One of these retrieves surface reflectance at M11; this choice is referred to as the SWIR scheme hereinafter; the other choice uses M5, this choice will be denoted as the SW scheme. The question is when to use them; that is, which scheme gives a better estimate of surface reflectance at the reference channel (M3) where retrieval of AOD is attempted. There are two components of the ρ^{sfc}_{M3} estimation: retrieved reflectance (ρ^{sfc}_{M5} or ρ^{sfc}_{M11}) and the spectral relationship. The SWIR scheme can retrieve ρ^{sfc}_{M11}accurately (except for heavy coarse-mode dominated aerosols) owing to the transparency of the atmosphere at longer wavelength. However, the relationship between M3 and M11 (via an intermediate M5 channel) is relatively uncertain (Table 3-11); even a perfect knowledge of ρ^{sfc}_{M11}would lead to an uncertainty of ~0.02 in the estimated ρ^{sfc}_{M3}. On the other hand, for the SW scheme, the M3 vs. M5 surface relationship is more robust as the RMSE of estimated ρ^{sfc}_{M3} is ~0.007 if ρ^{sfc}_{M5} is known, but retrieving accurate ρ^{sfc}_{M5} is challenging because of non-trivial atmospheric impacts. It should be noted that retrieving surface reflectance and AOD are not separate processes; they are performed simultaneously for each given τ_{550} within the searching loop, as described in detail below. Therefore, for cases with heavy aerosol loading, the M5 channel can be opaque with small surface signal, and simultaneous retrieval of surface and aerosol using visible channels could be subject to large uncertainties.

Given the pros and cons of the SW and SWIR schemes, it is attractive to design a hybrid approach which implements the SW scheme for low AOD cases when ρ^{sfc}_{M5} is likely to be

accurately retrieved and uses the SWIR scheme for high AODs when ρ_{M11}^{sfc} has a better chance to be accurate. However, a practical obstacle for this design is that AOD is not known a priori, and using retrieved AOD (either by SW or SWIR schemes) can be problematic since they are subject to errors especially for the cases when the scheme switch needs to be implemented. For example, a high AOD case may end up with a low AOD being retrieved from the SW scheme and the expected switch to SWIR scheme cannot be initiated due to the erroneous low value of the retrieval. In this algorithm, the hybrid scheme is implemented by a cross examination of ρ_{M3}^{sfc} retrieved from ρ_{M5}^{sfc} and ρ_{M11}^{sfc} based on the assumption that there is a greater chance for the SWIR scheme to be more accurate if the ρ_{M3}^{sfc} difference is large. This assumption is made largely from the observation that retrieved ρ_{M5}^{sfc} is much more sensitive to the unknown AOD than ρ_{M11}^{sfc} is, therefore, at certain unfavorable conditions (opaque atmosphere with inaccurate M3 vs. M5 relationship), lack of constraint on the magnitude of retrieved ρ_{M5}^{sfc} would induce an error much larger than that caused by the spectral relationship (with relatively accurate estimation of ρ_{M11}^{sfc}), given the relationship is derived from a representative training dataset with a well characterized uncertainty range. In this sense, SWIR scheme is generally more stable, while the SW scheme has a higher risk to be in large error.

The schematic illustration of this hybrid retrieval algorithm is shown in Figures 3-5 and 3-6. For each candidate aerosol model, the retrieval with the SW scheme is performed first, given the predominance of low AOD on a global scale. Then the applicability of the SWIR scheme is evaluated: if extrapolation is involved in the SW scheme (due to either AOD or surface reflectance being negative or beyond the upper limit in LUT), or if the difference between the ρ_{M3}^{sfc} estimated from ρ_{M5}^{sfc} and estimated from ρ_{M11}^{sfc} is larger than the prescribed threshold of 0.1, the algorithm switches to the SWIR scheme; and finally the retrieval residual is calculated. Among the four candidate aerosol models, the one (with its corresponding τ_{550}) that gives the minimal residual would be selected as the final result. Following the MODIS algorithm, the retrieval residual for each aerosol model is calculated from Eq. 3.4.13 with n=3 and λ is M1, M2 and M11 (for SW scheme) or M5 (for SWIR scheme). This residual represents the spectrally averaged percentage difference between retrieval and measurement, therefore, the aerosol model with the minimum residual is considered as the one that achieves the best fit across the spectrum. For ABI, lack of M1 and M2 channels leads to the residual to be calculated with a single wavelength, that is, M11 for SW scheme or M5 for SWIR scheme.

Aerosol optical depths in selected sensor channels (M1 to M11) are calculated from the spectral dependence of the aerosol normalized extinction coefficient n_{ext} of the retrieved aerosol model. Since n_{ext} for the land aerosol model is a function of τ_{550}, $n_{ext,\lambda}$ is linearly interpolated to the retrieved τ_{550}, and the optical depth at wavelength λ is calculated as $\tau_\lambda = n_{ext,\lambda} * \tau_{550}$.

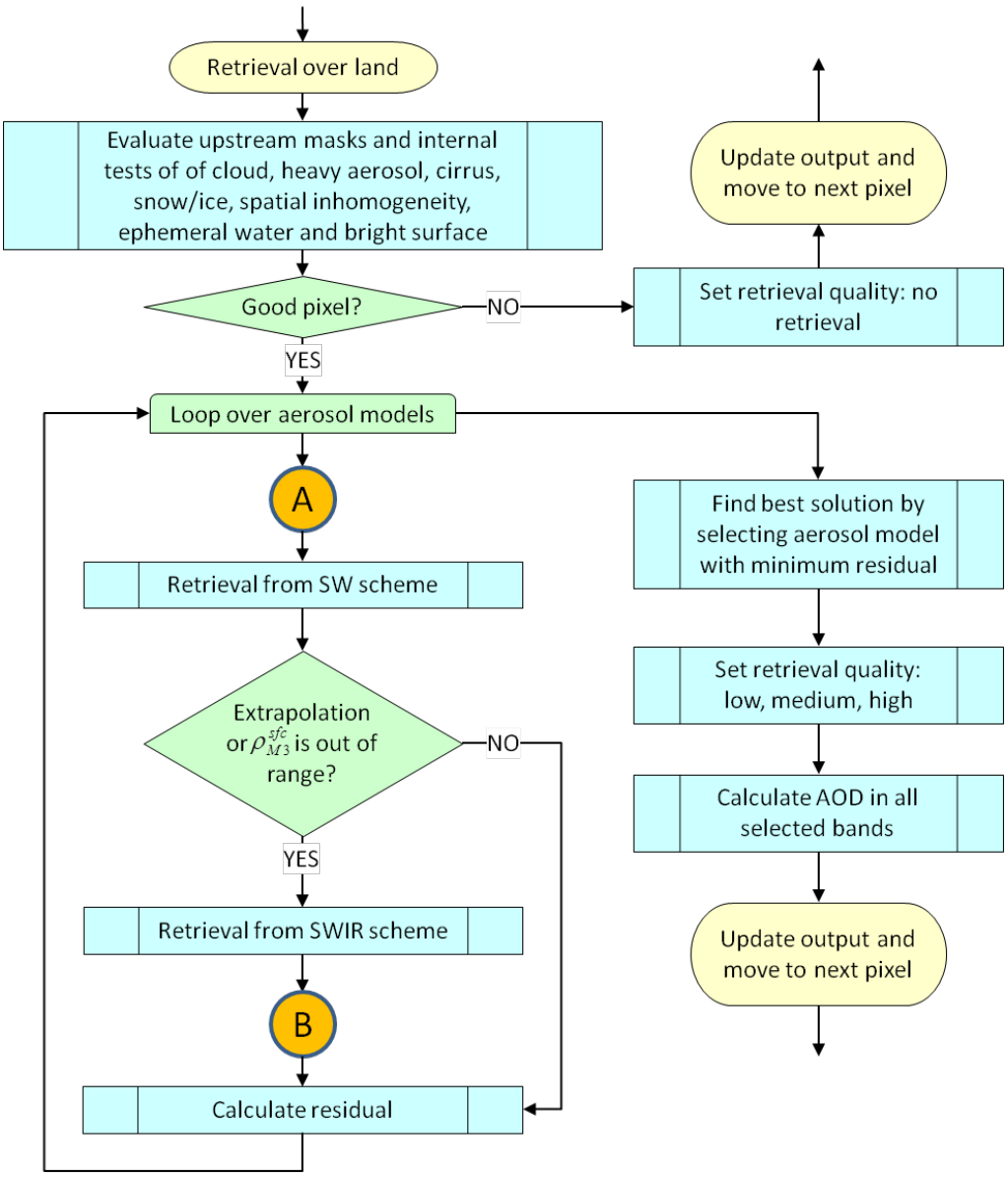

Figure 3-5. Flowchart of AOD retrieval over dark land.

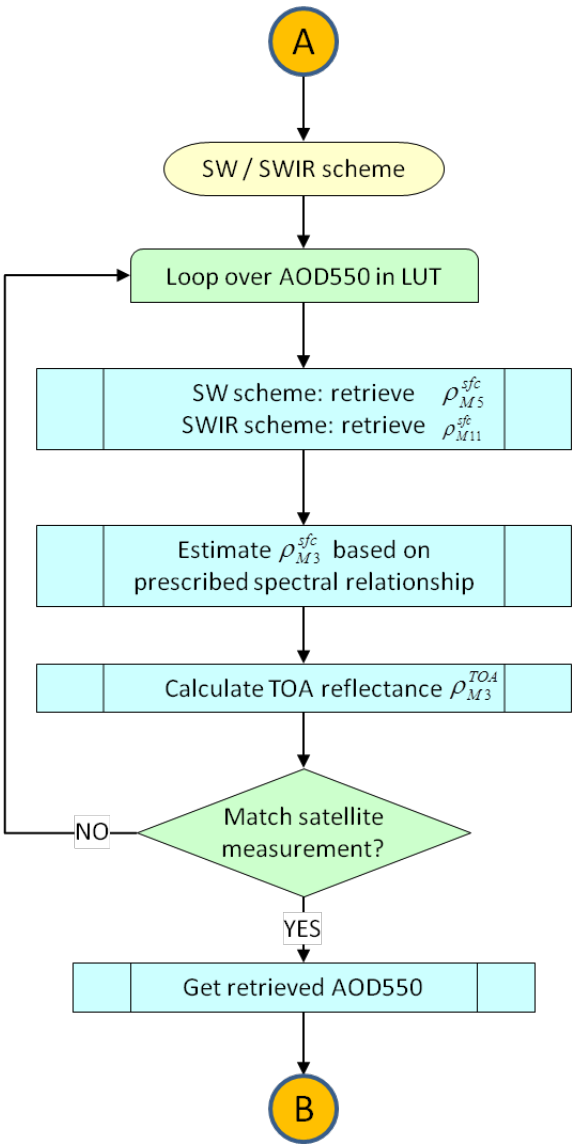

Figure 3-6. Flowchart of SW and SWIR scheme in aerosol retrieval over dark land.

The procedure of simultaneous retrieval of τ_{550} and surface reflectance is explained in detail here by taking the SW scheme as an example, which is the same as the SWIR scheme except the M5 channel is used instead of M11 for surface reflectance retrieval.

For any given aerosol model, a retrieval is performed by looping over τ_{550} in the look-up table in ascending order. At any step i in the loop, a Lambertian surface reflectance ($\rho_{lam}^{(i)}$) in the M5 channel is retrieved based on Eq. 3.4.18, which is derived from Eq. 3.4.17:

$$\rho_{lam}^{(i)} = \frac{R}{R*S_{R+A}+T_{R+A}^{\downarrow}T_{R+A}^{\uparrow}T^{H_2O}} \qquad (3.4.18)$$

where $R = \frac{\rho_{obs} - \rho_{atm}}{T^{O_3} T^{og}}$, and ρ_{atm} is the atmospheric path reflectance corresponding to the i^{th} AOD in LUT ($\tau_{550}^{(i)}$). Surface reflectance at M3 channel is then estimated through the prescribed relationships discussed in Section 3.4.3.3.1. When a valid $\rho_{lam,M3}^{(i)}$ is retrieved (value is between 0 and 1), the TOA reflectance in M3 channel ($\rho_{M3}^{cal,(i)}$) is calculated from $\tau_{550}^{(i)}$ and $\rho_{lam,M3}^{(i)}$. The loop of $\tau_{550}^{(i)}$ is terminated once $\rho_{M3}^{cal,(i)}$ converges to the observation (ρ_{M3}^{obs}). Here convergence means two adjacent steps in the loop, *i* and *i*+1, are found such that ρ_{M3}^{obs} falls within $\rho_{M3}^{cal,(i)}$ and $\rho_{M3}^{cal,(i+1)}$. The τ_{550} for the current aerosol model is determined by linear interpolation on the logarithm of reflectance:

$$\tau_{550} = \tau_{550}^{(i)} \frac{\ln \rho_{M3}^{cal,(i+1)} - \ln \rho_{M3}^{obs}}{\ln \rho_{M3}^{cal,(i+1)} - \ln \rho_{M3}^{cal,(i)}} + \tau_{550}^{(i+1)} \frac{\ln \rho_{M3}^{obs} - \ln \rho_{M3}^{cal,(i)}}{\ln \rho_{M3}^{cal,(i+1)} - \ln \rho_{M3}^{cal,(i)}} \qquad (3.4.19)$$

The final surface reflectance ρ_{lam} is calculated similarly from $\rho_{lam}^{(i)}$ and $\rho_{lam}^{(i+1)}$.

The retrieval of channel M5 (or M11 for SWIR scheme) surface reflectance essentially finds the surface reflectance that, when coupled with the atmosphere with a given aerosol optical depth, results in the observed TOA reflectance ρ_{M5}^{obs}. This retrieval yields a negative surface reflectance when the atmosphere is already brighter than the observed reflectance, that is when $\rho_{atm}(M5) > \rho_{toa}(M5)$ in Eq. 3.4.2. Similarly, the M5 surface reflectance retrieval can also lead to a value larger than unity when the atmosphere is "too dark", that is when $\rho_{atm}(M5) << \rho_{toa}(M5)$ even for the largest optical depth in the LUT. Since the surface is assumed to be Lambertian a negative or larger than unity surface reflectance is deemed unphysical and the iteration of AOD loop cannot proceed. Another special case that must be treated is when the observed TOA M3 reflectance is outside of the range of values calculated for a given aerosol model from the aerosol optical depth values in the LUT, and no valid solution is found. Both of these special cases are handled by extrapolation of the AOD and the surface reflectance using Eq. 3.4.19, in which the extrapolation bracket of [$\rho_{M3}^{cal,(i)}$, $\rho_{M3}^{cal,(i+1)}$] is determined by finding the index (*i*+*1*) where the absolute difference between $\rho_{M3}^{cal,(i+1)}$ and ρ_{M3}^{obs} is the smallest among all the LUT $\tau_{550}^{(j)}$ being iterated through. The extrapolation is not performed when less than two $\tau_{550}^{(j)}$ are iterated; in this case no retrieval is done and all values are set to missing. To avoid the unphysical surface reflectance calculated from the spectral relationship, the minimum value is set to 0.005 for M1 and M2, and 0.01 for all other channels.

3.4.3.4 Retrieval over bright land surface

3.4.3.4.1 Estimate spectral land reflectance ratio

Due to the significant variation of surface reflectance over bright land, spectral surface reflectance relationship is very different at different locations. Therefore, a static database is created to prescribe the surface spectral reflectance ratios (M1/M5, M2/M5 and M3/M5) at 0.1ºx0.1º spatial resolution. With this dataset, surface reflectance at M1, M2 and M3 channels can be calculated once the M5 reflectance is known.

To create this dataset, two-year worth (May 2012-April 2014) of clear-sky snow-free VIIRS TOA reflectances are collected over bright land surfaces ($\rho_{M11}^{obs} > 0.25$). Correction for the Rayleigh scattering and molecular absorption is performed along with the removal of aerosol impact with assumed background aerosol optical depth. To account for the non-Lambertian characteristics of surface reflectance, the lower bounds of retrieved reflectance ratios are used to fit a linear function of scattering angle (surface spectral reflectance ratio = offset + slope*ScatteringAngle) for the forward and backward reflection separately. To derive the lower bound of the atmospherically corrected ratios, retrieved ratios are separated into bins with a scattering angle width of 10º. In each bin, the lowest 10th percentile of the ratios is selected. This method is similar to the averaging of ratios between the minimum and the lowest 20th percentile. However, if there are outliers, the averaging method tends to be significantly influenced by these outliers. The choice of the lowest 10th percentile can eliminate the influence of the outliers as long as the outliers are less than the 10th percentile value. The lower bound lines are derived through a linear regression of these lowest 10th percentile ratios. The flowchart of this process is shown in Figure 3-7 and the detailed descriptions can be found in Zhang et al. [2016].

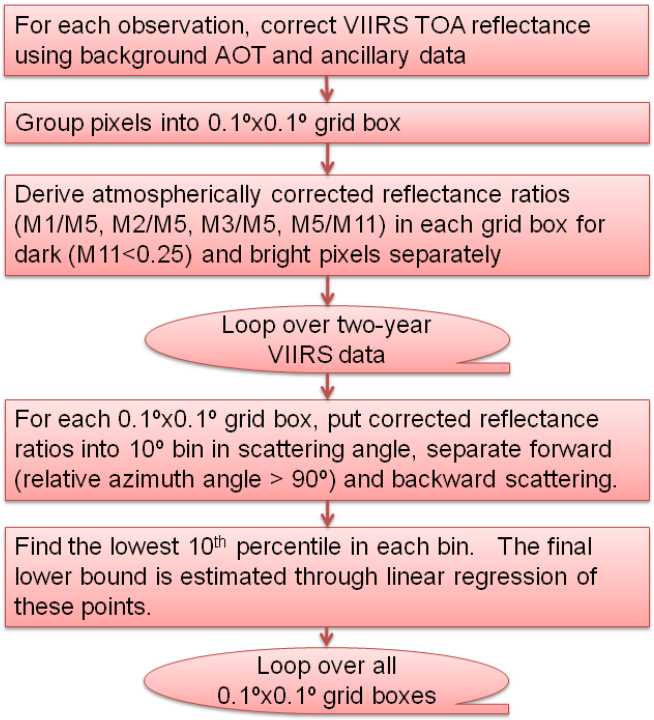

Figure 3-7. Flowchart showing the process for deriving the bright surface reflectance ratio database.

The global map of the derived bright surface reflectance ratios at a selected geometry for M1/M5, M2/M5, and M3/M5 is shown in Figure 3-8. The geometry is backward reflection with a scattering angle of 140º for each 0.1ºx0.1º grid box. As shown in this figure, the

bright pixels are mostly distributed over regions of Africa, western Asia, northwest China, Australia, and the western continental US; the reflectance ratios change from region to region. The spatial coverage is larger in the backward reflection than that in the forward reflection (not shown here); this is because surface reflectance is generally higher in the backward reflection and thus more bright pixels are collected in the training dataset. This dataset will be continually updated along with accumulated VIIRS observation.

For ABI, instead of the spectral ratio as a function of scattering angle at regular grids, a linear relationship with constant offset and slope is developed for each bright land pixels between channel B1 (M3) and B2 (M5). More details are described in Appendix E.

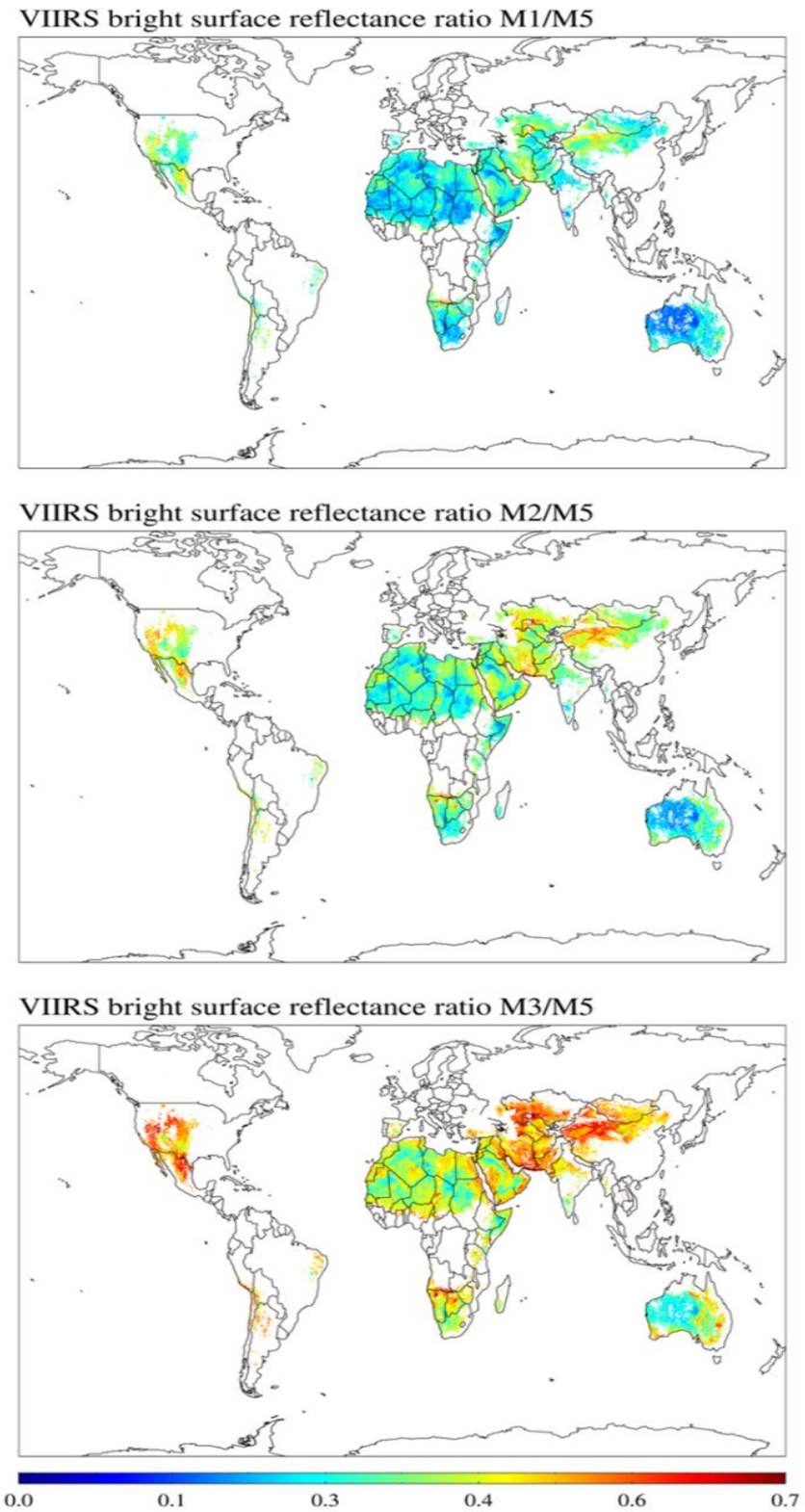

Figure 3-8. Surface reflectance ratios for bright surface (backscattering geometry with scattering angle 140º).

3.4.3.4.2 Aerosol retrieval over bright land surface

The aerosol retrieval over bright land surface is similar to the SW scheme over dark land in the sense that the surface reflectance at channel M5 is retrieved first; the difference is in the channels used to retrieve the AOD and to calculate the residual. Therefore a flowchart specific to the retrieval over bright land is not shown. If the auxiliary surface spectral reflectance relationship is missing, retrieval will be switched to the dark land scheme.

Within the region of North Africa and Arabian Peninsula (20ºW-60ºE and 0º-36ºN), the M3 band is used as the reference channel to retrieve AOD and the residual is calculated with the M1 and M2 channels. In this region, there is no aerosol model selection; the retrieval is forced to use dust model. This restriction is based on the observation that dust is the dominant aerosol type and the algorithm's ability to choose the correct aerosol model is dubious especially when dust occurs over high surface reflectance regions.

Over other bright regions, the M1 channel is used to retrieve AOD and M2 and M3 channels are used to compute the residual. Aerosol model selection is performed by choosing the best solution with minimum residual. This change of the reference channel (from M3 to M1) is based on the empirical argument that AOD retrieved from M1 channel is more accurate than from M3.

For ABI, lack of M1 and M2 channels will leave no residual channels to the retrieval, therefore, M3 channel is used to retrieve AOD with a prescribed aerosol model (generic aerosol model).

3.4.3.5 Internal Tests and Quality Control

Several simple internal tests are designed to screen out the contaminated pixels and identify low quality retrievals. Though they are not as sophisticated and particular as dedicated algorithms, they nevertheless give the aerosol algorithm a certain degree of self-reliance and reduce the dependence on the external inputs.

1) Internal cloud test: A brightness test $\rho_{\mathrm{M1}}^{\mathrm{TOA\text{-}ray}} > 0.4$ is used to screen out thick cloud; here $\rho_{\mathrm{M1}}^{\mathrm{TOA\text{-}ray}}$ is the Rayleigh scattering and gaseous absorption corrected TOA reflectance at M1 channel. The reason for removing the Rayleigh contribution is to reduce the angular dependence of the TOA reflectance so that a single threshold independent of viewing geometry can be applied. It should be noted that this test not only detects bright clouds, but also other bright scenes (e.g., snow and ice) unsuitable for aerosol retrievals. For ABI, M3 channel is used instead of M1.

2) Internal heavy aerosol test: potential heavy aerosol is detected if $f^{"}\left(\rho_{M2}^{obs-ray}\right) < -0.025$ (-0.07 for NOAA20 due to difference in the channel spectral response function), here $f^{"}\left(\rho_{M2}^{obs-ray}\right)$ is a parameter proportional to the second spectral derivative of the Rayleigh-scattering-corrected TOA reflectance at channel M2

calculated as: $f''(\rho_{M2}^{obs-ray}) = 4.3\rho_{M1}^{obs-ray} - 7.6\rho_{M2}^{obs-ray} + 3.3\rho_{M3}^{obs-ray}$. This test is based on the observation that usually Rayleigh-scattering-corrected TOA reflectance is concave downward at channel M2 for heavy smoke and dust, which is caused by the enhanced absorption at M1 where the background Rayleigh scattering is much stronger than M2. For ABI, currently there is no heavy aerosol test due to the lack of M1 and M2 channels.

An additional heavy aerosol test is included based on the VIIRS cloud mask (VCM) algorithm [JPSS, 2014]: if the input cloud mask is cloudy, but passes the internal cloud and cirrus test, then the pixel would be considered as potential heavy aerosol if the 3x3 TOA reflectance standard deviation at channel M3 (internal inhomogeneity test) is less than 0.006.

3) Internal cirrus test: Following the scheme adopted by the MODIS Enhanced Deep Blue aerosol algorithm [Hsu et al., 2013], cirrus is identified over non-desert area if $\rho_{M9}^{TOA} > 0.018$ and total precipitable water $TPW > 0.4\ cm$; and over desert area if $\rho_{M9}^{TOA} > 0.018$, and $TPW > 0.9\ cm$ or BT_{M15}-BT_{M16} > -1K. Here, BT_{M15} and BT_{M16} are the brightness temperatures in M15 (10.76 μm) and M16 (12.01 μm) channels. The input land/water mask is used to identify pixels over desert. To avoid the mis-identification of smoke plumes as cirrus, this test (and the thin cirrus test) is bypassed if heavy aerosol is detected by the internal test.

4) Internal thin cirrus test: Following the scheme of the operational VIIRS cloud mask [JPSS, 2014], thin cirrus is identified if $\rho_{M9}^{obs} > TC$, where TC is the thin cirrus threshold calculated as $TC = a + b\frac{TPW}{\mu_v}$. Here μ_v is the cosine of viewing zenith angle (up to 71°) and the maximum value for $\frac{TPW}{\mu_v}$ is 16cm; (a, b) are constants specified for dark land as (0.0126, -3.636e-4) and desert as (0.0276, -5.128e-4), respectively.

5) Internal inhomogeneity test: Standard deviation of ρ_{M1}^{TOA} (σ_{M1}^{3x3}) over 3 by 3 pixels is calculated for each land pixel and used as a measure of spatial inhomogeneity of the retrieval area. The spatial inhomogeneity could be caused by unfavorable conditions such as sub-pixel cloud, rugged terrain, etc. Using the M1 channel is due to the smaller surface contribution. A land pixel will pass this test if $\sigma_{M1}^{3x3} \leq 0.008$. For ABI, due to the lack of M1 channel, this test is set as $\sigma_{M3}^{3x3} \leq 0.012$.

6) Internal snow test: Following the MODIS algorithm, snow pixels are identified if the normalized difference ratio (r_s) is larger than 0.1 and the brightness temperature at M15 is lower than 285K. Here r_s is calculated from channels M7 (0.865μm) and M8 (1.24 μm) as: $r_s = \frac{\rho_{M7}^{obs-ray} - \rho_{M8}^{obs-ray}}{\rho_{M7}^{obs-ray} + \rho_{M8}^{obs-ray}}$ As channel M8 is not available from ABI, M10 would be used instead and the threshold is changed to 0.3.

7) Internal ephemeral water test: Land pixels covered by ephemeral water are identified when the TOA NDVI is less 0.1 and $\rho_{M7}^{obs-ray} < 0.1$. The latter criterion is used to

ensure only dark scenes are tested. The TOA NDVI is calculated as $\mathrm{NDVI} = \frac{\rho_{M7}^{\text{TOA-ray}} - \rho_{M5}^{\text{TOA-ray}}}{\rho_{M7}^{\text{TOA-ray}} + \rho_{M5}^{\text{TOA-ray}}}$.

Based on the external masks, internal tests and retrieval inputs and outputs, retrievals are categorized into various quality levels as listed in Table 3-12. In general, the high quality retrievals are recommended for quantitative applications due to their better overall performance; however, the lower quality retrievals also have their merit for the qualitative examination of local episodic events due to their greater spatial coverage.

Table 3-12. Criteria used for assigning retrieval quality over land.

Quality Level	Criteria
No Retrieval	1) Cloudy: input cloud mask is probably or confident cloudy and any internal cloud, cirrus or inhomogeneity test fails; 2) Snow/ice (input mask or internal test); 3) Ephemeral water (internal test); 4) Fire (input mask) 5) Retrieval failed due to missing inputs or numeric error.
Low	1) Air mass (sum of inverse cosine solar and viewing zenith angles) > 5 (6 for ABI); 2) Fail internal cloud test (but input cloud mask is clear); 3) Fail internal cirrus test (but input cloud mask is clear); 4) External cloud mask is cloudy (but pass internal tests, not heavy aerosol); 5) Coastal area (input land/water mask); 6) Extrapolation due to unphysical surface reflectance retrieved ; 7) $\sigma_{M1}^{3x3} < 0.008$ ($\sigma_{M3}^{3x3} > 0.012$ for ABI); 8) Retrieval residual > 0.5;
Medium	1) Cloud shadow (input mask); 2) Thin cirrus (internal test); 3) Adjacent to cloudy pixel; 4) Adjacent to snow pixel (within 3-pixel distance) 5) Land cover type is barren or sparsely vegetated; 6) TOA $\mathrm{NDVI}_{\mathrm{SWIR}}$ is out of range (-0.1, 0.8); 7) TOA redness ratio is out of range (0.4, 1.6); 8) $\sigma_{M1}^{3x3} > 0.004$ ($\sigma_{M3}^{3x3} > 0.006$ for ABI) 9) Retrieval residual > 0.4 10) Retrieved τ_{550} is out of range (-0.05, 5.0)
High	Remaining retrievals

3.4.4 Calculation of aerosol particle size parameter

The wavelength (λ) dependence of aerosol optical depth is usually described as $\tau \propto \lambda^{-\alpha}$, where τ is the optical depth and α is the Ångström exponent. Large/small values of Ångström exponent indicate small/large particles, respectively. The Ångström exponent

over ocean is calculated as the linear slope of aerosol optical depth versus wavelength in log-scale for two wavelength pairs (M4, M7) and (M7, M10) for VIIRS and (M5,M7) and (M7,M10) for ABI:

$$\alpha_{M4/5;M7} = -\frac{\ln \tau_{M4/5} - \ln \tau_{M7}}{\ln \lambda_{M4/5} - \ln \lambda_{M7}} \quad (3.4.20)$$

$$\alpha_{M7;M10} = -\frac{\ln \tau_{M7} - \ln \tau_{M10}}{\ln \lambda_{M7} - \ln \lambda_{M10}} \quad (3.4.21)$$

3.4.5 **Look-up table**

Two lookup tables (LUT), one for the atmosphere (aerosol plus molecules at standard pressure) and one for the ocean surface reflectance, store reflectances, transmittances and other quantities pre-calculated for discrete states of the atmosphere and the ocean surface. The tables are calculated with the vector version of the 6S radiative transfer code [Vermote et al., 1997; Kotchenova et al., 2006; 2007]. The atmospheric LUT is produced for a non-reflecting surface (surface reflectance is zero). This increases flexibility since potentially any surface can be used to couple the atmosphere with in the retrieval.

3.4.5.1 **Atmospheric look-up table**

The atmospheric LUT contains radiative functions and aerosol normalized extinction coefficients used to retrieve aerosol optical depth. Table 3-13 lists the contents of VIIRS LUT. The corresponding discrete values for each dimension are listed in Table 3-14. The ABI atmospheric lookup table contains less number of channels (Nchn=6, Nlndchn=3, Nwatchn=4), and expanded viewing angle coverage (Nsenzen=25).

Table 3-13. Contents of VIIRS atmospheric look-up table

Data Set Name	Description	Size of Dimensions
tau550	Aerosol optical depth at 550nm in LUT	(20) (Ntau)
solar_zenith_angle	Solar zenith angle in LUT	(21) (Nsolzen)
sensor_zenith_angle	Sensor zenith angle in LUT	(20) (Nsenzen)
scattering_angle_position	Scattering angle indexing vector	(420) (Nsolzen x Nsenzen)
land_aer_nor_ext_coef	Normalized extinction coefficient for land aerosol models in channels M1-M11	(11,4,20) (Nchn, Nlndaer, Ntau)
land_aer_sph_alb	Atmospheric spherical albedo corresponding to candidate land aerosol models	(7,4,20) (Nlndchn, Nlndaer, Ntau)
land_aer_trans	One-way atmospheric transmittance corresponding to candidate land aerosol models	(7,4,20,21) (Nlndchn, Nlndaer, Ntau, Nsolzen)

land_aer_refl	Atmospheric reflectance corresponding to candidate land aerosol models	(7,4,20,5527) (Nlndchn, Nlndaer, Ntau, Nscat)
water_aer_nor_ext_coef	Normalized extinction coefficient for ocean aerosol models in channels M1-M11	(11,9) (Nchn, Nwataer)
water_aer_sph_alb	Atmospheric spherical albedo corresponding to candidate ocean aerosol models	(7,9,20) (Nwatchn, Nwataer, Ntau)
water_aer_trans	One-way atmospheric transmittance corresponding to candidate ocean aerosol models	(7,9,20,21) (Nwatchn, Nwataer, Ntau, Nsolzen)
water_aer_refl	Atmospheric reflectance corresponding to candidate ocean aerosol models	(7,9,20,5527) (Nwatchn, Nwataer, Ntau, Nscat)
ray_sph_alb	Rayleigh scattering spherical albedo	(11) (Nchn)
ray_trans	Rayleigh transmittance	(11,21) (Nchn, Nsolzen)
ray_refl	Rayleigh reflection	(11,5527) (Nchn, Nscat)

Table 3-14. Discrete values/description of VIIRS atmospheric LUT dimensions

Dimension Name	**Variable Name in** Table	**Number of Values**	**Discrete Values/Description**
AOD at 550nm	Ntau	20	0.00, 0.01, 0.05, 0.10, 0.15, 0.20, 0.30, 0.40, 0.60, 0.80, 1.00, 1.20, 1.40, 1.60, 1.80, 2.00, 2.50, 3.00, 4.00, 5.00
Solar zenith angle	Nsolzen	21	0°, 4°, 8°, 12°, 16°, 20°, 24°, 28°, 32°, 36°, 40°, 44°, 48°, 52°, 56°, 60°, 64°, 68°, 72°, 76°, 80°
Sensor zenith angle	Nsenzen	20	0.0°, 2.84°, 6.52°, 10.22°, 13.93°, 17.64°, 21.35°, 25.06°, 28.77°, 32.48°, 36.19°, 39.90° 43.61°, 47.32°, 51.03°, 54.74°, 58.46°, 62.17° 65.88°, 69.59°
Channels	Nchn	11	Channels M1 to M11
Channels for land aerosol radiative functions	Nlndchn	7	Channels M1, M2, M3, M4, M5, M8, M11
Land aerosol models	Nlndaer	4	Dust, Generic, Urban, Smoke
Scattering angle	Nscat	5527	Every 4° interval in the range from 180-(θ_s+θ_v) to 180-|θ_s-θ_v| for all pairs combination of solar zenith angle (θ_s) and sensor zenith angle (θ_v)
Ocean aerosol models	Nwataer	9	Four fine modes plus five coarse mode
channels for ocean aerosol radiative functions	Nwatchn	7	Channels M4, M5, M6, M7, M8, M10, M11

For the ABI lookup table, the sensor zenith angle range is expanded to include five more nodes (73.29°, 77.01°, 80.72°, 84.43°, 88.14°) and the number of scattering angles (Nscat) is increased to 7727; six shortwave channels (Nchn) are M3, M5, M7, M9, M10

and M11; three land channels (Nlndchn) are M3, M5 and M11; four water channels (Nwatchn) are M5, M7, M10 and M11.

3.4.5.1.1 Normalized spectral aerosol extinction coefficient

Normalized spectral aerosol extinction coefficients are provided for all candidate aerosol models in channels M1 to M11. For the land aerosol models, the coefficients are functions of optical depth and interpolation on the optical depth dimension is needed to apply to the retrieved value.

3.4.5.1.2 Spherical albedo

Atmospheric spherical albedos (S_{R+A}, subscript R+A represents combined contributions from both molecules and aerosols) are provided for each aerosol model and optical depth for the channels used in the retrieval. Since the spherical albedo is the integrated bidirectional reflectance distribution function over both illumination and viewing hemispheres, it does not depend on geometry and there is no need for interpolation.

3.4.5.1.3 Transmittance

One-way atmospheric transmittances (T_{R+A}) are provided for each aerosol model and optical depth for the channels used in the retrieval. The total transmittance is the sum of direct and diffuse components and assumed to be azimuthally invariant. Transmittances at twenty-one discrete zenith angles (for 0° to 80° in step of 4°) are provided to describe the dependence on illumination and viewing geometry. The downward and upward transmittance ($T_{R+A}^{\uparrow}$ and $T_{R+A}^{\downarrow}$) are estimated by linear interpolation of the one-way transmittance LUT to the solar zenith angle and sensor zenith angle, respectively.

3.4.5.1.4 Reflectance

Under the plane-parallel assumption, dependence of atmospheric reflectance on geometry is usually specified by solar zenith angle θ_s, view zenith angle θ_v and corresponding azimuth angles. When no provision is made for preferentially oriented scatterers, and thus scattering depends only on the angle between the incident and scattered beam (scattering angle, Θ), not on the incident and scattered directions separately, the dependence can be described by the scattering angle. For a given pair of θ_s and θ_v, the realizable scattering angle spans a range of $[\Theta_{min}, \Theta_{max}]$ depending on the relative azimuth angle (φ), where $\Theta_{min}=180°-(\theta_s+\theta_v)$ and $\Theta_{max}=180°-|\theta_s-\theta_v|$. As a result, the actual scattering angle range varies for different combinations of θ_s and θ_v.

Normally, the atmospheric reflectance is calculated for discrete values of θ_s, θ_v and φ in a lookup table to describe its angular dependence. However, such scheme leads to a varying

resolution in scattering angle for different atmospheric paths. For example, there are the same number (number of discrete φ values) of reflectances pre-calculated for the case of θ_s=10°; θ_v=10° and the case θ_s=60°; θ_v=60°, where the former extends over a range of 20° scattering angle (from 160° to 180°) and the latter spreads 120° (from 60° to 180°). Therefore, a fixed resolution in relative azimuth angle might result in deficient or redundant representation of the scattering angle dependence for certain combinations of θ_s and θ_v.

For the current aerosol retrieval algorithm, the atmospheric reflectance lookup table is generated aiming to achieve a fixed resolution (4°) in scattering angle for all discrete combinations of θ_s and θ_v (there are 21 discrete values of θ_s and 20 θ_v, a total of 420 combinations). Since the range of scattering angle varies for different (θ_s, θ_v), instead of being arranged as a rectangular array where extra space will be wasted, the reflectance entries (corresponding to a given aerosol model, aerosol optical depth, and wavelength) are organized as a one-dimensional array. Within the array, there are 420 blocks corresponding to the individual pairs of (θ_s^i, θ_v^j). The sequence of blocks is ordered by looping over the viewing zenith angle first (j=1, 20) then followed by the solar zenith angle (i=1, 21). Each block contains a varying number of reflectance entries with scattering angles separated by 4° from Θ_{max} to Θ_{min} (the last interval might be less than 4° if Θ_{max}- Θ_{min} is not an integer multiple of 4°). There are a total of 5527 reflectance entries pre-calculated to represent the angular dependence of atmospheric reflectance. In order to find the block corresponding to a given (θ_s^i, θ_v^j), an indexing vector with 420 elements is created to save the starting position of each block within the reflectance array. Figure 3-9 shows the layout of the atmospheric reflectance array and indexing vector, and the way the starting position of each block is accessed.

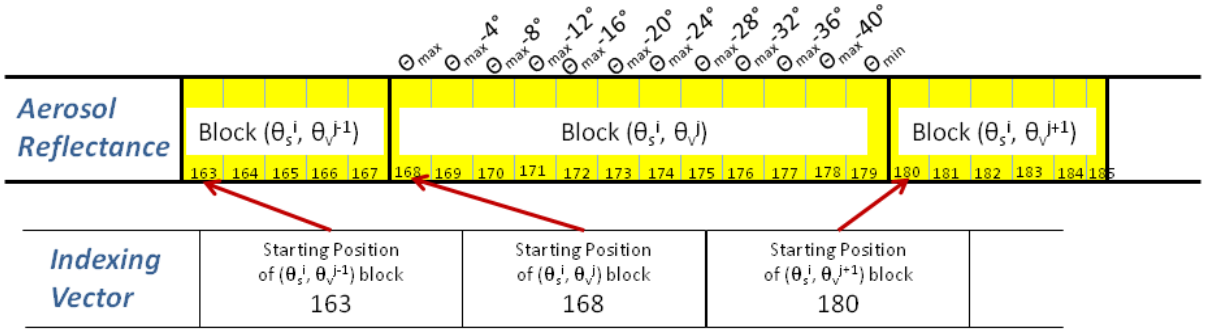

Figure 3-9. The layout of atmospheric reflectance array for a given aerosol model, aerosol optical depth and wavelength (top) and indexing vector (bottom). The starting position of each block can be accessed by the corresponding element in the indexing vector.

In the aerosol retrieval, atmospheric reflectance corresponding to a given aerosol model, aerosol optical depth, wavelength and geometry (θ_s, θ_v and φ) is determined by linear interpolation on the values stored in the lookup table. The interpolation on geometry is implemented as follows:

1. The solar zenith angle bracket [θ_s^{i-1}, θ_s^i] containing θ_s and the linear interpolation fraction f_s are determined such that θ_s= f_s* θ_s^{i-1}+(1- f_s)*θ_s^i.

2. The viewing zenith angle bracket $[\theta_v^{j-1}, \theta_v^j]$ containing θ_v and the linear interpolation fraction f_v are determined such that $\theta_v = f_v * \theta_v^{j-1} + (1 - f_v) * \theta_v^j$.

3. For each pair of $(\theta_s^{i-1}, \theta_v^{j-1})$, $(\theta_s^{i-1}, \theta_v^j)$, $(\theta_s^i, \theta_v^{j-1})$, and (θ_s^i, θ_v^j), atmospheric reflectance corresponding to the instantaneous relative azimuth angle φ is interpolated from the reflectance array stored in the lookup table. For example, for the pair of (θ_s^i, θ_v^j):

    a. The corresponding position (k) in the indexing vector is determined by $k = i * n_v + j$, where n_v is the number of tabulated viewing zenith angles (=20), and the array index is assumed to start from zero following the convention in the C programming language. Therefore, the starting position of the block is read out from the k^{th} element of the indexing vector, and the number of entries in this block is determined by the difference between the $(k+1)^{th}$ and k^{th} elements. The block of pre-calculated reflectances corresponding to the scattering angles from Θ_{max} to Θ_{min} for the current zenith angle pair are then extracted from the reflectance array.

    b. The scattering angle Θ corresponding to the measurement relative azimuth angle φ is calculated from

    $$\cos \Theta = -\cos \theta_s^i * \cos \theta_v^j - \sin \theta_s^i * \sin \theta_v^j * \cos \varphi$$

    Linear interpolation is performed to calculate the atmospheric reflectance $\rho_{i,j}$ of the scattering angle Θ from the block of reflectance.

4. With the four atmospheric reflectances $\rho^{i-1,j-1}$, $\rho^{i-1,j}$, $\rho^{i,j-1}$, and $\rho^{i,j}$ corresponding to the four pairs of tabulated bracket zenith angles, instantaneous atmospheric reflectance is then estimated as:

$$\rho = f_s * f_v * \rho^{i-1,j-1} + f_s * (1-f_v) * \rho^{i-1,j} + (1-f_s) * f_v * \rho^{i,j-1} + (1-f_s) * (1-f_v) * \rho^{i,j}$$

3.4.5.2 **Ocean surface sunglint reflectance look-up table**

The ocean surface sunglint reflectance LUT is to account for its bidirectional reflection (BRDF) and to store the quantities needed for the analytical coupling of the atmosphere with the surface. Table 3-15 lists the contents of this LUT, the corresponding discrete values for each dimension are listed in Table 3-16. There is no entry for wind direction as it is considered fixed at a westerly direction.

Table 3-15. Contents of ocean sunglint surface reflectance look-up table

Data Set Name	Description	Size of Dimensions
rhobar	Ocean surface sunglint hemispherical-directional reflectance $\overline{\rho_{sgt}}$ which represents the portion of downwelling atmospheric diffuse radiation reflected upward direct to the satellite sensor	(7,9,20,21,21,21,4) (Nwatchn, Nwataer, Ntau, Nsolzen, Nsenzen, Nrelazi, Nwpd)
sgalb	Ocean surface sunglint spherical albedo $\overline{\overline{\rho_{sgt}}}$ $\overline{\overline{\rho_{sgt}}}$	(7,4) (Nwatchn, Nwpd)

Table 3-16. Discrete values of ocean reflectance LUT dimensions

Dimension Name	Variable Name in Table 3-15	Number of Values	Discrete Values
Relative Azimuth Angle	Nrelazi	21	0°, 9°, 18°, 27°, 36°, 45°, 54°, 63°, 72°, 81°, 90°, 99°, 108°, 117°, 126°, 135°, 144°, 153°, 162°, 171°, 180°
Zenith angle	Nsolzen Nsenzen	21	0°, 4°, 8°, 12°, 16°, 20°, 24°, 28°, 32°, 36°, 40°, 44°, 48°, 52°, 56°, 60°, 64°, 68°, 72°, 76°, 80°
Wind speed (m/s)	Nwpd	4	1.0, 4.0, 6.0, 12.0

3.4.5.2.1 Ocean surface reflectivity

The ocean surface sunglint diffuse reflectances $\overline{\rho_{sgt}}$, representing the portion of downwelling atmospheric diffuse radiation reflected upward direct to the satellite sensor, are provided for each ocean aerosol model and optical depth for the channels used in the retrieval. The dependence on geometry and surface roughness of the reflectance is represented by the extra dimensions of solar/sensor zenith angle, relative azimuth angle and wind speed. Linear interpolation on these dimensions is used to estimate $\overline{\rho_{sgt}}$ for any given illumination and observation geometry and surface wind speed.

Applying the reciprocity principle, the diffuse reflectance $\overline{\rho'_{sgt}}$, representing the portion of downwelling atmospheric direct radiation reflected diffusely skyward to the satellite sensor, can be regarded as $\overline{\rho_{sgt}}$ with exchanged solar zenith (θ_s) and sensor zenith (θ_v) angles, i.e., $\overline{\rho'_{sgt}}(\theta_s, \theta_v) = \overline{\rho_{sgt}}(\theta_v, \theta_s)$. Consequently, $\overline{\rho'_{sgt}}$ at any given geometry and wind speed is determined via the interpolation of the $\overline{\rho_{sgt}}$ LUT by switching the zenith angles.

3.4.5.2.2 Ocean surface spherical albedo

The ocean surface sunglint spherical albedo ($\overline{\rho_{sgt}}$) LUT is to account for the diffuse downwelling radiation that is scattered diffusely upward to the satellite sensor. It is assumed to be independent of the atmosphere and therefore only a function of surface wind speed and spectral channels. There is no interpolation involved with this parameter.

3.4.6 Gas transmittance parameterization

To simplify the radiative transfer model in the aerosol retrieval, the transmission of gases is parameterized as an analytical function of the effective absorber amount. The coefficients appearing in the analytical expressions are determined for the sensor bands to account for the absorption for water vapor, ozone, and by the rest of the gases (O_3, O_2, CO_2, N_2O).

The analytical functions are fitted with the path absorber amount and channel-dependent coefficients *C*. The path absorber amount is the product of the column absorber amount *u* and the air mass M for water vapor and ozone, while it is simply M for the other gases due to the constant content. The column water vapor and ozone amounts are supplied as inputs to the algorithm. The air mass M is

$$M = \frac{1}{\cos\theta_s} + \frac{1}{\cos\theta_v} \quad (3.4.22)$$

where θ_s and θ_v are solar and local zenith angles, respectively.

The transmission for water vapor is expressed as:

$$T_\lambda^{H_2O} = exp\left[C_{1,\lambda}^{H_2O} \cdot M \cdot u_{H_2O} + C_{2,\lambda}^{H_2O} \cdot \ln(M \cdot u_{H_2O}) + C_{3,\lambda}^{H_2O} \cdot M \cdot u_{H_2O} \cdot \ln(M \cdot u_{H_2O})\right] \quad (3.4.23)$$

Where $T_\lambda^{H_2O}$ is the water vapor transmission at a given wavelength, u_{H_2O} is the column water vapor amount in unit cm, and $C_{i,\lambda}^{H_2O}$ are band-dependent coefficients.

Similarly, ozone transmission is calculated as:

$$T_\lambda^{O_3} = exp\left[-C_\lambda^{O_3} \cdot M \cdot u_{O_3}\right] \quad (3.4.24),$$

where u_{O_3} is the input column ozone amount in unit atm-cm.

The transmission by gases other than water vapor and ozone, including O_2, CO_2, N_2O, and CH_4, is modeled as:

$$T_\lambda^{og} = exp\left[M \cdot \left(C_{1,\lambda}^{Gas} \cdot P + C_{2,\lambda}^{Gas} \cdot \ln P\right) + \ln M \cdot \left(C_{3,\lambda}^{Gas} \cdot P + C_{4,\lambda}^{Gas} \cdot \ln P\right) + M \cdot \ln M \cdot \left(C_{5,\lambda}^{Gas} \cdot P + C_{6,\lambda}^{Gas} \cdot \ln P\right)\right] \quad (3.4.25)$$

where $P = P_{sfc}/P_0$, P_0 = 1013 mb and P_{sfc} is the input surface pressure. Table 3-17 lists the constant coefficients *C* used for the gaseous absorption calculation.

Table 3-17. Gaseous absorption coefficients for sensor channels.*

VIIRS Channels	$C_{1,\lambda}^{H_2O}$	$C_{2,\lambda}^{H_2O}$	$C_{3,\lambda}^{H_2O}$	$C_{\lambda}^{O_3}$	$C_{1,\lambda}^{Gas}$	$C_{2,\lambda}^{Gas}$	$C_{3,\lambda}^{Gas}$	$C_{4,\lambda}^{Gas}$	$C_{5,\lambda}^{Gas}$	$C_{6,\lambda}^{Gas}$
M1	4.04E-05	-9.86E-04	-7.37E-06	2.85E-04	-2.81E-04	1.16E-03	2.82E-04	-1.12E-03	7.43E-05	-3.05E-04
M2	-7.24E-07	-1.25E-04	7.14E-08	2.88E-03	-2.83E-05	1.04E-04	2.90E-05	-1.02E-04	7.52E-06	-2.71E-05
M3	6.78E-06	-3.73E-04	-1.23E-06	1.80E-02	-1.18E-04	3.66E-04	1.21E-04	-3.75E-04	3.13E-05	-9.67E-05
M4	-1.23E-04	-2.47E-04	2.07E-05	8.39E-02	-9.96E-05	3.11E-04	1.02E-04	-3.23E-04	2.65E-05	-8.18E-05
M5	-5.17E-04	-3.06E-05	7.73E-05	4.33E-02	-1.98E-03	8.46E-03	1.78E-03	-9.55E-03	5.19E-04	-2.32E-03
M6	-5.34E-03	1.87E-03	8.72E-04	1.07E-02	-1.83E-03	3.98E-03	2.10E-03	-5.13E-03	4.96E-04	-1.07E-03
M7	-2.51E-03	7.13E-04	3.81E-04	7.67E-05	-2.76E-05	1.12E-03	8.44E-06	2.02E-04	2.69E-06	-9.69E-06
M8	-3.77E-03	2.38E-03	5.91E-04	1.53E-08	-9.04E-04	7.37E-03	1.24E-05	-5.93E-04	1.46E-04	-1.19E-03
M10	-1.15E-03	8.63E-04	1.38E-04	0.0	-2.09E-02	3.94E-03	3.02E-03	4.04E-02	4.25E-03	4.55E-03
M11	-1.62E-03	1.01E-03	2.65E-04	0.0	-4.71E-02	3.98E-02	-1.27E-02	-4.23E-02	7.72E-03	-1.37E-02

* Coefficients for NOAA-20 VIIRS are listed in Table B-3; Table C-3 for ABI

3.4.7 **Calculation of molecular atmospheric functions**

Molecular scattering is important in the radiative transfer computation and satellite remote sensing especially in the blue spectral range. Since the blue channel is the reference (primary) channel for aerosol retrieval over land, variation of molecular reflectance and transmission need to be incorporated in an accurate and efficient manner. Instead of expanding the lookup table with an extra dimension on surface pressure, analytical formulas [Vermote and Tanré, 1992] are used to compute molecular scattering, and to adjust the atmospheric functions pre-calculated at standard pressure to local conditions. With the contribution of polarization being implicitly considered, the analytical expressions were shown to be valid for a large range of observation conditions.

Molecular reflection is calculated as the sum of single-scattering contribution and the correction for higher orders of scatterings. The relevant formulas are from subroutine CHAND for Rayleigh scattering function in the 6S code [Vermote et al., 2006]. According to these the Rayleigh (molecular) reflectance ρ_R corresponding to the cosines of solar and local zenith angles, μ_s and μ_v, azimuth angles ϕ_s, ϕ_v and the Rayleigh optical depth τ is computed as:

$$\rho_R = \sum_{m=0}^{2}(2-\delta_{0,m})\times\rho_1^m(\mu_s,\mu_v,\tau)\times\cos[(m(\pi-(\phi_s-\phi_v))]+ \\ \left(1-e^{-\tau/\mu_s}\right)\times\left(1-e^{-\tau/\mu_v}\right)\times\sum_{m=0}^{2}(2-\delta_{0,m})\times\Delta^m(\tau)\times P^m(\mu_s,\mu_v)\times\cos[(m(\pi-(\phi_s-\phi_v))] \quad (3.4.26)$$

Here $\delta_{0,s}$ is the Kronecker delta, $\rho_1^m(\mu_s,\mu_v,\tau)$ is the single-scattering reflectance corresponding to the m^{th} term of the phase function. The first three single-scattering reflectance terms (m=0, 1, 2) are:

$$\rho_1^m(\mu_s,\mu_v,\tau) = P^m\times(1-e^{-\tau\left(\frac{1}{\mu_s}+\frac{1}{\mu_v}\right)})\times\frac{1}{4(\mu_s+\mu_v)} \quad (3.4.27)$$

The first three terms of the Fourier series expansion of the Rayleigh phase function P^m (m=0,1,2) appearing in the equations above are:

$$P^0 = 1+(3\mu_s{}^2-1)(3\mu_v{}^2-1)*\frac{1-\frac{\delta}{2-\delta}}{1+2\frac{\delta}{2-\delta}}*\frac{1}{8}$$

$$P^1 = -\mu_s\mu_v(1-\mu_s{}^2)^{1/2}(1-\mu_v{}^2)^{1/2}*\frac{1-\frac{\delta}{2-\delta}}{1+2\frac{\delta}{2-\delta}}*\beta*1.5$$

$$P^2 = (1-\mu_s{}^2)(1-\mu_v{}^2) * \frac{1-\frac{\delta}{2-\delta}}{1+2\frac{\delta}{2-\delta}} * \beta * 0.375 \qquad (3.4.28)$$

Here δ is the depolarization factor set to 0.0279, and the β factor equals to 0.5.

The Rayleigh optical depth τ is calculated as $\tau = \tau_0 * \frac{P}{P_0}$, where τ_0 is the Rayleigh optical depth at standard surface pressure P_0 (Table 3-18), and P is the local actual pressure. τ_0 is pre-calculated using the 6S subroutine ODRAYL and the sensor spectral response function for standard pressure and temperature profiles.

Adjustment of optical depth $\Delta^s(\tau)$ corresponding to the multiple-scattering term is approximated as:

$$\Delta^s(\tau) = a^s + b^s \ln(\tau) \qquad (3.4.29)$$

Where $a^0 = a_0^0 + a_1^0(\mu_s + \mu_v) + a_2^0\mu_s\mu_v + a_3^0(\mu_s^2 + \mu_v^2) + a_4^0(\mu_s\mu_v)^2$,

$\{a_n^0\}_{n=0,1,\ldots,4}$ = {0.332438, 0.162854, -0.309248, -0.103244, 0.114933} and

$b^0 = b_0^0 + b_1^0(\mu_s + \mu_v) + b_2^0\mu_s\mu_v + b_3^0(\mu_s^2 + \mu_v^2) + b_4^0(\mu_s\mu_v)^2$,

$\{b_n^0\}_{n=0,1,\ldots,4}$ = {-6.7771E-02, 1.577E-03, -1.2409E-02, 3.2417E-02, -3.5037E-02}.

and $a^1 = 0.19666$, $a^2 = 0.145459$; $b^1 = -0.054391$, $b^2 = -0.029108$.

Table 3-18. Rayleigh optical depth at standard surface pressure for the sensor channels*

Channel (VIIRS wavelength: µm)	**VIIRS** τ_0	**ABI** τ_0
M1 (0.412)	0.3189	
M2 (0.445)	0.2336	
M3 (0.488)	0.1605	0.1852
M4 (0.555)	0.0978	
M5 (0.672)	0.0442	0.0542
M6 (0.746)	0.0289	
M7 (0.862)	0.0161	0.0157
M8 (1.240)	0.0037	
M10 (1.610)	0.0013	0.0013
M11 (2.250)	0.0003	0.0003

* Rayleigh optical depth for NOAA-20 VIIRS are listed in Table B-4; Table C-4 for ABI

The Rayleigh reflectance ρ_R is calculated at the actual surface pressure and at the standard pressure, respectively, and used in Eq. 3.4.2 in Section 3.4.1. The dependence on pressure

is realized through the Rayleigh optical depth τ that enters in the calculation of the Rayleigh reflectance.

The Rayleigh transmission $T_R(\mu)$ and spherical albedo S_R are used to correct the optical functions stored in the LUT to the local pressure, which are computed at standard surface pressure. Specifically, the LUT transmissions $T_{R+A}^{\downarrow}$ and $T_{R+A}^{\uparrow}$ in Eq. 3.4.6 and in Eq. 3.4.17 need to be multiplied by the ratio of Rayleigh transmission $T_R(\mu)$ at actual pressure to that at standard pressure; the LUT spherical albedo S_{R+A} in Eq. 3.4.6 and in Eq.(3.4.17) is corrected by adding the difference between the Rayleigh spherical albedo S_R at actual pressure and that at standard pressure. The pressure correction is realized through the Rayleigh optical depth τ .

The analytical expression of Rayleigh transmission function is based on the two-stream method,

$$T_R(\mu) = \frac{[\frac{2}{3} + \mu] + [\frac{2}{3} - \mu]e^{-\tau/\mu}}{\frac{4}{3} + \tau} \qquad (3.4.30)$$

where μ is the cosine of the solar/view zenith angle for downward/upward transmittance, respectively.

For conservative molecular scattering, the spherical albedo S is given by:

$$S_R = \frac{1}{4+3\tau}[3\tau - 4E_3(\tau) + 6E_4(\tau)] \qquad (3.4.31)$$

where E_n is the exponential integral ($E_n(x) = \int_1^\infty \frac{e^{-xt}}{t^n} dt$). The exponential integral is estimated as:

$$E_1(\tau) = \sum_{i=0}^{5} c_i \tau^i - \ln\tau \quad \mathrm{E_1(\tau) = \sum_{i=0}^{5} c_i \tau^i - \ln \tau}$$

(3.4.32)

where τ is the Rayleigh optical depth, coefficients c_i = -0.57721566, 0.99999193, -0.24991055, 0.5519968, -0.00976004, 0.00107857 for i=0 to 5. The recurrence relation is used to calculate $\mathrm{E_n(x)}$ $E_n(x)$ for n>0:

$$E_{n+1}(\tau) = \frac{1}{n}(e^{-\tau} - \tau E_n(\tau)). \qquad (3.4.33)$$

3.4.8 **Algorithm output**

The output of the current algorithm includes aerosol optical depth, aerosol type, and particle size parameter. The parameters are given below in Table 3-19 .. In addition, a number of flags indicating the quality of retrievals are provided. The overall quality flag is set to 'no retrieval' when the retrieval is not applicable or fails, and set to 'low', 'medium' or 'high' quality from the quality control process. The detailed quality flags used to document the inputs, internal tests, retrieval path and performance are listed in Table 3-20 .

Table 3-19 . AOD and APSP algorithm outputs

Name	Type	Description	Dimension
AOD550	output	Retrieved aerosol optical depth at 550 nm	pixel (xsize, ysize)
AOD_channel	output	Retrieved aerosol optical depth in sensor channels M1 to M11	pixel (xsize, ysize) x Nchn
AngsExp1	output	Ångström Exponent calculated from AOD at M4 and M7 over ocean	pixel (xsize, ysize)
AngsExp2	output	Ångström Exponent calculated from AOD at M7 and M10 over ocean	pixel (xsize, ysize)
QCAll	output	Overall quality flag for aerosol retrieval: 0: high quality; 1: medium quality; 2: low quality; 3: no retrieval	pixel (xsize, ysize)
QCExtn,QCInput, QCTest, QCPath, QCRet	output	Detailed input and output quality and critical path flags (see Table 3-20)	pixel (xsize, ysize) x 5
AerMdl	output	Aerosol model selected from prescribed models during the retrieval; 0: oceanic aerosol; 1: dust over land; 2: generic aerosol over land; 3: urban aerosol over land; 4: smoke over land.	pixel (xsize, ysize)
FineMdlIdx	output	Index of fine mode aerosol model over ocean	pixel (xsize, ysize)
CoarseMdlIdx	output	Index of coarse mode aerosol model over ocean	pixel (xsize, ysize)
FineModWgt	output	Fine mode weight over ocean	pixel (xsize, ysize)
SfcRefl	Diagnostic output	Surface reflectance of land and ocean	pixel (xsize, ysize) x Nchn
Residual	Diagnostic output	Retrieval residual of best solution	pixel (xsize, ysize)
SpaStddev	Diagnostic output	3 by 3 standard deviation of TOA reflectance at M1/M11 (land/ocean)	pixel (xsize, ysize)
AOD550LndMdl	Diagnostic output	Retrieved AOD at 550nm for each land aerosol model	pixel (xsize, ysize) x 4
ResLndMdl	Diagnostic output	Retrieval residual for each land aerosol model	pixel (xsize, ysize) x 4
Longitude	Location	Longitude of each pixel	pixel (xsize, ysize)

Latitude	Location	Latitude of each pixel	pixel (xsize, ysize)

Table 3-20 Detailed input and output quality and critical path flags

Name	Bits	Quality Flag Name	Meaning
QCExtn	0,1	Input cloud mask	0: confidently clear; 1: probably clear; 2: probably cloudy; 3: confidently cloudy
	2	Input snow mask	0: no; 1: yes
	3	Input cloud shadow mask	0: no; 1: yes
	4	Input fire mask	0: no; 1: yes
	5	Input glint mask	0: no; 1: yes
	6	Input heavy aerosol mask	0: no; 1: yes
QCInput	0	Input location	0: good; 1: bad - if 1. longitude beyond [-180°,180°] 2. latitude beyond [-90°,90°]
	1	Input geometry	0: good; 1: bad - if 1. zenith angle beyond [0°,90°] 2. azimuth angle beyond [-360°,360°]
	2	Input ancillary data	0: good; 1: bad - if 1. TPW beyond [0,20] cm 2. ozone beyond [0,1] atm-cm 3. surface pressure beyond [500,1500] mb 4. wind speed beyond [0,100] m/s 5. wind direction beyond [0°,360°]
	3	Input reflectance and brightness temperature	0: good; 1: bad - if 1. M1-M11 reflectance beyond [0,1] 2. M15 or M16 brightness temperature beyond [200,350] K 3. M6 reflectance is saturated
QCTest	0	Cloud test	0: no; 1: yes
	1	Cirrus test	0: no; 1: yes
	2	Thin cirrus test	0: no; 1: yes
	3	Inhomogeneity test	0: no; 1: yes
	4	Snow/ice test	0: no; 1: yes
	5	Ephemeral water test	0: no; 1: yes
	6	Shallow water test	0: no; 1: yes
	7	Heavy aerosol test	0: no; 1: yes
QCPath	0	Retrieval over water	0: no; 1: yes
	1	Bright land surface	0: no; 1: yes
	2	Sunglint over water	0: no; 1: yes
	3	SW scheme over dark land	0: no; 1: yes
	4	SWIR scheme over dark land	0: no; 1: yes
	5	Retrieval over bright land	0: no; 1: yes

	6	Retrieval over bright land with dark land scheme	0: no; 1: yes
QCRet	0	Retrieval failed	0: no; 1: yes 1. Missing critical channel reflectances (M3/5/11 over dark land; M1/2/3/5 over bright land; M6 over ocean) 2. Cannot calculate NDVI and redness ratio over dark land 3. Missing ancillary surface reflectance dataset over bright land 4. Arithmetic error (divide by 0)
	1	Large airmass	0: no; 1: yes
	2	Barren land cover type	0: no; 1: yes
	3	Extrapolation	0: no; 1: yes
	4	Large residual	0: no; 1: yes Larger than 0.5 over land; 0.3 over ocean
	5	$NDVI_{SWIR}$ out-of-range	0: no; 1: yes Beyond [-0.1,0.8] over land
	6	Redness ratio out-of-range	0: no; 1: yes Beyond [0.4,1.6] over land
	7	Adjacent to cloud or snow	0: no; 1: yes

In addition, the following metadata information is included in the output:

- MeanAOD : (average of retrieved AOD550)
- RetrievalPct : (percentage of pixels eligible for AOD retrieval)
- MeanAODHighQuality: (average of retrieved high quality AOD550)
- HighQualityPct: (percentage of pixels have high quality AOD retrieval)

Following global attributes are included in the output:

- Conventions : CF-1.5
- Metadata_Conventions : CF-1.5, Unidata Dataset Discovery v1.0
- Metadata_Link : output filename
- ascend_descend_data_flag : 0 (ascend) or 1 (decend)
- cdm_data_type : swath
- channel_center_wavelength: 0.412um,0.445um,0.488um,0.555um,0.672um, 0.746um,0.865um,1.240um,1.378um,1.610um,2.250um,10.76um,12.01um
- channels_used: M1,M2,M3,M4,M5,M6,M7,M8,M9,M10,M11,M15,M16
- date_created :
- day_night_data_flag : night or day
- end_orbit_number :
- geospatial_bounds :
- geospatial_first_scanline_first_fov_lat :
- geospatial_first_scanline_first_fov_lon :
- geospatial_first_scanline_last_fov_lat :

- geospatial_first_scanline_last_fov_lon :
- geospatial_last_scanline_first_fov_lat :
- geospatial_last_scanline_first_fov_lon :
- geospatial_last_scanline_last_fov_lat :
- geospatial_last_scanline_last_fov_lon :
- geospatial_lat_units: degrees_north
- geospatial_lon_units: degrees_east
- history :JRR-AOD v2r0
- id : 306f1124-f260-4909-87df-c8aafee9dc49
- institution : DOC/NOAA/NESDIS/NDE->S-NPP Data Exploitation, NESDIS, NOAA, U.S. Department of Commerce
- instrument_name : VIIRS
- naming_authority : gov.noaa.nesdis.nde
- processing_level : NOAA Level 2
- production_environment : ITE
- production_site : NSOF
- project : JPSS Risk Reduction: Enterprise Aerosol Optical Depth/Particle Size Products
- references :
- resolution : 750M
- satellite_name : NPP
- standard_name_vocabulary : CF Standard Name Table (version 17, 24 March 2011)
- start_orbit_number :
- summary : Enterprise Aerosol Optical Depth/ Aerosol Particle Size Products
- time_coverage_end :
- time_coverage_start :
- title : JRR-AOD

4 Preliminary Validation

4.1 Validation Data

The performance of the algorithm using VIIRS data is evaluated based on the validation against AERONET measurement. Retrievals over AERONET stations are performed for the period of October 26, 2012 to December 31, 2015, and the high and top-2 (high and medium) quality results are evaluated.

AERONET Level 2 Quality Assured direct sun observations of AOD are accurate to within 0.01 [Holben et al., 1998; Eck et al., 1999; Holben et al. 2001]. AERONET provides the best means of quantitatively validating satellite-derived AOD parameters. However, the validation sites are spatially limited and do not offer a complete global evaluation. Especially lacking in the ocean-based AERONET data base leads to an inadequacy to evaluate aerosol products over ocean.

Following the MODIS validation approach [Ichoku et al., 2002], matching with AERONET measurements requires at least 400 pixel retrievals within a circle of 20-km radius centered on the ground stations and at least 2 ground measurements within one-hour time window centered on the VIIRS overpass time. Spatial and temporal averages are performed for each match-up and the retrieval performance is evaluated in terms of accuracy (retrieval bias), precision (standard deviation of retrieval error) and number of available matches. Evaluation of aerosol size parameter (Ångström Exponent) requires the AERONET measured τ_{550} larger than 0.15 due to the susceptible capacity of satellite retrievals under a low aerosol-signal condition [Remer et al., 2002].

4.2 Validation Results

Validation results are listed in Table 4-1 for τ_{550} in the low (<0.1), medium (between 0.1and 0.8) and high (>0.8) value ranges over land (including both dark and bright surface), and in the low (<0.3) and high (≥0.3) value ranges over water, as well as the overall performance of τ_{550} and AE (0.555 vs. 0.865μm) over water. Small positive bias of τ_{550} is shown over land (0.02) and ocean (0.03) for the high quality retrievals with the precision of retrieval over water being almost twice that of land (0.05 vs. 0.11), which are comparable to those of MODIS [Levy, et al., 2015]. For the top-2 quality (high and medium) retrievals, accuracy and precision are inferior to those of high quality. Both the high and top-2 quality τ_{550} and AE retrievals meet the requirements (Table 2-1 and Table 2-2). It is recommended that the high quality results be used for quantitative analysis, and top-2 quality retrievals could be applied to the qualitative applications. The scatter plots of the retrieved VIIRS τ_{550} and AE against the AERONET measurements are shown in
Figure for over land and water.

Table 4-1. Validation statistics of high and top-2 quality VIIRS AOD at 550 nm and Ångström Exponent over cocean (0.555 vs. 0.865μm).

Statistics	**AOD550 Over Land** High/Top2 Quality	**AOD550 Over Water** High/Top2 Quality	**AE Over Water (0.555 vs. 0.865μm)** High/Top2 Quality
Low AOD: AERONET τ_{550} < 0.1 over land; τ_{550} < 0.3 over water			
Accuracy	0.035 / 0.058	0.030 / 0.048	
Precision	0.073 / 0.101	0.037 / 0.051	
Number	27,083 / 34,170	11,077 / 14,322	
Medium AOD: 0.1 ≤ AERONET τ_{550} ≤ 0.8 over land			
Accuracy	0.001 / 0.036		
Precision	0.122 / 0.151		
Number	23,614 / 30,180		
High AOD: AERONET τ_{550} > 0.8 over land; τ_{550} ≥ 0.3 over water			
Accuracy	-0.029 / -0.003	0.023 / 0.054	
Precision	0.380 / 0.396	0.105 / 0.124	
Number	1,208 / 1,265	935 / 1,316	
All retrievals			

Accuracy	0.018 / 0.047	0.030 / 0.049	0.050 / 0.001
Precision	0.112 / 0.138	0.046 / 0.060	0.377 / 0.370
Number	51,676 / 65,615	12,012 / 15,638	3,186 / 4,303

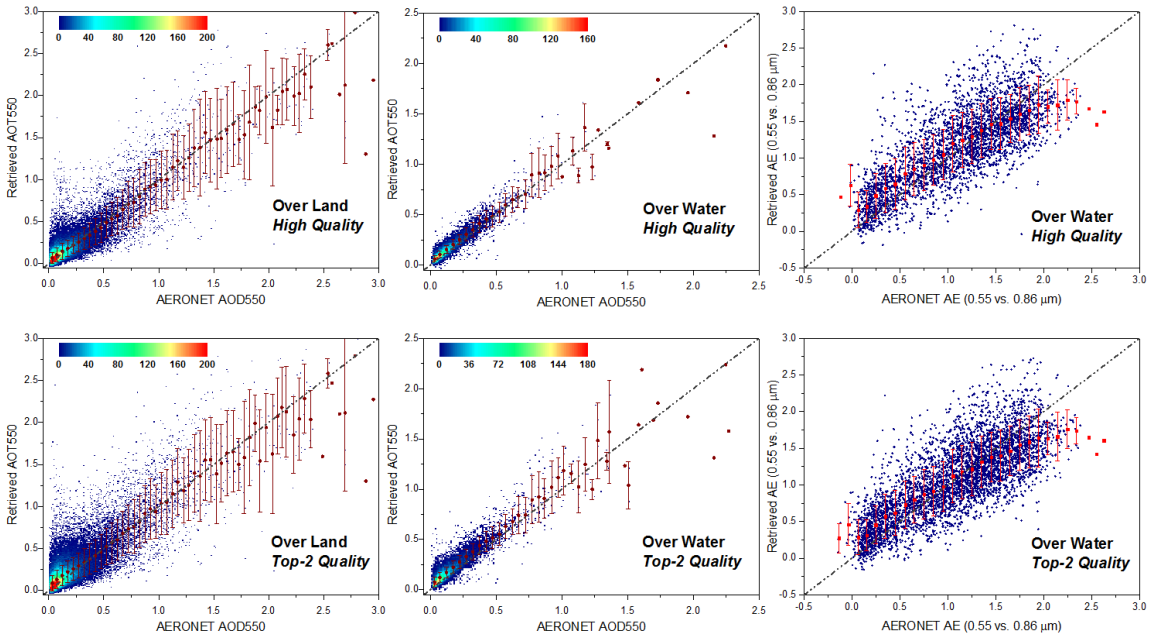

Figure 4-1. Scatter plots of high (top) and top-2 (bottom) quality retrieved VIIRS τ_{550} against AERONET measurements over land (left) and water (middle); and retrieved VIIRS AE (0.555 vs. 0.865µm) against AERONET measurements over water (right).

5 PRACTICAL CONSIDERATIONS

5.1 Numerical Computation Considerations

The LUT approach uses pre-calculated values of spectral atmospheric transmittances, reflectances, spherical albedo and surface BRDF as functions of AOD at 550 nm, aerosol models, geometries and ocean surface wind speeds. In the LUT, following the NPP/VIIRS approach [Vermote et al., 2006], the TOA is given as a function of scattering angle with an interval of 4 degrees. The range of scattering angles is calculated from the solar and local zenith angles and the relative azimuth angle. This method provides a relatively rapid search of the LUT. Just like in the standard MODIS algorithm [Remer et al., 2005], the interval halving method is used in LUT for searching for the "best" combination of fine and coarse mode of ocean aerosol models; this increases efficiency as well.

5.2 Programming and Procedural Considerations

The aerosol retrieval is carried out pixel by pixel. It requires calibrated and geo-located sensor reflectances, upstream cloud, fire and snow/ice mask as sensor-specific dynamic

input, which could be common to retrieval of other products and handled in the framework outside of the aerosol retrieval software package. The programming design uses modules, providing the flexibility for ease upgrades.

The data that need to be configurable for future updates include algorithm coefficients (LUT and land surface reflectance relationship) and criterion values (e.g. selecting atmospheric conditions) are put in an external file for the convenience of updates.

5.3 Quality Assessment and Diagnostics

The quality assessment of retrievals is described in Section 3.4.2.5 and 3.4.3.5. Valid retrievals are assigned low, medium or high quality based on the inputs and retrieval diagnostic variables (e.g., retrieval residual). It is recommended that high quality results be used for quantitative analysis and the top-2 (above-low) quality retrievals be used for qualitative demonstration and investigation.

There are several diagnostics including the spectral surface reflectance at the channels used for retrieval, retrieval residual, and individual retrieval results for each candidate land aerosol models that can be outputted as set by a configuration flag. Combined with the outputs of AOD and selected aerosol models, these diagnostics can provide more information for diagnosing the deficiencies of the retrieval algorithm for future improvements. Writing out the diagnostics will increase the output file size, so it is recommended only for diagnosis mode and not suggested to be used for operational process, except the residuals and individual retrieval results for each candidate land aerosol models that are required by the surface reflectance downstream product.

5.4 Exception Handling

The quality control flags from the flagged Level 1b sensor input data, including bad sensor input data, missing sensor input data and validity of each aerosol channel are checked. The algorithm also checks for conditions not favorable for aerosol retrieval and generates quality control flags based on the input cloud, fire, snow/ice, glint, cloud shadow and land/water flags, as well as the internal test results. In addition, the algorithm checks for the availability of the ancillary input data files (LUTs, coefficients and surface cover type), attempt to divide by zero, and errors associated with dynamic memory allocation and deallocation.

6 ASSUMPTIONS AND LIMITATIONS

This section describes the limitations and assumptions in the current version of the aerosol retrieval algorithm, and potential future enhancements to the algorithm.

6.1 Performance

The following assumptions have been made in the current algorithm developing:

- Aerosol shape is spherical except for the dust over land.
- The vertical profile of aerosol concentration is assumed to be exponentially decreasing with a scale height of 2km. The impact of fixed aerosol profile may be tolerated at sensor channels where molecular scattering and absorption is minimal.
- Surface reflectance of ocean can be calculated and that of land can be estimated with sufficient accuracy;
- Land surface is dark and Lambertian. (An alternative algorithm over bright land surface is currently being developed that may extend the retrievals for snow-free land surface.)
- Calibrated and geo-located radiances in relevant sensor channels are available.
- Ancillary data are available.

The limitations in the current retrieval algorithm are:

- Retrieval limited to dark surface. (This limitation will be eliminated in the next delivery of the algorithm that will include retrieval over bright snow-free surface.) ;
- Retrieval limited to clear-sky conditions;
- Retrieval limited to daytime only;
- Retrievals may be impacted by residual cloud, snow, shadow, and other undetected unfavorable conditions.

6.2 Assumed Sensor Performance

The calibrated and geo-located channel radiances are assumed to be available for the current aerosol retrieval algorithm. A loss of channel M3 over land and M7 over ocean will disable the algorithm as they are reference channels for retrieving aerosol in this algorithm.

REFERENCES

Ackerman, A.S., O.B. Toon, D.E. Stevens, A.J. Heymsfield, V. Ramanathan, and E.J. Welton, Reduction of tropical cloudiness by soot, *Science*, 288, 1042-1047, 2000.

Albrecht, B.A., Aerosols, cloud microphysics, and fractional cloudiness, *Science*, 245, 1227-1230, 1989.

Bessho, K., K. Date, M. Hayashi, A. Ikeda, T. Imai, H. Inoue, Y. Kumagai, T. Miyakawa, H. Murata, T. Ohno, A. Okuyama, R. Oyama, Y. Sasaki, Y. Shimazu, K. Shimoji, Y. Sumida, M. Suzuki, H. Taniguchi, H. Tsuchiyama, D. Uesawa, H. Yokota, and R. Yoshida, An introduction to Himawari-8/9 - Japan's new-

generation geostationary meteorological satellites. *J. Meteor. Soc. Japan*, 94, doi:10.2151/jmsj.2016-009, 2016.

Bohren, C.F., and D.R. Huffman, *Absorption and Scattering of Light by Small Particles*, John Wiley, Hoboken, N.J., 1983.

Chameides, W.L., et al., A case study of the effects of atmospheric aerosols and regional haze on agriculture: An opportunity to enhance crop yields in China through emission controls? *Proc. Natl. Acad. Sci.*, 96, 13,626-13,633, 1999.

Charlson, R.J., S.E. Schwartz, J.M. Hales, R.D. Cess, J.A. Coakley, J.E. Hansen, and D.J. Hofmann, Climate forcing by anthropogenic aerosols, *Science*, 255, 423-430, 1992.

Coakley, J.A., R.D. Cess, and F.B. Yurevich, The effect of tropospheric aerosols on the Earth's radiation budget: a parameterization for climate models, *J. Atmos. Sci.*, 40, 116-138, 1983.

Cox, C. and W. Munk, Statistics of the sea surface derived from sun glitter. *J. Mar. Res.*, 13, 198-208, 1954.

Diner, D.J., J.C. Beckert, T.H. Reilly, C.J. Bruegge, J.E. Conel, R. Kahn, J.V. Martonchik, T.P. Ackerman, R. Davies, S.A.W. Gerstl, H.R. Gordon, J-P. Muller, R. Myneni, R.J. Sellers, B. Pinty, and M.M. Verstraete, Multiangle Imaging SpectroRadiometer (MISR) description and experiment overview, *IEEE Trans. Geosci. Remt. Sensing,* **36**, 1072-1087, 1998.

Dubovik, O., et al., Application of spheroid models to account for aerosol particle nonsphericity in remote sensing of desert dust, *J. Geophys. Res.*, 111, D11208, doi:10.1029/2005JD006619, 2006.

Eck, T. F., B. N. Holben, J. S. Reid, O. Dubovik, A. Smirnov, N. T. O'Neill, I. Slutsker, and S. Kinne, Wavelength dependence of the optical depth of biomass burning, urban, and desert dust aerosols, *J. Geophys. Res*., 104, 31,333–31,349, doi:10.1029/1999JD900923, 1999.

Fraser, R.S., Satellite measurement of mass of Sahara dust in the atmosphere. *Appl. Opt.,* **15,** 2471–2479, 1976.

Geogdzhayev, I.V., M.I. Mishchenko, W.B. Rossow, B. Cairns, and A.A. Lacis, Global two-channel AVHRR retrievals of aerosol properties over the ocean for the period of NOAA-9 observations and preliminary retrievals using NOAA-7 and NOAA-11 data. *J. Atmos. Sci.*, **59**, 262-278, doi:10.1175/1520-0469(2002)059<0262:GTCARO>2.0.CO;2, 2002.

Griggs, M., Measurements of atmospheric aerosol optical thickness using ERTS-1 data, *J. Air pollut. Control Assoc*., 25, 622-626, 1975.

Hansen, J., M. Sato, and R. Ruedy, Radiative forcing and climate response, *J. Geophys. Res.*, 102, 6831-6864, 1997.

Higurashi A. and T. Nakajima, "Development of a two channel aerosol retrieval algorithm on global scale using NOAA AVHRR." *J. Atmos. Sci*., **56**, 924–941, 1999.

Holben B.N., et al., AERONET - A federated instrument network and data archive for aerosol characterization, *Rem. Sens. Environ.*, 66, 1-16, 1998.

Holben, B.N., et al., An emerging ground-based aerosol climatology: Aerosol Optical Depth from AERONET, *J. Geophys. Res.*, 106, 12,067-12,097, 2001

Hsu, N. C., Tsay, S. C., King, M. D., & Herman, J. R. (2006). Deep blue retrievals of Asian aerosol properties during ACE-Asia. *Ieee Transactions on Geoscience and Remote Sensing, 44*(11), 3180-3195. doi: 10.1109/tgrs.2006.879540

Hsu, N. C.,M.-J. Jeong, C. Bettenhausen, A.M. Sayer, R. Hansell, C. S. Seftor, J. Huang, and S.-C. Tsay, Enhanced Deep Blue aerosol retrieval algorithm: The second generation, *J. Geophys. Res. Atmos.*, 118, 9296–9315, doi:10.1002/jgrd.50712, 2013.

Ichoku, C., et al., A spatio-temporal approach for global validation and analysis of MODIS aerosol products, *Geophys. Res. Lett.*, 29(12): art. no.-1616, 2002.

Jackson, J. M., H. Q. Liu, I. Laszlo, S. Kondragunta, L. A. Remer, J. F. Huang and H. C. Huang (2013). Suomi-NPP VIIRS aerosol algorithms and data products. *Journal of Geophysical Research-Atmospheres* **118**(22): 12673-12689.

Joint Polar Satellite System (JPSS) (2014). Joint Polar Satellite System (JPSS) VIIRS Cloud Mask (VCM) Algorithm Theoretical Basis Document (ATBD). http://www.star.nesdis.noaa.gov/jpss/documents/ATBD/D0001-M01-S01-011_JPSS_ATBD_VIIRS-Cloud-Mask_E.pdf.

Kahn, R.A., B.J. Gaitley, M.J. Garay, D.J. Diner, T. Eck, A. Smirnov, and B.N. Holben, Multiangle Imaging SpectroRadiometer global aerosol product assessment by comparison with the Aerosol Robotic Network. *J. Geophys. Res*. **115,** D23209, doi: 10.1029/2010JD014601, 2010.

Kaufman, Y. J., and L. Remer, "Detection of forests using mid-IR reflectance: An application for aerosol studies," *IEEE Trans. Geosci*. *Remote Sensing,* vol. 32, pp. 672–683, 1994.

Kaufman, Y. J., and D. Tanré, Algorithm for Remote Sensing of Troposheric Aerosol from MODIS, *http://eospso.gsfc.nasa.gov/atbd/modistables.html*, 1996

Kaufman, Y. J., D. Tanré, et al., Operational remote sensing of tropospheric aerosol over land from EOS moderate resolution imaging spectroradiometer, *J. Geophys. Res.*, 102(D14): 17051-17067, 1997.

King, M.D., D.M. Byrne, B.M. Herman and J.A. Reagan, Aerosol size distribution obtained by inversion of optical depth measurements, *J. Atmos. Sci*., 35, 2153- 2167, 1978.

Knapp, K. R., Vonder Haar, T. H., & Kaufman, Y. J. (2002). Aerosol optical depth retrieval from GOES-8: Uncertainty study and retrieval validation over South America. *Journal of Geophysical Research-Atmospheres, 107*(D7-8). doi: Artn 4055 10.1029/2001jd000505

Koepke, P., Effective reflectance of oceanic whitecaps, *Appl. Opt.*, 23, 1816-1823, 1984.

Kondragunta, S., I. Laszlo, H. Zhang, P. Ciren and A. Huff (2020). Chapter 17 - Air quality applications of abi aerosol products from the GOES-R Series. *The GOES-R Series*. S. J. Goodman, T. J. Schmit, J. Daniels and R. J. Redmon, Elsevier: 203-217.

Koren, I.Y., Y.J. Kaufman, L.A. Remer, and J.V. Martins, Measurement of the effect of Amazon smoke on inhibition of cloud formation, *Science*, 303, 1342, 2004.

Kotchenova S.Y., E.F. Vermote, R. Matarrese, and F.J. Klemm, Jr., Validation of a vector version of the 6S radiative transfer code for atmospheric correction of satellite data. Part I: Path radiance, *Appl. Opt.*, 45, 6762-6774, 2006.

Kotchenova S.Y. and E.F. Vermote, Validation of a vector version of the 6S radiative transfer code for atmospheric correction of satellite data. Part II. Homogeneous Lambertian and anisotropic surfaces, *Appl. Opt.*, 46, 4455-4464, 2007.

Laszlo, I., Ciren, P., Liu, H. Q., Kondragunta, S., Tarpley, J. D., & Goldberg, M. D. (2008). Remote sensing of aerosol and radiation from geostationary satellites. *Advances in Space Research, 41*(11), 1882-1893. doi: DOI 10.1016/j.asr.2007.06.047

Laszlo, I. (2018). Remote sensing of tropospheric aerosol optical depth from multispectral monodirectional space-based observations. *Comprehensive Remote Sensing*. S. Liang. Oxford, Elsevier: 137-196.

Levy, R.C., L.A. Remer, and O. Dubovik, Global aerosol optical properties and application to Moderate Resolution Imaging Spectroradiometer aerosol retrieval over land, *J. Geophys. Res.*, 112(D13210), doi: 10.102, 2007a.

Levy, R. C., L. A. Remer, S. Mattoo, E. F. Vermote, and Y. J. Kaufman (2007), Second-generation operational algorithm: Retrieval of aerosol properties over land from inversion of Moderate Resolution Imaging Spectroradiometer spectral reflectance, *J. Geophys. Res.,* 112, D13211, doi:10.1029/2006JD007811, 2007b.

Levy, R. C., Munchak, L. A., Mattoo, S., Patadia, F., Remer, L. A., and Holz, R. E.: Towards a long-term global aerosol optical depth record: applying a consistent aerosol retrieval algorithm to MODIS and VIIRS-observed reflectance, *Atmos. Meas. Tech.*, 8, 4083-4110, doi:10.5194/amt-8-4083-2015, 2015.

Liu, H. Q., L. A. Remer, J. F. Huang, H. C. Huang, S. Kondragunta, I. Laszlo, M. Oo and J. M. Jackson (2014). Preliminary evaluation of S-NPP VIIRS aerosol optical thickness. *Journal of Geophysical Research-Atmospheres* 119(7): 3942-3962.

Mekler Y., H. Quenzel, G.Ohring, and I.Marcus , Relative atmospheric aerosol content from ERTS observations. *J. Geophys. Res*., **82**, 967–972, 1977.

Pope, C Arden; et al., Cancer, cardiopulmonary mortality, and long-term exposure to fine particulate air pollution, *J. Amer. Med. Assoc.* 287: 1132–1141, doi:10.1001/jama.287.9.1132, 2002.

Prados, A. I., Kondragunta, S., Ciren, P., & Knapp, K. R. (2007). GOES Aerosol/Smoke product (GASP) over North America: Comparisons to AERONET and MODIS observations. *Journal of Geophysical Research-Atmospheres, 112*(D15). doi: Artn D15201 10.1029/2006jd007968

Ramanathan, V., P.J. Crutzen, J.T. Kiehl, and D. Rosenfeld, Aerosols, climate, and the hydrological cycle, *Science*, 294, 2119-2124, 2001

Rao, C.R.N, EP McClain, and LL Stowe, Remote sensing of aerosols over the oceans using AVHRR data theory, practice, and applications. *Int. J. Remote Sens.* **10**(4–5), 743–749, 1989.

Remer, L. A., D. Tanré, Y. J. Kaufmann, C. Ichoku, S. Mattoo, R. Levy, D. A. Chu, B. Holben, O. Dubovik, A. Smirnov,J. V. Martins, R.-R. Li, and Z. Ahmad, Validation of MODIS aerosol retrieval over ocean, *Geophys. Res. Lett*.,29(12), doi:10.1029/2001GL013204, 2002.

Remer, L. A., Y. J. Kaufman, et al., The MODIS aerosol algorithm, products, and validation, *J. Atmos. Sci.*, 62(4), 947-973, 2005

Remer, L. A., D. Tanre, Y.J. Kaufman, R. Levy and S. Mattoo, Algorithm for Remote Sensing of Tropospheric aerosol from MODIS: Collection 5, Product ID MOD04/MYD04, 2006.

Rosenfeld, D., and I.M. Lensky, Satellite-based insights into precipitation formation processes in continental and maritime convective clouds, *Bull. Am. Met. Soc.*, 79, 2457-2476, 1998.

Sayer, A. M., Hsu, N. C., Bettenhausen, C., & Jeong, M. J. (2013). Validation and uncertainty estimates for MODIS Collection 6 "Deep Blue" aerosol data. *Journal of Geophysical Research-Atmospheres, 118*(14), 7864-7872. doi: 10.1002/jgrd.50600

Stowe L. L., R. Hitzenberger, and A. Deepak, Report on *Experts Meeting on Space Observations of Tropospheric Aerosols and Complementary Measurements*, WCRP-48, WMO/TD-No. 389, World Meteorological Organization, 1990.

Stowe, L. L., A. M. Ignatov, and R. R. Sing, Development, validation, and potential enhancements to the second-generation operational aerosol product at the National Environmental Satellite, Data, and Information Service of the National Oceanic and Atmospheric Administration, *J. Geophys. Res*., 102, 16,923-16,934, 1997.

Tanré, D., Y. J. Kaufman, et al., Remote sensing of aerosol properties over oceans using the MODIS/EOS spectral radiances, *J. Geophys. Res.,* 102(D14), 16971-16988, 1997.

Tanré D., F.M. Bréon, J.L. Deuzé, O. Dubovik, F. Ducos, P. François, P. Goloub, M. Herman, A. Lifermann, F. Waquet, Remote sensing of aerosols by using polarized, directionnal and spectral measurements within the A-Train: the PARASOL mission, *Atmos. Meas. Tech.*, **4**, 1383-1395, doi:10.5194/amt-4-1383-1395-2011, 2011.

Twomey, S., The influence of pollution on the shortwave albedo of clouds, *J. Atmos. Sci.*, 34, 1149-1152, 1977.

Vermote, E. and D. Tanré, Analytical expressions for radiative properties of planar rayleigh scattering media, including polarization contributions. *J. Quant. Spectrosc. Radiat. Tansfer*, Vol. 47, No. 4, 305-314, 1992.

Vermote, E. F., D. Tanre, J. L. Deuze, M. Herman, and J. J. Morcrette, Second Simulation of the Satellite Signal in the Solar Spectrum, 6S: An overview, *IEEE Trans. Geosci. Remote Sens.,* 35(3), 675-686, 1997.

Vermote, E. F., D. Tanré, J. L. Deuzé, M. Herman, J. J. Morcrette, S. Y. Kotchenova, and T. Miura, Second Simulation of the Satellite Signal in the Solar Spectrum (6S), 6S User Guide Version 3, November, 2006, http://www.6s.ltdri.org

Vermote, E. F., and S. Kotchenova, Atmospheric correction for the monitoring of land surfaces, *J. Geophys. Res*., 113, D23S90,doi:10.1029/2007JD009662, 2008.

Wang, M., and H.R. Gordon, Radiance reflected from the ocean-atmosphere system: synthesis from individual components of the aerosols size distribution, *Appl. Opt.*, 33, 7088-7095, 1994.

Yu, H., S.C. Liu, and R.E. Dickinson, Radiative effects of aerosols on the evolution of the atmospheric boundary layer, *J. Geophys. Res.*, 107, 4142, 2002.

Zhang H. et al., An enhanced VIIRS aerosol optical thickness (AOT) retrieval algorithm over land using a global surface reflectance ratio database, submitted to *J. Geophys. Res.*, 2016.

APPENDIX

A. Sunglint directional reflectance

In calculating the reflectance of water Cox and Munk (1954) considered the system of coordinates (P,X,Y,Z) where P is the observed point, Z the altitude, PY is pointed to the sun direction and PX to the direction perpendicular to the sun plane. Using spherical trigonometry, the components of surface slope Z_x and Z_y which is so inclined to reflect an incoming ray from the sun toward the satellite can be related to the sun-satellite geometry through:

$$Z_X = \frac{-\sin(\theta_v)\sin(\phi_s - \phi_v)}{\cos(\theta_s)+\cos(\theta_v)}; \quad \text{(A-1)}$$

$$Z_Y = \frac{\sin(\theta_s)+\sin(\theta_v)\cos(\phi_s - \phi_v)}{\cos(\theta_s)+\cos(\theta_v)} \quad \text{(A-2)}$$

To simplify the calculation, the (P,X,Y) coordinate system is rotated to a new set of principal axes (P, X', Y') with PY' parallel to the wind direction. The slope components are now expressed as:

$$Z'_X = \cos(\chi) Z_X + \sin(\chi) Z_Y; \quad \text{(A-3)}$$

$$Z'_Y = -\sin(\chi) Z_X + \cos(\chi) Z_Y, \quad \text{(A-4)}$$

where χ is the relative azimuth angle between sun and wind direction. The possibility for the occurrence of such slope is calculated as:

$$p(Z'_X, Z'_Y) = (2\pi\sigma'_X\sigma'_Y)^{-1} \exp\left(-\frac{\xi^2+\eta^2}{2}\right) \times \left\{ \begin{array}{l} 1-\frac{1}{2}C_{21}(\xi^2-1)\eta - \frac{1}{6}C_{03}(\eta^3-3\eta) + \frac{1}{24}C_{40}(\xi^4-6\xi^2+3) + \\ \frac{1}{4}C_{22}(\xi^2-1)(\eta^2-1) + \frac{1}{24}C_{04}(\eta^4-6\eta^2+3) \end{array} \right\} \quad \text{(A-5)}$$

where $\xi = Z'_X / \sigma'_X$ and $\eta = Z'_Y / \sigma'_Y$. σ'_X and σ'_Y are the root mean square values of Z'_X and Z'_Y, the skewness coefficients C_{21} and C_{03}, and the peakedness coefficients C_{40}, C_{22} and C_{04} have been defined by Cox and Munk for a clean surface as follows:

$$\sigma'^{\,2}_X = 0.003 + 0.00192ws; \quad \sigma'^{\,2}_Y = 0.00316ws$$

$$C_{21} = 0.01 - 0.0086ws; \; C_{03} = 0.04 - 0.033ws$$

$$C_{40} = 0.40, \; C_{22} = 0.12; \; C_{04} = 0.23,$$

where WS is the wind speed with a lower limit of 0.1 m/s and upper limit of 14 m/s to ensure numerical stability.

The directional reflectance is written as:

$$\rho_{sgt}(\theta_s,\theta_v,\phi_s,\phi_v)=\frac{\pi\cdot p(Z_X^{'},Z_Y^{'})\cdot R(n_r,n_i,\theta_s,\theta_v,\phi_s,\phi_v)}{4\cdot\cos\theta_s\cdot\cos\theta_v\cdot\cos^4\beta}, \quad \text{(A-6)}$$

where β is the tilt ($\tan\beta=\sqrt{Z_X{}^2+Z_Y{}^2}$).

Fresnel's reflection Coefficient $R(nr,ni,\theta_s,\theta_v,\phi_x,\phi_v)$ is computed as:

$$R(nr,ni,\theta_s,\theta_v,\phi_s,\phi_v)=\frac{1}{2}\left\{\frac{\left[(n_r^2-n_i^2)\cos\theta_i-u\right]^2+\left[2n_rn_i\cos\theta_i+v\right]^2}{\left[(n_r^2-n_i^2)\cos\theta_i+u\right]^2+\left[2n_rn_i\cos\theta_i-v\right]^2}+\frac{(\cos\theta_i-u)^2+v^2}{(\cos\theta_i+u)^2+v^2}\right\} \quad \text{(A-7)}$$

where,

$$u^2=\frac{1}{2}\left\{\left|n_r^2-n_i^2-\sin^2\theta_i\right|+\sqrt{(n_r^2-n_i^2-\sin^2\theta_i)^2+4n_r^2n_i^2}\right\}$$

$$v^2=\frac{1}{2}\left\{-\left|n_r^2-n_i^2-\sin^2\theta_i\right|+\sqrt{(n_r^2-n_i^2-\sin^2\theta_i)^2+4n_r^2n_i^2}\right\}$$

$$\cos\theta_i=\sqrt{\frac{1}{2}\left[1+\cos\theta_s\cos\theta_v+\sin\theta_s\sin\theta_v\cos(\phi_s-\phi_v)\right]}$$

$$\sin\theta_i=\sqrt{\frac{1}{2}\left[1-\cos\theta_s\cos\theta_v-\sin\theta_s\sin\theta_v\cos(\phi_s-\phi_v)\right]}$$

Normalized integral of downward diffuse radiation by sunglint directional reflectance $\overline{\rho_{sgt}}$ is pre-calculated using the 6S RTM and stored in LUT for varying geometry (solar zenith angle, local zenith angle, and relative azimuth (sun – satellite)), aerosol model and optical depth, and surface wind speed (see Section 3.4.2.3). $\overline{\rho_{sgt}^{'}}$ is the normalized integral of upward diffuse radiation by sunglint directional reflectance and can be obtained from the same LUT as $\overline{\rho_{sgt}}$ by swapping solar zenith and local zenith angles. Linear interpolation is used for intermediate values of arguments from LUT. Noted that wind direction is fixed when calculating $\overline{\rho_{sgt}}$ and $\overline{\rho_{sgt}^{'}}$ in the glint LUT, but not for explicit calculation of specular reflection (calculated with analytical Fresnel Equation).

The sunglint spherical albedo $\overline{\overline{\rho_{sgt}}}$ is also calculated following 6S RTM. In each VIIRS channel, the sunglint spherical albedo decreases with wind speed from 2 to 14 m/s by about 5%, therefore it is parameterized as a function of surface wind speed.

B. Spectral Constants for NOAA20 VIIRS

Table B-1 Whitecap effective reflectance $\rho_{wc\text{-}eff}$ and underwater reflectance ρ_w for NOAA-20 VIIRS.

Channel (wavelength: µm)	ρ_{wc-eff}	ρ_w
M4 (0.559)	0.2200	0.0064
M5 (0.671)	0.2200	0.0009
M6 (0.746)	0.2177	0.0
M7 (0.879)	0.2110	0.0
M8 (1.240)	0.1669	0.0
M10 (1.621)	0.1010	0.0
M11 (2.263)	0.0619	0.0

Table B-2 Seawater index of refraction for NOAA-20 VIIRS

Channel (wavelength: µm)	Refractive Index	
	Real Part	Imaginary Part
M4 (0.559)	1.339	2.577E-09
M5 (0.671)	1.337	2.145E-08
M6 (0.746)	1.336	1.467E-07
M7 (0.879)	1.334	4.054E-07
M8 (1.240)	1.329	3.557E-05
M10 (1.621)	1.322	8.860E-05
M11 (2.263)	1.297	4.984E-04

Table B-3. Gaseous absorption coefficients for NOAA-20 VIIRS channels.

VIIRS Channels	$C_{1,\lambda}^{H_2O}$	$C_{2,\lambda}^{H_2O}$	$C_{3,\lambda}^{H_2O}$	$C_{\lambda}^{O_3}$	$C_{1,\lambda}^{Gas}$	$C_{2,\lambda}^{Gas}$	$C_{3,\lambda}^{Gas}$	$C_{4,\lambda}^{Gas}$	$C_{5,\lambda}^{Gas}$	$C_{6,\lambda}^{Gas}$
M1	0.0	0.0	0.0	0.0	0.0	0.0	0.0	0.0	0.0	0.0
M2	0.0	0.0	0.0	2.72E-03	0.0	0.0	0.0	0.0	0.0	0.0
M3	0.0	0.0	0.0	1.93E-02	0.0	0.0	0.0	0.0	0.0	0.0
M4	-5.15E-05	-2.40E-04	5.79E-06	9.41E-02	0.0	0.0	0.0	0.0	0.0	0.0
M5	-7.65E-04	-1.13E-03	9.91E-05	4.70E-02	0.0	0.0	0.0	0.0	0.0	0.0
M6	-2.62E-03	-2.41E-03	3.63E-04	1.03E-02	-1.69E-04	5.96E-04	-3.02E-04	-9.03E-03	7.97E-05	-1.46E-04
M7	-1.11E-03	2.15E-04	1.47E-04	0.0	0.0	0.0	0.0	0.0	0.0	0.0
M8	-2.17E-03	-1.92E-03	2.89E-04	0.0	-3.44E-04	5.26E-04	-9.61E-04	-1.20E-03	2.53E-05	-1.32E-04
M10	-9.32E-04	4.49E-04	1.10E-04	0.0	-1.52E-02	2.12E-02	-6.99E-03	-4.48E-02	3.05E-03	-4.40E-03
M11	-6.81E-04	-1.18E-03	8.82E-05	0.0	-4.85E-02	4.44E-03	-1.09E-02	-9.91E-03	7.99E-03	-6.99E-04

Table B-4. Rayleigh optical depth at standard surface pressure for the NOAA-20 VIIRS channels

Channel (wavelength: µm)	**NOAA-20 VIIRS** τ_0
M1 (0.415)	0.3222
M2 (0.450)	0.2328
M3 (0.492)	0.1583
M4 (0.569)	0.0930
M5 (0.671)	0.0445
M6 (0.746)	0.0283
M7 (0.879)	0.0154
M8 (1.240)	0.0037
M10 (1.621)	0.0013
M11 (2.263)	0.0003

C. Spectral Constants for ABI

Table C-1 Whitecap effective reflectance $\rho_{wc\text{-}eff}$ and underwater reflectance ρ_w for ABI bands.

ABI Band (wavelength: μm)	ρ_{wc-eff}	ρ_w
B2 (0.64)	0.2200	0.00131
B3 (0.86)	0.2120	0.0
B5 (1.6)	0.1005	0.0
B6 (2.2)	0.0625	0.0

Table C-2 Seawater index of refraction for ABI bands

ABI Band (wavelength: μm)	**Refractive Index**	
	Real Part	**Imaginary Part**
B2 (0.64)	1.337	1.540E-08
M7 (0.86)	1.335	3.322E-07
M10 (1.6)	1.323	8.698E-05
M11 (2.2)	1.298	4.558E-04

Table C-3. Gaseous absorption coefficients for ABI bands.

ABI bands (VIIRS)	$C_{1,\lambda}^{H_2O}$	$C_{2,\lambda}^{H_2O}$	$C_{3,\lambda}^{H_2O}$	$C_{\lambda}^{O_3}$	$C_{1,\lambda}^{Gas}$	$C_{2,\lambda}^{Gas}$	$C_{3,\lambda}^{Gas}$	$C_{4,\lambda}^{Gas}$	$C_{5,\lambda}^{Gas}$	$C_{6,\lambda}^{Gas}$
B1 (M3)	0.0	0.0	0.0	1.25E-02	0.0	0.0	0.0	0.0	0.0	0.0
B2 (M5)	-2.54E-03	-3.93E-05	2.28E-04	8.53E-02	-5.04E-04	1.29E-03	-1.21E-03	-2.35E-03	1.72E-04	-2.95E-04
B3 (M7)	-1.53E-03	-1.79E-05	6.62E-05	0.0	0.0	0.0	0.0	0.0	0.0	0.0
B5 (M10)	-1.19E-03	9.45E-07	-5.64E-05	0.0	-1.48E-02	2.07E-02	-6.63E-03	-4.36E-02	2.95E-03	-4.30E-03
B6 (M11)	-3.71E-03	-4.03E-05	-6.29E-04	0.0	-3.30E-02	1.89E-03	-1.17E-02	-6.72E-03	4.65E-03	-1.69E-04

Table C-4. Rayleigh optical depth at standard surface pressure for the ABI bands

ABI Bands (wavelength: µm)	τ_0
B1 (0.47)	0.1852
B2 (0.64)	0.0542
B3 (0.86)	0.0157
B4 (1.37)	0.0024
B5 (1.60)	0.0013
B6 (2.20)	0.0003

Table C-5. ABI coefficients in the spectral surface reflectance relationship for various categories of dark land cover types.

Channels	c_0	c_1	c_2	c_3	c_4	c_5	c_6	c_7	RMSE	R^2	%Error
Forest, land cover type 1-5, #: 657,135 (37.60%)											
M5 vs. M11	0.018	-0.028	0.0	-5.4E-05	0.25	0.32	0.0	7.5E-04	0.0058	0.93	9.16
M3 vs. M5	0.0057	0.018	0.0	1.3E-04	0.81	-0.48	0.0	-1.7E-03	0.0046	0.86	10.0
M11 vs. M5	-3.4E-03	0.017	0.0	4.0E-04	2.63	-1.85	0.0	-3.8E-03	0.010	0.96	7.88
Woodland and woodedgrass, land cover type 6 and 7, #:595,564 (34.07%)											
M5 vs. M11	0.011	-9.1E-03	0.0	-1.4E-05	0.39	2.3E-03	0.0	8.9E-04	0.0085	0.87	9.98
M3 vs. M5	-5.4E-03	0.011	0.0	1.2E-04	0.63	-0.084	0.0	-6.4E-04	0.0060	0.82	11.71
M11 vs. M5	0.097	-0.092	0.0	-9.0E-05	0.94	0.064	0.0	3.8E-03	0.014	0.90	9.22
Closed/open shrublands, land cover type 8 and 9, #:118,055 (6.75%)											
M5 vs. M11	9.2E-03	-0.024	0.0	9.6E-05	0.56	-0.033	0.0	4.0E-04	0.015	0.77	9.44
M3 vs. M5	3.4E-04	0.016	0.0	1.7E-04	0.60	-0.25	0.0	-8.7E-04	0.0098	0.74	9.47
M11 vs. M5	0.086	-0.092	0.0	3.0E-04	0.92	0.025	0.0	-4.4E-04	0.019	0.79	7.53
Grasses and cropland, land cover type 10 and 11, #:349,043 (19.97%)											
M5 vs. M11	0.049	-0.068	0.0	-1.5E-04	0.23	0.25	0.0	1.9E-03	0.015	0.82	12.9
M3 vs. M5	-9.4E-03	0.017	0.0	2.5E-04	0.70	-0.25	0.0	-1.7E-03	0.0073	0.86	10.42
M11 vs. M5	0.13	-0.12	0.0	2.9E-04	0.63	-0.23	0.0	2.2E-03	0.019	0.88	9.91
Urban, land cover type 13, #:19,669 (1.13%)											
M5 vs. M11	-7.9E-03	7.2E-03	0.0	1.2E-05	0.97	-0.25	0.0	-3.1E-03	0.013	0.82	10.89
M3 vs. M5	0.0046	0.017	0.0	3.1E-05	0.81	-0.034	0.0	-1.2E-03	0.0049	0.94	7.42
M11 vs. M5	0.13	-0.13	0.0	5.9E-05	-6.9E-03	0.25	0.0	7.7E-03	0.013	0.91	8.28
Barren, land cover type 12, #:15 (0.00%)											
M5 vs. M11	1.13	5.70	0.0	-2.4E-02	-3.5	-20.8	0.0	0.092	0.0014	0.99	0.64
M3 vs. M5	-0.044	-1.57	0.0	2.8E-03	0.88	6.6	0.0	-1.3E-02	0.0016	0.99	0.89
M11 vs. M5	0.84	-0.44	0.0	-9.5E-03	-2.40	1.07	0.0	4.1E-02	0.0026	0.98	0.89
All, land cover type 1-13, #:1,747,931 (100%)											
M5 vs. M11	-0.020	0.018	0.0	6.3E-05	0.69	-0.13	0.0	-9.8E-04	0.013	0.85	13.03
M3 vs. M5	-1.4E-03	9.8E-03	0.0	1.0E-04	0.63	-0.15	0.0	-6.5E-04	0.0064	0.89	11.19
M11 vs. M5	0.12	-0.13	0.0	5.7E-05	0.58	0.22	0.0	3.8E-03	0.017	0.91	10.12

D. GOES-17 ABI Cooling System Issue and Algorithm Mitigation

During post-launch testing of the GOES-17 ABI instrument, an issue with the instrument's cooling system was discovered. The loop heat pipe (LHP) subsystem, which transfers heat from the ABI electronics to the radiator, is not operating at its designed capacity. The consequence of this is that the ABI detectors cannot be maintained at their intended temperatures under certain orbital conditions. Inadequate cooling of the infrared channels leads to partial loss of imagery during some of the overnight hours before and after the vernal and autumnal equinoxes.

Infrared signals with long wavelengths can be swamped by infrared light emitted by warm parts of the imager, degrading the signal. Cooling the detectors reduces this thermal "noise" in observations. During some nighttime hours during certain parts of the year (before and after the vernal and autumnal equinoxes), the sun heats up seven of the ABI detectors (bands 8-16) faster than they can be cooled. The detectors become warmer than they're designed to operate, and they begin to radiate at temperatures closer to the wavelengths they're attempting to detect from the Earth. Eventually, local emissions and dark current noise overwhelm the signal from the Earth, and the channels saturate, meaning a useful signal is not available.

As aerosol retrieval is performed at daytime using shortwave channels (ABI bands 1-6), the direct impact on the retrieved AOD value is insignificant; however, the indirect impact through using the upstream retrieval products derived with affected Infrared channels (e.g., ABI cloud mask) need to be addressed. The indirect impacts from the ABI cloud mask would affect the AOD "retrievability" and quality control in the following two ways: (1) if cloudy pixels are misclassified as clear-sky, they are very likely to be identified by the internal tests (using SW channels) of the AOD algorithm, so for this scenario, algorithm would have some extra low-quality retrievals that are not supposed to be retrieved; (2) for the scenario of clear pixels misidentified as cloudy, they would likely pass the internal cloud tests, and as a result, algorithm would lose some high-quality retrievals by degrading them to be low-quality.

At current stage, the algorithm mitigation would simply copy the variable "granule_level_quality_flag" from the ABI cloud mask output to the AOD output with a new variable name "cloud_mask_granule_level_quality_flag". This variable is a 64 bit sized mask where each bit can represent a different QC condition. Currently, only bit 0, bit 1 and bit 63 are in use. Bit 0 is reserved for missing channel degradation (such as when the FPT threshold is exceeded and a channel gets turned off), bit 1 is for missing ancillary SST degradation, and bit 63 is reserved for a complete failure of IR channels. User would check this flag (larger than 0) for the potential degrade of the GOES-17 ABI cloud mask.

Further investigation is on-going to fully examine the impacts on the pixel level.

E. ABI Bright Land Spectral Reflectance Relationship

A constant linear relationship between surface reflectance at ABI channel B1 (M3) and B2 (M5)

$$\rho_{M3}^{sfc} = c_0 + c_1 \rho_{M5}^{sfc} \qquad \text{(E.1)}$$

is developed for each GOES pixels where bright surface is identified, where c_0 and c_1 are numerical constants.

This relationship is derived from the ABI full-disk measurements during the period of 5/22/-12/31/2019 for GOES-16. The surface reflectance at B1 and B2 over the bright land pixels ($\rho_{M11}^{TOA} > 0.25$) are retrieved from the measured TOA clear-sky reflectance based on Eq. 3.4.18. In this process, due to a lack of instantaneous AOD map over full-disk domain, a constant τ_{550} of 0.05 associated with the generic aerosol model is assumed to represent the dominant clean-air condition. This assumption is built upon the observation that, given a relatively long time period, the high AOD cases are not dominant in the GOES domain, and hopefully the incorrectly retrieved surface reflectance can be eliminated as low-value outliers in the analysis. The linear relationship (E.1) is derived for each pixels where enough valid samples (solar zenith angle < 65°) are available (# > 100). The removal of outliers is achieved by performing a linear regression with all samples first, then removing the points lying 0.005/0.01 above/below the fitting line, and the final linear relationship is derived by the regression with remaining samples. Same process also applies to GOES-17 during the period of 7/13/-12/31/2019

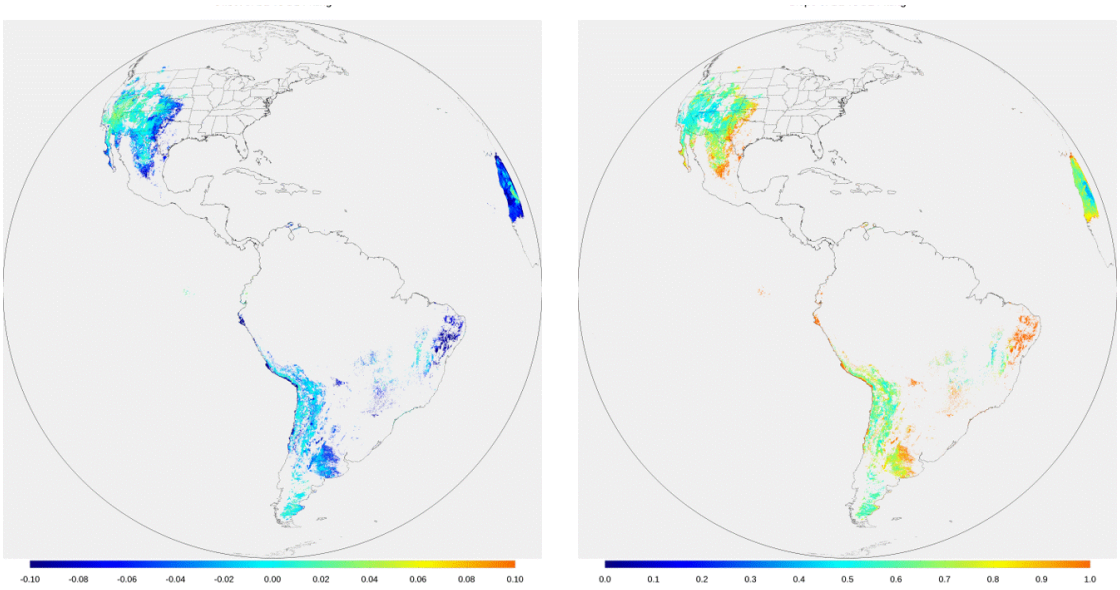

Figure E-1. The offset (left) and slope (right) of the bright land spectral surface relationship for GOES-16.

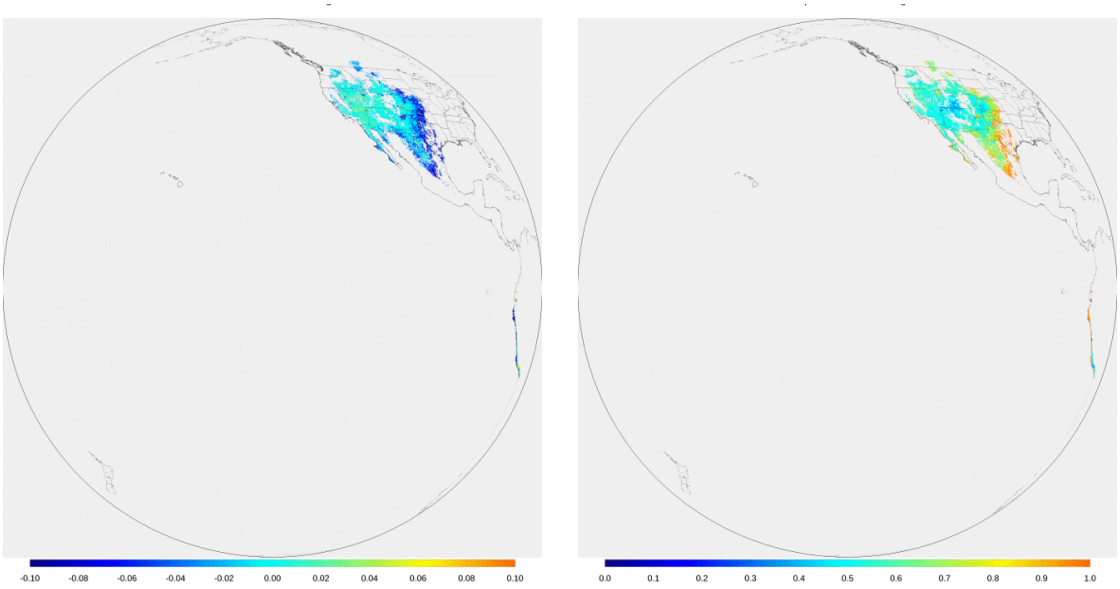

Figure E-2. The offset (left) and slope (right) of the bright land spectral surface relationship for GOES-17.